DISSERTATION

ELECTROCHEMILUMINESCENT AND ELECTROLUMINESCENT DEVICES CONTAINING POLYPYRIDINE TRANSITION METAL COMPLEXES

Submitted by

Corey J. Bloom

Department of Chemistry

In partial fulfillment of the requirements

for the degree of Doctor of Philosophy

Colorado State University

Fort Collins, Colorado

Spring, 2003

ProQuest Information and Learning Company
300 North Zeeb Road
P.O. Box 1346
Ann Arbor, MI 48106-1346

COLORADO STATE UNIVERSITY

February 18, 2003

We hereby recommend that the dissertation prepared under our supervision by Corey J. Bloom entitled *Electrochemiluminescent and Electroluminescent Devices Containing Polypyridine Transition Metal Complexes* be accepted as fulfilling in part the requirements for the degree of Doctor of Philosophy.

Committee on Graduate Work

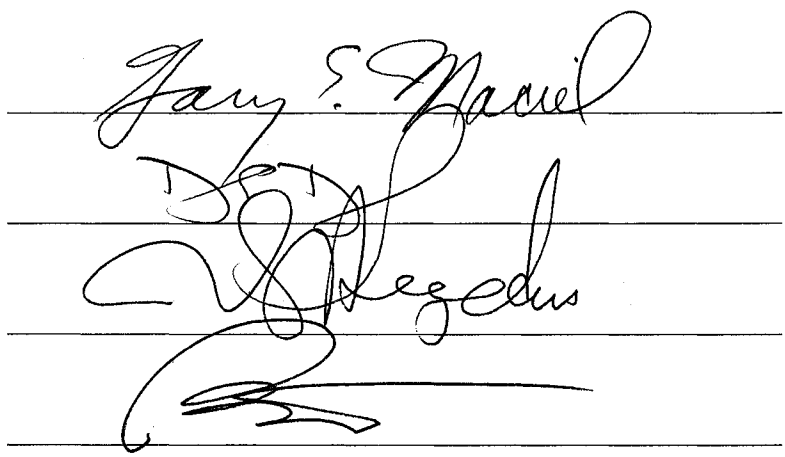

Adviser

Department Head

ABSTRACT OF DISSERTATION

Electrochemiluminescent and Electroluminescent Devices Containing Polypyridine Transition Metal Complexes

Polypyridine coordination complexes of transition metal cations, most notably tris(2,2'-bipyridine)ruthenium(II)-based compounds, "$[Ru(LL)_3]$", have a number of properties which make them of interest for both fundamental and applied studies. Stability in a number of oxidation states, along with interesting photochemical and photophysical behavior (including excited states that are in some cases relatively long-lived), are among the potentially useful characteristics of these complexes. Extensive research toward understanding the fundamental nature of these materials has brought the field to a point where the relationships between chemical structure and physical behavior of these metal complexes are well understood. As a consequence, it is now possible to predictably control the properties of these complexes through intelligent synthetic design. Using this knowledge, several materials composed of carefully designed and treated polypyridine metal complexes are described here for use in solid state devices exhibiting emission of light driven by electrical energy.

Light emitting devices based on solid thin layers of organic compounds and/or inorganic coordination complex materials fall into two general categories, electro*chemi*luminescent (ECL) and electroluminescent (EL) systems. The basic

description of the two device motifs is quite similar; however, there are a number of critical differences in the mechanisms by which they operate. These considerations in turn dictate the choices of materials employed in the construction of the two types of devices. The introductory chapter in this work describes in detail the conceptual differences between ECL and EL devices, and the resulting materials requirements.

In the second chapter, an ECL system is described based on a substituted $[Ru(LL)_3]$ monomer complex which exhibits intense emission following either photo- or electrochemically-generated excitation. A solid state "sandwich cell" device is constructed following thermal polymerization of the complex to yield electrochemically active thin films. The performance of this device is reported, and is found to be superior to previously reported similar ECL devices, owing to the rational design of the emitting material.

In the third chapter, a series of three polymerizable complexes, including the same $[Ru(LL)_3]$-based complex used in the ECL devices along with two similar compounds, is examined. In this work the electronic properties of the three films are studied after careful electrochemical reduction to yield conductive polymers, with emphasis on conductivities and work functions. These materials are considered for use as the cathode layers for EL devices employing commonly reported emissive compounds. The reduced $[Ru(LL)_3]$ conducting polymer with the lowest work function was successfully used as a cathode in devices with two common EL materials. These results sufficed as proof-of-concept for the use of reduced coordination complexes as cathodes in EL devices, but their performance was less than ideal. The inferior performance of these devices is most likely due to the inherent limitations imposed by the use of compounds that necessitated

thermal polymerization, as well as the need for electrochemical treatment prior to device construction.

Finally, the fourth chapter describes a related set of three coordination complexes of ruthenium and chromium (discrete molecules rather than polymers) that are also electrochemically reduced and subsequently used as cathode materials for EL devices. However, these complexes can be vapor deposited in the conductive state, and thus have important advantages in actual devices. The performance of systems including layers of these vapor deposited complexes is evaluated and is significantly improved over those devices reported in the previous chapter.

Corey J. Bloom
Department of Chemistry
Colorado State University
Fort Collins, CO 80523
Spring 2003

ACKNOWLEDGEMENTS

First and foremost, I would like to thank my adviser, Mike Elliott. It has truly been a pleasure working in the group, and I have grown a great deal as a scientist and a person under your supervision. I would also like to thank many members of the Elliott group both past and present, for help and comic relief in the lab, and some good memories outside of work as well. I am particularly grateful for the assistance of Dan Derr and Francois Pichot in the early stages of my education at C.S.U., and Shawn Sapp for several productive and enjoyable years sharing lab space in C116.

I will also be forever thankful for the love and support of my wife Wendy and the rest of my family, as well as many good friends in Fort Collins. The adventures snowboarding and skiing with the boys at Mary Jane and Steamboat, playing golf, camping and backpacking (including the "death march"), playing softball with the Mechanics, and hanging at Charolais Pines, the Trailhead and The East Coast were the best of times. Thanks, guys; Nate, Jorin, Bercot, Brian, Duane, Limoges, Grant, J.W., Shawn, and everybody else too numerous to list. The good memories will remain, the rest will fade. I wish the best of luck to you all in the future.

TABLE OF CONTENTS

LIST OF FIGURES

Chapter One.

Chapter Two.

Chapter Three.

LIST OF TABLES

CHAPTER ONE

INTRODUCTION TO ELECTROCHEMILUMINESCENT AND ELECTROLUMINESCENT DEVICES

Background:

There is currently a great demand for improved technologies providing light emission in flat panel displays. An ideal device would be inexpensive to construct, would operate with intense emission and low power consumption, and would have a long lifetime. Among the known possible device motifs, many of the most promising designs studied to date have involved the use of thin layers of organic compounds in the solid state as emissive materials.[1] The detailed construction and mechanism of operation of such devices is variable, but they share in common some basic characteristics. In general, the devices are composed of one or more layers of organic materials (and/or inorganic coordination complexes) in a sandwich configuration between two conducting electrodes. The active organic materials can be either polymers or discrete molecules, and can be deposited via spin coating from solution or thermal vapor deposition. Both of these methods are relatively inexpensive, and particularly well suited for use in relatively large, planar types of displays. With the application of a potential across the electrodes, current is passed by one of several possible mechanisms and materials are forced into an excited state, from which there is a good probability of photon emission. The electrodes biased with positive and negative potentials are referred to as the anode and cathode, respectively.

Electrochemiluminescent Devices:

Light emitting devices of the above description fall into two general categories, with emission governed by either electrochemiluminescent (ECL) or electroluminescent

(EL) mechanisms.[2-6] Although the basic description of such systems is very similar, there are some important differences in the mechanism by which these devices operate, and thus in the requirements for the materials employed in their construction. In ECL, chemical species produced at the two electrodes meet at a plane near the center of the device and undergo a chemical reaction that yields a product in the excited state, with subsequent emission of a photon.

In ECL devices there are several stringent requirements for the active material. It must be possible for redox reactions to occur at both electrodes in the solid state, and for the two electro-generated species to move towards the center of the device. In specially designed solids, the conduction of charged species can occur via the process of "electron hopping". In this case, reversible electron transfer reactions (driven by a gradient in the concentration of the redox species of interest) take place between neighboring active sites in differing oxidation states. The result is that charged moieties can be moved across a solid film without *physical* movement of the redox sites.[7-10] Because the charged entities are effectively moving by a diffusion mechanism (but the redox sites themselves are immobile), this process is also referred to as "apparent diffusion". Although the active sites themselves need not move, mobile counterions must be present in order to maintain charge neutrality at the local level, and to further allow the equilibration of the Fermi levels of the organic material and the adjacent electrode.[1] Finally, the chemiluminescent reaction that occurs when the charged species collide in the film must be completely reversible, in that it must yield the *initial* reactants as the final products. If this were not the case, these reactants would be quickly depleted and the production of reactive species at the two electrodes would no longer be possible.

Polymers composed of substituted tris(bipyridine)ruthenium (II) complexes, hereafter $[Ru(LL)_3]^{2+}(X^-)_2$, are among the few known materials fulfilling all of the requirements for an ECL device.[2-4,11] In these "redox polymer" systems, discrete electrochemically active complexes which can exist in a number of stable oxidation states are present.[12-14] Furthermore, electron transfer between complexes is facile, allowing for the necessary apparent diffusion of redox species across a solid film (provided the presence of physically mobile counterions).[8,13,15] In addition, it is possible to control the behavior of the complexes comprising the films, including redox potentials and photophysical properties, by varying the exact chemical composition of the bipyridine ligands.[16-18] Finally, and of key importance to the light emitting technologies under consideration here, the electro-generated reduced and oxidized forms of $Ru(LL)_3$ can efficiently undergo the chemiluminescence reaction defined below:[16,19]

$$[Ru(LL)_3]^{3+} + [Ru(LL)_3]^{1+} \rightarrow [Ru(LL)_3]^{2+} + [Ru(LL)_3]^{2+}* \rightarrow 2[Ru(LL)_3]^{2+} + h\nu$$

The useful redox, photophysical, and photochemical properties of $[Ru(LL)_3]^{2+}$-based materials are all a consequence of the unique electronic structure of the complexes. **Figure 1.1** depicts the chemical structure of the $[Ru(bpy)_3]^{2+}$ ion, and **Figure 1.2** is a simplified molecular orbital (MO) diagram for the d^6 Ru^{2+} ion in the roughly octahedral ligand field resulting from complexation with 3 bipyridine units[19]. The large ligand field stabilization energy for the d^6 ion in the complex is evident from this diagram. In addition, the consequences of oxidation and reduction(s) of the complex can be deduced from the MO representation. Oxidation would result in the removal of an electron from the metal-based t_{2g} orbital, and reductions proceed with the addition of one or more

electrons to the ligand-based π_L^* antibonding manifold. The excited state complex formed following absorption of light of appropriate energy ($\lambda \sim 500$ nm), or the chemiluminesence electron transfer reaction discussed above, consists of an electron promoted from the metal-based t_{2g} orbital to the ligand π_L^* orbital. This first excited state is thus referred to as a metal-to-ligand-charge-transfer (MLCT) state. The complex in this singlet ^{1}MLCT state then quickly undergoes an intersystem crossing to a triplet ^{3}MLCT state, from which emission or non-radiative recombination eventually takes place.[16,19] Again, synthetic modifications that alter the physical and electronic structure of the bipyridine rings can thus have significant effects on the redox potentials and excited state behavior of the complex.

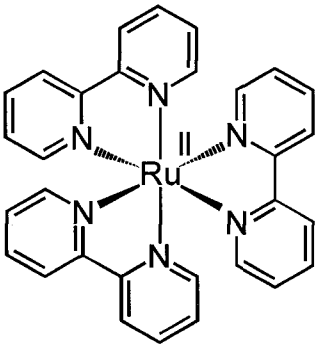

Figure 1.1: The chemical structure of the tris(bipyridine)ruthenium (II) ion. Counterions are not included in this representation.

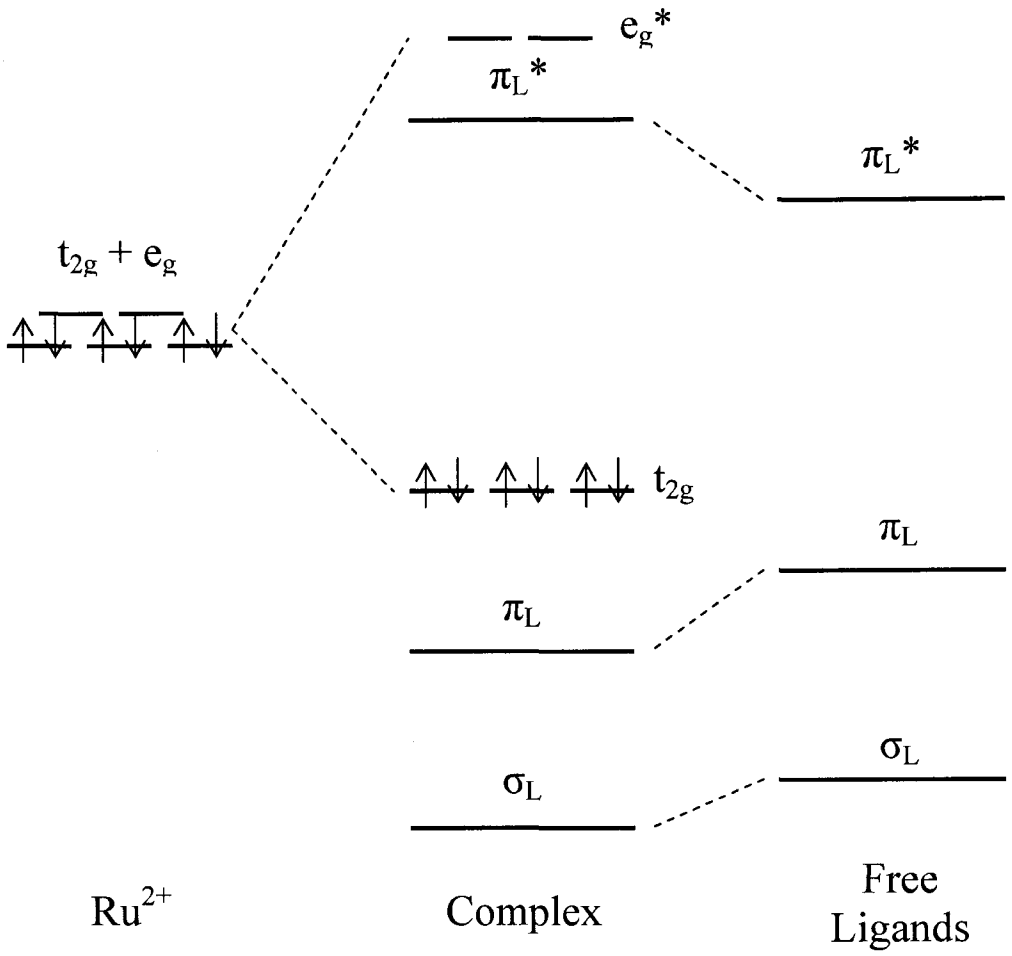

Figure 1.2: A simplified MO of the $[Ru(bpy)_3]^{2+}$ complex in O_h symmetry. Electrons are shown only in the metal-based orbitals, but the ligand π_L and σ_L orbitals are also fully occupied.

As a consequence of the above properties, it is possible to make an ECL device employing a $[Ru(LL)_3]$-based polymer as the sole active material (most often in a "sandwich" configuration between two electrodes). When provided with mobile counterions which can locally maintain charge neutrality (by employing relatively small, electrochemically inactive anions such as PF_6^- and initially swelling the polymer film with solvent), and when a sufficient voltage bias is applied across the polymer film, the 2+ charged complexes are oxidized to the 3+ state at the anode and simultaneously are

reduced to the 1+ species at the cathode. Both species effectively diffuse towards the center of the film via electron hopping between complexes, where they meet and undergo the chemiluminescence reaction described above. After steady-state conditions are achieved, concentration gradients of the $[Ru(LL)_3]$ complexes, along with corresponding gradients of counterions, are produced within the polymer layer (this is generally referred to as the "mixed-valent" state), and the film can be dried to yield a fully solid-state ECL device.[3,4] **Figure 1.3** contains a conceptual diagram of an $[Ru(LL)_3]$-polymer based ECL device during steady-state operation.

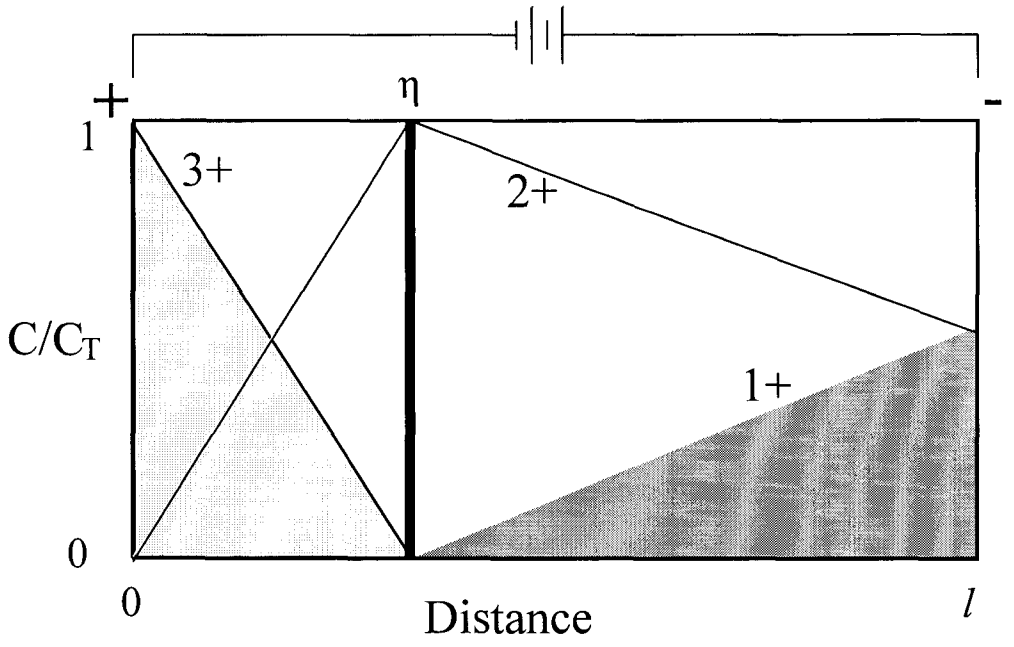

Figure 1.3: A representation of the cross-section of an ECL device based on a $[Ru(LL)_3]^{2+}$ polymer at steady state.

In the above representation of an ECL device in operation, the x-axis represents distance across the polymer film, and the y-axis is normalized concentration of redox centers. The *total* concentration of metal complexes (irrespective of charge) is assumed

to be equal throughout the film. At the anode (left side, x = 0) the complexes are oxidized to $[Ru(LL)_3]^{3+}$ while the reduction to $[Ru(LL)_3]^{1+}$ takes place at the cathode at ℓ. Concentration gradients of both the charged complexes and the counter anions form as the 3+ and 1+ species effectively diffuse towards the center of the film, where they meet at η and undergo the chemiluminescence reaction described above. The two shaded areas represent the integrated amount of 3+ and 1+ complexes, and because the total number of anions is fixed the two areas must be equal to maintain charge neutrality.

By intelligent design of the $[Ru(LL)_3]$-based complexes, and appropriate choice of electrode materials and operation parameters, the performance of these ECL devices can be optimized. In **Chapter 2**, a particularly efficient ECL system employing the design described above and composed of a strongly luminescent $[Ru(LL)_3]$ compound is examined in detail.

Electroluminescent Devices:

Electroluminescent devices are governed by a significantly different mechanism, and are subsequently engineered with different concerns.[5,6,20,21] **Figure 1.4** is a simplified diagram of an EL device in operation. In these systems, with the application of a voltage bias, electrons and holes are injected from the electrodes into the conduction band (CB) and valence band (VB) of the organic compounds, respectively (or LUMO and HOMO depending on the material).[1] Under the influence of the applied potential gradient, these charge carriers then migrate towards the center of the film where an electron-hole pair has a high likelihood of radiative recombination. Such EL devices are analogous to inorganic light emitting diodes (LEDs), and are thus commonly also

referred to as organic light emitting diodes or devices (OLEDs). The terms "EL device" and "OLED" are generally treated as interchangeable, and they will be used as such here.

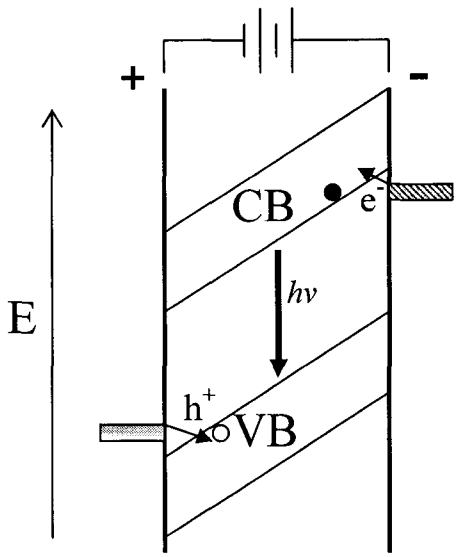

Figure 1.4: Representation of an EL device in operation.

In the simplified depiction of an EL device above, the x axis represents distance across the organic layer, while the y axis represents energy. With an applied voltage, the energy of the cathode (again on the right side) is raised relative to the anode. The energy bands in the wide bandgap organic semiconductor tilt accordingly to a degree determined by the potential gradient, assuming no band bending. Holes injected from the anode and electrons from the cathode are driven towards the center of the film, where they recombine to form an excited state with a high probability of relaxation by emission of light.

Note the important differences in the operation of OLEDs as compared to ECL devices. In an EL system, gradients of chemical species are not produced, and there is no

requirement of counterions for charge balance. Charge carriers in an EL device move via migration in response to a potential field. Again, in ECL devices mobile counterions can screen charges, causing any potential drop to occur at the electrode interface, and thus charges move by the apparent diffusion of redox species driven by a chemical potential resulting from the concentration gradient. For these reasons, the requirements for the organic materials comprising EL devices are not as restrictive as in ECL systems. Electrons and holes must be a least fairly mobile in the appropriate bands (or orbitals) in the materials, and they must eventually meet in a material that will form an excited state with a high probability of photon emission. Devices composed of either polymers or small molecule organic compounds (and coordination complexes), or both, are thus common, as are multilayer devices engineered to provide for the most efficient operation.[1,5,22,23]

In contrast to the situation in ECL devices, in OLEDs the choice of electrode composition is critical and has a direct effect on the performance of the device. Injection of electrons into the CB, and holes into the VB, is through an energy barrier determined largely by the difference in energy of the Fermi level (E_F) of the electrode in question and the adjacent band in the organic material. Accordingly, cathode materials with high E_F (and thus low work functions, Φ, the difference between E_F and the energy of a free electron in vacuum) are generally employed to provide for facile electron injection into the CB. By the same reasoning, the anode must be composed of a conductor with a low E_F (or high Φ) to minimize the barrier for injection of a hole into the VB. Cathodes are thus generally composed of low Φ metals such as calcium and magnesium, while transparent conducting metal oxides like indium/tin oxide (ITO) are the most commonly

used anode materials.[5,21,24] Keeping in mind that one electrode must be transparent to allow for the escape of light, ITO and other conducting oxides are a logical choice for anode materials as they inherently have high work functions.

Athough OLEDs constructed as described above operate efficiently and with intense emission, device lifetime is still problematic. One of the most common causes of failure cited is degradation of the cathode material itself, along with problems at the interface between the organic layer and the metal cathode.[6,25-27] It stands to reason that replacing the reactive metal cathode with a low work function conductor composed of organic material may provide for a more compatible junction with the active layer.

It has previously been reported that, after careful electrochemical treatment involving reduction to the zero charged state and ejection of counterions, $[Ru(LL)_3]$-based redox polymers such as those employed as the emissive layers in ECL devices become much more conductive than in other "mixed-valent" states.[28,29] Because these polymers have been electrochemically reduced, the E_F is significantly raised to yield low Φ conductors that are promising candidates for use as cathodes in EL devices using common emissive materials. Furthermore, the ability to control the redox potentials of the $Ru(LL)_3$ complexes comprising the polymers via synthetic chemistry affords a series of chemically similar materials ostensibly with different Φ. In **Chapter 3**, theory is developed to predict the work functions of these reduced conducting polymers, and several EL devices are constructed and analyzed using the polymer with the lowest Φ as a cathode material. In this configuration, the $Ru(LL)_3$-based polymer is used only as an electronic material, and does not directly participate in the light emission step.

OLEDs utilizing reduced polymers as cathodes were successful, but device performance was less than ideal, most likely due in large part to engineering problems associated with the necessity of electrochemical treatment of the polymer film, and the constraints this places on device construction. In **Chapter 4**, several electrochemically reduced coordination complexes of ruthenium and chromium are examined. In this case the structurally symmetrical bis(terpyridine) ruthenium, $[Ru(LLL)_3]^0$, and tris(bipyridine) chromium, $[Cr(LL)_3]^0$, complexes are employed. These neutral complexes are isolated and thermally vapor deposited for use as cathodes in EL devices. With the advantage of more flexible design of device architecture, significantly improved device performance was evident.

It is the unique properties of metal polypyridine complexes that makes these varying applications in light emitting schemes possible, and ties this body of work together. The *large* difference in potential between the $[Ru(LL)_3]^{3+}$ and $[Ru(LL)_3]^{1+}$ oxidation states, which places their electron transfer reaction in the Marcus inverted region,[30,31] along with the behavior of the $[Ru(LL)_3]^{2+*}$ species consequently formed, are critical in the ECL device discussed in **Chapter 2**. At the same time, it is the *small* potential separation between the 1+, 0, and 1- charged $Ru(LL)_3$ complexes (and the related $[Ru(LLL)_2]^0$ and $[Cr(LL)_3]^0$ species), and the facile electron transfer between neighboring complexes in the solid state, which governs the application of the conducting materials employed as cathodes for EL devices in **Chapters 3 and 4**.

REFERENCES

(1) Sheats, J. R.; Antoniadis, H.; Hueschen, M.; Leonard, W.; Miller, J.; Moon, R.; Roitman, D.; Stocking, A. *Science* **1996**, *273*, 884.

(2) Abruna, H. D.; Bard, A. J. *J. Am. Chem. Soc.* **1982**, *104*, 2641.

(3) Maness, K. M.; Terrill, R. H.; Meyer, T. J.; Murray, R. W.; Wightman, R. M. *J. Am. Chem. Soc.* **1996**, *118*, 10609.

(4) Maness, K. M.; Masui, H.; Wightman, R. M.; Murray, R. W. *J. Am. Chem. Soc.* **1997**, *119*, 3987.

(5) Tang, C. W.; VanSlyke, S. A. *Appl. Phys. Lett.* **1987**, *51*, 913.

(6) Burroughs, J. H.; Bradley, D. D. C.; Brown, A. R.; Marks, R. N.; Mackay, K.; Friend, R. H.; Burns, P. L.; Holmes, A. B. *Nature* **1990**, *347*, 539.

(7) Kaufman, F.; Engler, E. M. *J. Am. Chem. Soc.* **1979**, *101*, 547.

(8) Facci, J. S.; Schmehl, R. H.; Murray, R. W. *J. Am. Chem. Soc.* **1982**, *104*, 4959.

(9) Daum, P.; Lenhard, J. R.; Rolison, D.; Murray, R. W. *J. Am. Chem. Soc.* **1980**, *102*, 4649.

(10) Shigehara, K.; Oyama, N.; Anson, F. C. *J. Am. Chem. Soc.* **1981**, *103*, 2522.

(11) Lee, J. K.; Yoo, D.; Handy, E.; Rubner, M. F. *Appl. Phys. Lett.* **1996**, *69*, 1686.

(12) Chidsey, C. E. D.; Murray, R. W. *J. Phys. Chem.* **1986**, *90*, 1479.

(13) Peerce, P. J.; Bard, A. J. *J. Electroanal. Chem.* **1980**, *114*, 89.

(14) Daum, P.; Murray, R. W. *J. Phys. Chem.* **1981**, *85*, 389.

(15) Buttry, D. A.; Anson, F. C. *J. Electroanal. Chem.* **1983**, *130*, 333.

(16) Juris, A.; Balzani, V.; Barigelletti, F.; Campagna, S.; Belser, P.; VonZelemsky, A. *Coord. Chem. Rev.* **1988**, *84*, 85.

(17) Elliott, C. M.; Herschenhart, E. J. *J. Am. Chem. Soc.* **1982**, *104*, 7519.

(18) Wacholtz, W. F.; Auerbach, R. A.; Schmehl, R. S. *Inorg. Chem.* **1986**, *25*, 227.

(19) Kalyanasundaram, K. *Photochemistry of Polypyridine and Porphyrin Complexes*; Harcourt Brace Jovanovich: London, **1992**.

(20) Miyata, S.; Nalwa, H. S. *Organic Electroluminescent Materials and Devices*; Gordon and Breach: Netherlands, **1997**.

(21) Gustafsson, G.; Cao, Y.; Treacy, G. M.; Klavetter, F.; Colaneri; Heeger, A. J. *Nature* **1992**, *357*, 472.

(22) Troadec, D.; Veriot, G.; Antony, R.; Moliton, A. *Synth. Met.* **2001**, *124*, 49.

(23) Parthasarathy, G.; Burrows, P. E.; Khalfin, V.; Kozlov, V. G.; Forrest, S. R. *Appl. Phys. Lett.* **1998**, *72*, 2138.

(24) Matsumura, M.; Akai, T.; Saito, M.; Kimura, T. *J. Appl. Phys.* **1996**, *79*, 264.

(25) Lazzaroni, R.; Bredas, J. L. *Plast. Engin.* **1998**, *43*, 185.

(26) Birgeson, J.; Fahlman, M.; Brohms, P.; Salaneck, W. R. *Synth. Met.* **1996**, *80*, 125.

(27) Choung, V. E.; Mason, M. G.; Tang, C. W.; Gao, Y. *Appl. Phys. Lett.* **1998**, *72*, 2689.

(28) Elliott, C. M.; Redepenning, J. G.; Balk, E. M. *J. Electroanal. Chem.* **1986**, *213*, 203.

(29) Elliott, C. M.; Redepenning, J. G.; Balk, E. M.; Schmittle, S. J. *Electronically Conducting Films of Poly(trisbipyridine)-Metal Complexes;* ACS Symposium Series 360 (Inorganic and Organometallic Polymers), American Chemical Society: Washington, DC, **1988**, p. 420.

(30) Marcus, R. A. *Angew. Chem. Int. Engl. Ed.* **1993**, *32*, 1111.

(31) Wallace, W. L.; Bard, A. J. *J. Phys. Chem.* **1979**, *83*, 1350.

CHAPTER TWO

A HIGHLY EFFICIENT SUBSTITUTED TRIS(BIPYRIDINE)RUTHENIUM(II) POLYMER-BASED ELECTROCHEMILUMINESCENT DEVICE

A portion of the material presented in this chapter was published in

The Journal of the American Chemical Society, **1998**, *120*, 6781-6784.

Introduction:

One of the many interesting and useful properties of the tris(bipyridine)ruthenium(II) complex is intense photoluminescence from the ^{3}MLCT excited state. The emission quantum yield (Φ_E) in the solution state is generally reported in the range of 7% in dry acetonitrile.[1] This complex also exhibits electrochemically generated luminescence (ECL) in dilute solution via the reaction[2,3]

$$[Ru(LL)_3]^{3+} + [Ru(LL)_3]^{1+} \longrightarrow [Ru(LL)_3]^{2+} + [Ru(LL)_3]^{2+*} \longrightarrow 2[Ru(LL)_3]^{2+} + h\nu$$

Moreover, in acetonitrile solution the quantum efficiency for ECL emission (Φ_{ECL}), at 5%, is only modestly smaller than Φ_E under similar conditions.[2,3] Thus, at least in the solution state, it has been demonstrated that the electrogenerated chemical reaction depicted above can yield the highly luminescent excited species with a probability approaching unity.

More recently, ECL has been observed in the solid state from electrochemically formed films of poly-Ru(vbpy)$_3$, where vbpy is 4-vinyl-4'-methyl-2,2'-bipyridine.[4,5] The most successful of these studies, at least in terms of emission stability, has involved a dual electrode arrangement employing an interdigitated array electrode (IDA) where the polymer spans the gap (<5μm) separating the "fingers" of the two electrodes.[5] In this configuration when appropriate voltages are applied, oxidation of $Ru(LL)_3^{2+}$ ensues at one electrode and reduction at the other. As described in **Chapter 1**, time-independent gradients of $[Ru(LL)_3]^{3+}$ and $[Ru(LL)_3]^{1+}$ are established in the polymer at steady-state. At the interface of these two gradients the light emitting reaction detailed above occurs.

Furthermore, the electrochemical process which generates $[Ru(LL)_3]^{3+}$ and $[Ru(LL)_3]^{1+}$ is a voltage-driven disproportionation reaction that does not change the net charge of the system, thus there is no requirement for charge compensating ions to enter or leave the polymer. Consequently, such assemblies can be operated entirely in the solid state (i.e., in the absence of electrolyte solution). Although devices based on poly-$Ru(vbpy)_3$ exhibit good reproducibility and light emission stability, Φ_{ECL} has proven to be meager ($\approx$ 0.03%).[5] Other $Ru(bpy)_3$-based ECL systems not involving vbpy polymerization have also been examined and operate with comparable efficiencies.[6-8]

Tris(bipryidine)ruthenium(II) complexes in which the bipyridines are substituted in the 4- and 4'- positions with –COOR functions exhibit significantly enhanced solution photoluminescence when compared with the unsubstituted analogue. For example, in O_2-free acetonitrile at room temperature the ethyl ester-substituted complex has $\Phi_E \approx 30\%$.[9] In addition, these electron-withdrawing ester functions shift $E^{\circ\prime}(3+/2+)$ by ca. 300 mV and $E^{\circ\prime}(2+/1+)$ by ca. 380 mV in the positive direction, relative to the parent tris(bipryidine)ruthenium(II) complex.[10] Given the very high quantum efficiency for photoluminescence of the ethyl ester complex, it stands to reason that solid state ECL devices composed of $[Ru(LL)_3]^{2+}$-based monomers with ester substitution in the 4- and 4'- positions of the bipyridine ligands would perform substantially better than the previously studied systems. To this end, the **M2** complex reported here and shown in **Figure 2.1** can be thermally polymerized to yield electrochemically active thin polymer films (hereafter referred to as polymer **P2**). Devices comprising **P2** films as the ECL material are constructed and not only have substantially greater Φ_{ECL} than previously

reported $[Ru(LL)_3]^{2+}$-based ECL devices, but have efficiencies comparable with the best organic LED's available.

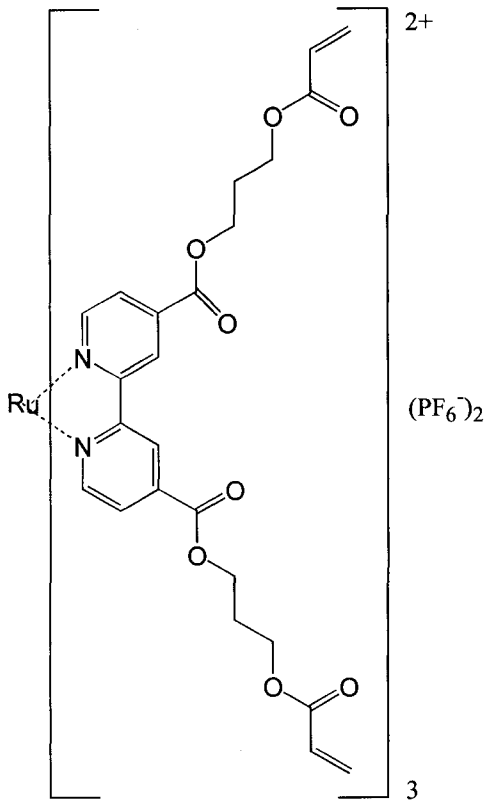

Figure 2.1: Structure of the monomer **M2**. The synthesis is detailed below in the Experimental Section.

Experimental:

4,4'-bis[(3-acrylyl-propoxy)carbonyl]-2,2'-bipyridine, (DEAB). 4,4'-dicarboxy-2,2'-bipyridine was prepared from 4,4'-dimethyl-2,2'-bipyridine (DMB, Reilly Industries, Indianapolis) following the procedure described by Oki and Morgan.[11] The carboxylic acid was converted to the acid chloride by refluxing 4 g of finely ground acid in 150 ml of thionyl chloride under nitrogen for 6-12 hours or until the solution became essentially clear. Excess thionyl chloride was removed by rotoevaporation. To minimize hydrolysis

by atmospheric moisture, the crude acid chloride was immediately converted to the bis-1,3-propanediol ester.

Typically, 60 ml of 1,3-propanediol was added to ca. 4 g of the diacid chloride dissolved in 300 ml of dichlormethane. This solution was heated to reflux for 1 hour, cooled to room temperature and extracted 4 times with 0.2 M aqueous sodium carbonate to remove excess diol. The dichloromethane layer, containing the intermediate product, 4,4'-bis[(3-hydroxypropoxy)carbonyl]-2,2'-bipyridine, was brought to dryness by rotoevaporation and the solid redissolved in a mixture of 300 ml of acetonitrile containing a large excess of acryloyl chloride. This solution was heated at reflux for 45 minutes and the solvent was then removed by rotoevaporation. The resulting thick liquid was diluted with 75 ml of 5% (by volume) triethylamine in water. This solution was extracted 4 times with dichloromethane, the organic fractions combined and dried over sodium sulfate before being evaporated to dryness. During the course of the reaction ca. 10% of the acrylate vinyl groups were hydrochlorinated by HCl produced in the reaction. To reverse this reaction the crude product was heated at reflux under nitrogen in a 5% V/V solution of triethylamine in dichloromethane for 4 hours. Finally, the DEAB ligand was purified by chromatography (silica, 1/3 acetone/dichloromethane) giving the product in 60% overall yield. ^{1}H NMR (δ in ppm from TMS in $CDCl_3$, multiplicity, integration): 2.2 (q., 2H); 4.3 (t., 2H); 4.5 (t., 2H); 5.8 (d., 1H): 6.1 (d. of d., 1H); 8.8 (d., 1H); 8.9 (s., 1H).

$[Ru(DEAB)_3](PF_6)_2$, M2. $Ru(DMSO)_4Cl_2$[12,13] (162 mg) was dissolved in approximately 30 ml of ethylene glycol and heated to reflux until an orange color developed. This

solution was cooled to 120° C whereupon 4.2 equivalents (685 mg) of the DEAB ligand was added. After 2 hours at this temperature, the solution was cooled to room temperature, diluted with 150 ml of water, and a few ml of saturated aqueous NH_4PF_6 added. The orange precipitate was collected by filtration and chromatographed on silica eluting with acetonitrile. Three bands, each of which contained a tris(bipyridine)ruthenium complex, resulted: **a** (rf = 0.9), **b** (rf = 0.5) and **c** (rf = 0.1). All had identical visible spectra and all fluoresced under long wavelength UV light. The ^1H NMR spectra of each was very similar, however, the integration for the acrylate protons were slightly less than expected in the case of **b** and **c**. In addition, no peak in the electrospray mass spectrum of either **b** or **c** could be matched with fragments from the anticipated structure. The ^1H NMR, mass spectrum, and chromatographic retention times all suggest that **b** and **c** are quite likely the dimer and trimer, respectively, of the monomer, **a**. The fraction containing **a** was reduced in volume to 10 ml and added to 60 ml of diethyl ether, whereupon the complex precipitated as a fine powder. The solid was collected by centrifugation, washed with diethyl ether and redissolved in acetonitrile. This solution was stored at –20° C and was used for casting films of **M2**. The yield of component **a** was 35%. 1H NMR (δ in ppm from TMS in $CDCl_3$, multiplicity, integration): 2.2 (m., 2H); 4.3 (t., 2H); 4.5 (t., 2H); 5.8 (d., 1H): 6.1 (d. of d., 1H); 6.4 (d, 1H); 8.0 (m., 2H); 9.0 (s., 1H). Electrospray MS: m/z = 753.2

Electrochemistry: Solution phase cyclic voltammetry of the **M2** monomer was performed in a Luggin capillary cell with a glassy carbon working electrode (WE), Ag/Ag^+ 0.1 M in DMSO reference electrode (RE), and a Pt wire counter electrode (CE).

The electrolyte solution was 0.1 M $TBA^+PF_6^-$ in CH_3CN, and the scan rate was 100 mV/sec. Electronic equipment used consisted of a P.A.R. model 173 potentiostat coupled to model 175 programmer with output to a Yokogawa X/Y recorder. **P2** polymer films were prepared by drop-coating onto a glassy carbon WE, followed by polymerization for approx. 4 hours at 150° C. Voltammetry was performed on **P2** films using the same equipment and conditions as for **M2** solutions.

ECL Sandwich-Cell Preparation: The anode of each sandwich cell consisted of a rectangular piece (ca. 2x1 cm) of ITO coated glass (resistance: 300 Ω/square). Each ITO electrode was cleaned by successive sonication in acetonitrile and ethanol, followed by gently swabbing the surface with a dichloromethane-soaked cotton swab.

The cleaned ITO electrode was heated for 10 seconds with a heat gun and 2-3 drops of monomer solution in acetonitrile (ca. 20 μl, 0.3 M) deposited onto the ITO surface. The solution was allowed to evaporate slowly under an inverted beaker, resulting in a highly uniform film (thickness ~ 500 nm by profilometry) of the monomer. In order to make electrical contact to the ITO, the monomer film was removed from an approximately 0.75 cm strip along one edge of the electrode surface with a dichloromethane-soaked cotton swab. The film was then polymerized at 150° C for one to three hours.

At the junction of the bare ITO and the edge of the polymer film, a thin layer (approx. 1 mm thick and 5 mm wide) of TorrSeal® epoxy resin was applied slightly overlapping the polymer but leaving a free area of ITO at the very end of the slide. After curing the epoxy at 70° C overnight, a rectangular piece of gold mesh (2000 lines/inch, 3-

5 μm thick, Buckbee-Mears, St. Paul, MN) of dimenisions slightly narrower than the exposed polymer film was carefully laid down on top of the polymer film so that it partially covered the insulating epoxy layer, defining a device area of ca. 0.5 cm^2. This gold mesh served as the cathode and allowed solvent vapors to swell the underlying film. At this point, another drop of monomer solution was deposited at the bottom end of the gold grid. This solution was pulled, by capillary action, into the entire grid. This second monomer layer served as an adhesive between the first polymer layer and the gold minigrid. The monomer was swabbed from the part of the gold surface lying atop the epoxy (for a subsequent electrical contact). The assembly was then heated at 150° C for one additional hour to polymerize the new monomer film sufficiently to ensure intimate contact between the gold electrode and the original **P2** film. Independent electrical contacts were made to the ITO anode and gold cathode using fine Teflon-insulated copper wires and silver paint. After the silver paint had thoroughly dried, these electrical contacts were buried under a second layer of epoxy to avoid their exposure to solvent. Finally, the entire device was placed in a 70° C oven overnight.

Results and Discussion:

In acetonitrile solution **M2** exhibits electrochemical reductions and photoluminescence (Φ_E) virtually identical to the ethyl ester-substituted complex.[6,7] Unlike $Ru(vbpy)_3$, **M2** shows no tendency to polymerize electrochemically. Rather, the monomer can be cast as the PF_6^- salt from acetonitrile solution (spin-, dip- or spread-coated) to form uniform glassy films when dry. These films can be polymerized thermally (150°C, ≥ 1 hr) or photochemically (UV) yielding robust, electroactive films of

P2. Cyclic voltammetry of both the **M2** monomer in solution and a **P2** polymer film is displayed in **Figure 2.2**.

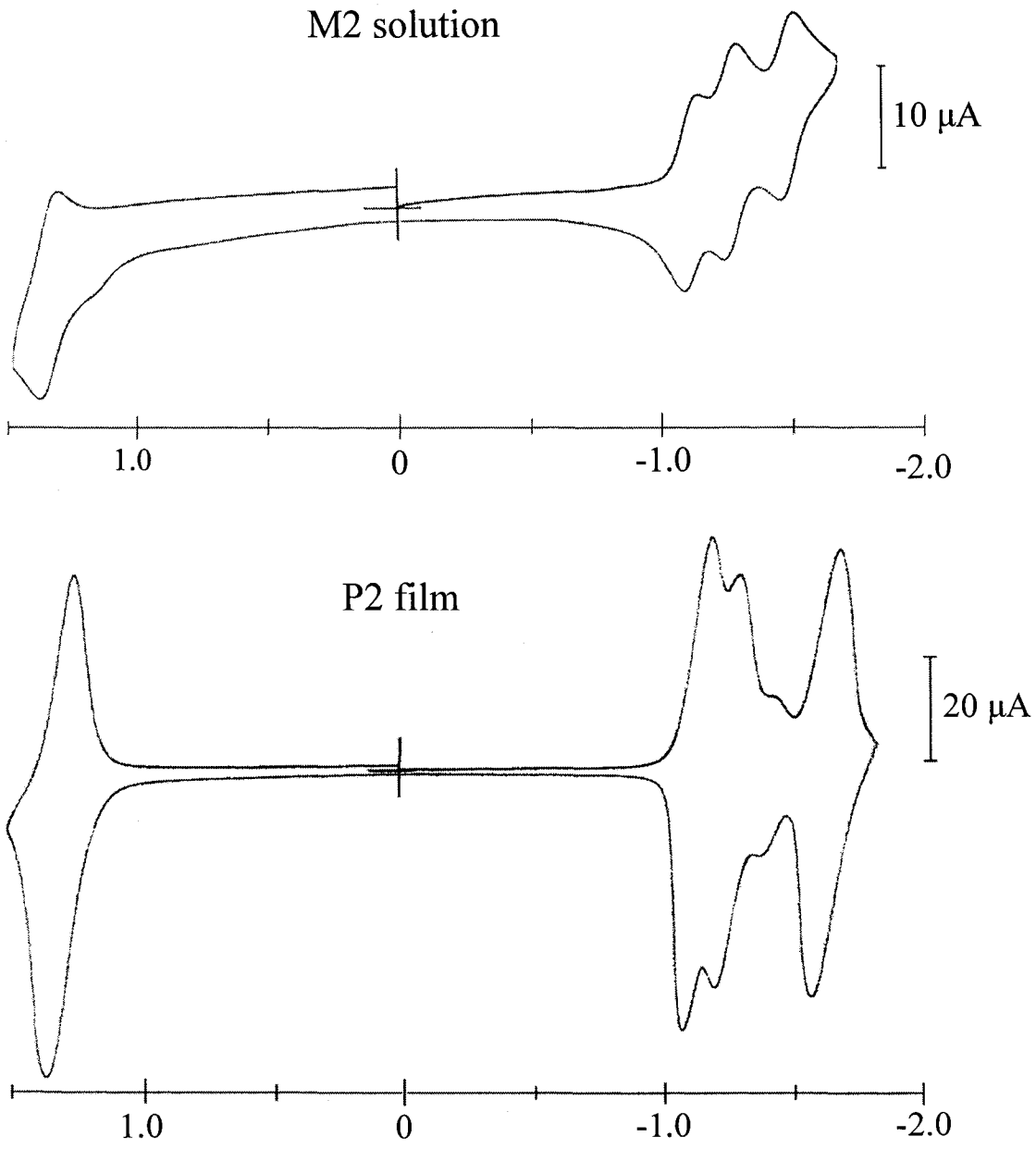

Figure 2.2: Cyclic voltammograms of the M2 monomer in solution and a P2 polymer film on glassy carbon WE's. In both cases, $E_{½}(3+/2+) - E_{½}(2+/1+) \sim 2.4$ V.

A group of 12 so-called "sandwich-cell" devices were fabricated from **P2** as described in detail in the Experimental Section. Briefly, these cells consist of a ~ 0.5 μm film of the polymer sandwiched between an optically transparent indium/tin oxide coated glass (ITO) anode and a porous gold "minigrid" (2000 lines/inch) mesh cathode. A diagram of the design of these ECL devices is depicted in **Figure 2.3**. To initiate the ECL reaction and establish the steady-state redox site gradients within the polymer film, each sandwich cell was first exposed to acetonitrile saturated N_2 in a vial stoppered with a septum through which the electrode leads passed. A bias of 2.5 volts was imposed between the Au cathode and ITO anode. Within a few seconds of applying the bias, visible luminescence was typically evident through the ITO electrode. The assembly was removed from the vial inside of an inert atmosphere box and allowed to dry under bias. As the polymer dried (over a period of about 5 minutes) the current decreased, finally stabilizing at a value typically 10% of the current initially observed with the polymer fully solvent swollen. Concomitantly with the decrease in current, the light emission diminished.

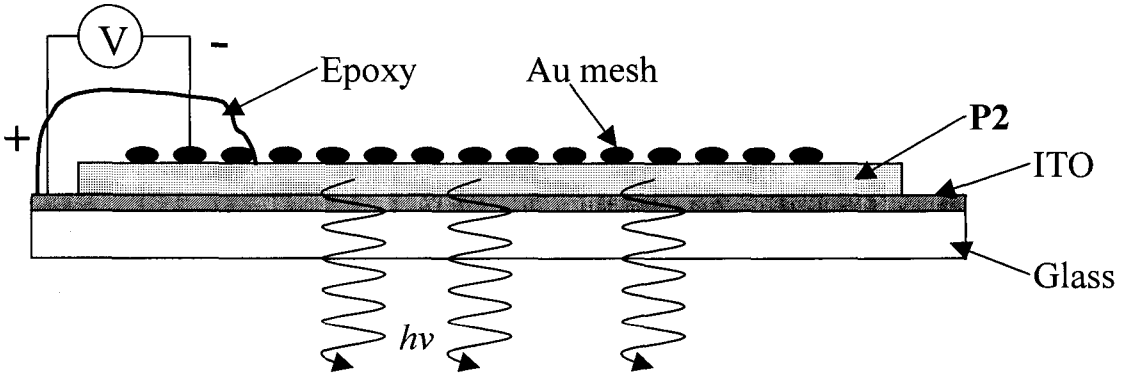

Figure 2.3: Sandwich electrode design. Drawing is **not** to scale.

The ECL emission of each fully dried assembly was measured (Center for Advanced Multifunctional Polymers and Molecular Assemblies, University of Arizona, Tucson) from the ITO side using a silicon photodiode mounted in a special housing calibrated to measure the external emission quantum yield. *External* and *internal* emission quantum yields (or efficiencies) differ in that the former is the number of photons escaping the front surface of the device per electron passed while the latter is the number of photons generated per electron passed. Of the 12 devices investigated, 6 emitted below the measurement threshold of the silicon detector. For the remaining 6 devices, each behaved in qualitatively similar fashion; however, there was considerable variation in resistance and *external* Φ_{ECL}. Current densities at 5.0 V bias ranged from 1 to 29 mA/cm^2 and external Φ_{ECL} ranged from 0.06% to 0.92%. By comparison with devices of similar construction and known *internal* quantum efficiency, it is estimated that the *internal* quantum efficiencies of the present devices is 4-6 X larger than the *external* efficiency directly measured.[14] Consequently, for the most efficient of the devices tested the internal Φ_{ECL} should be ~ 4.5%. **Figures 2.4-2.6** present data obtained from this most efficient device.

Figure 2.4 is a plot of the current density (mA/cm^2) and light intensity (mW) versus bias voltage. In **Figure 2.5,** external Φ_{ECL} is plotted vs bias voltage, as calculated from the data shown in **Figure 2.4**. As is evident from this data, both the emission intensity and current increase approximately monotonically with bias voltage above ~ 2.5 V. The quantum efficiency is maximized at ~ 5 V and decreases slightly at higher bias voltages. When these devices are operated at bias voltages $\geq$ 10 V there is a

noticeable decay of emission with time that accelerates as the voltage is increased. Presumably this decay at high drive voltages is due to damage caused to the polymer film at higher current densities, likely by the buildup of heat in the **P2** film itself and/or at the electrode interfaces.

Figure 2.6 depicts a plot of emission intensity and current density vs time (for the same device examined in the two previous figures) after removing the bias for 5 minutes and then reapplying a 5 V bias at t = 0. After roughly 2 minutes the current and emission recovered and reached steady values that exhibited minimal decay after approximately 9 minutes of operation. This result also serves to illustrate that, at room temperature, there is very limited counter ion mobility within this material when dry. For example, once the redox concentration gradient is established in a swollen film and the polymer dried, the bias voltage can be removed and reapplied after ~ 24 hours and visible ECL emission typically reappears within 5-10 minutes.

The considerable variability in the ECL efficiency of these cells from one device to another most certainly arises from their rather primitive design and construction. That point notwithstanding, the performance of the most efficient device demonstrates that, at a minimum with proper engineering, internal $\Phi_{ECL} > 4\%$ are attainable with **P2** polymers. Moreover, it is unlikely that the specific result reported herein represents the maximum efficiency possible from an optimized device based on this polymer system, but rather a lower limit to what might be possible.

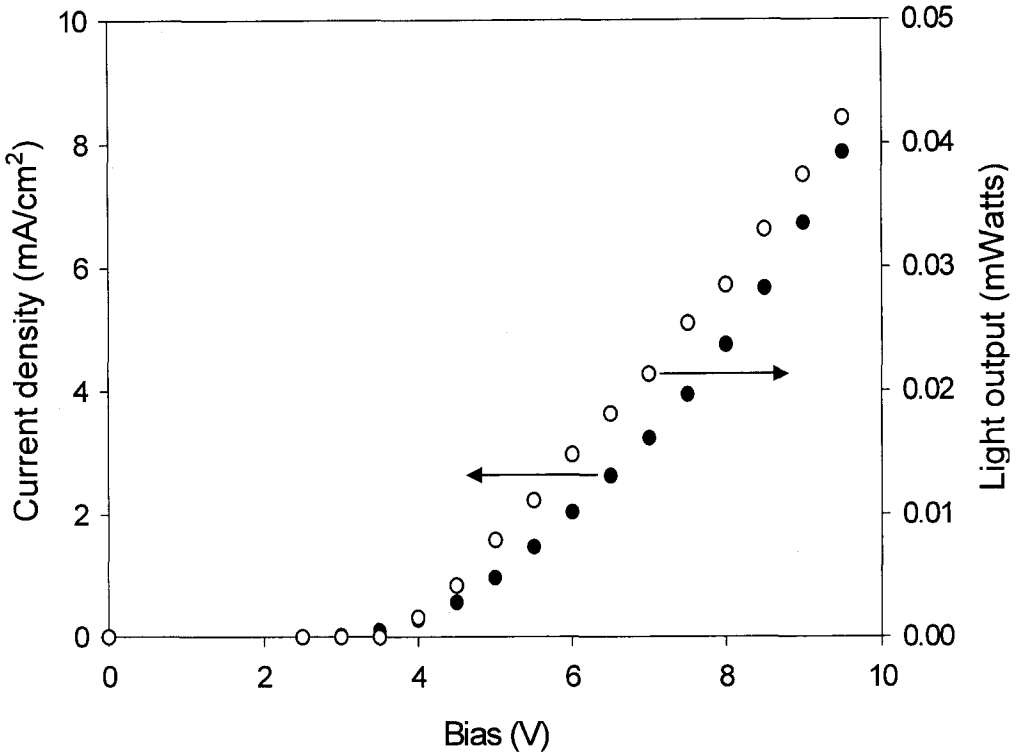

Figure 2.4: Performance data for an ECL sandwich device composed of a **P2** polymer film. Current density (closed circles) and light output (open circles) vs voltage.

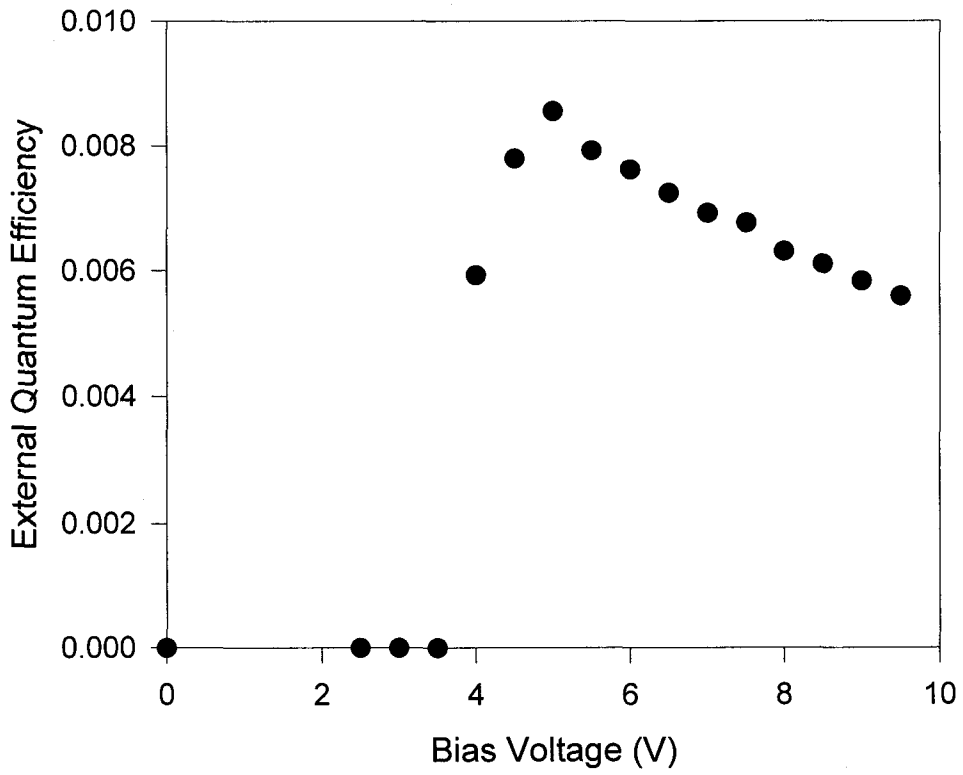

Figure 2.5: External Φ_{ECL} vs V for the same device as the above figure.

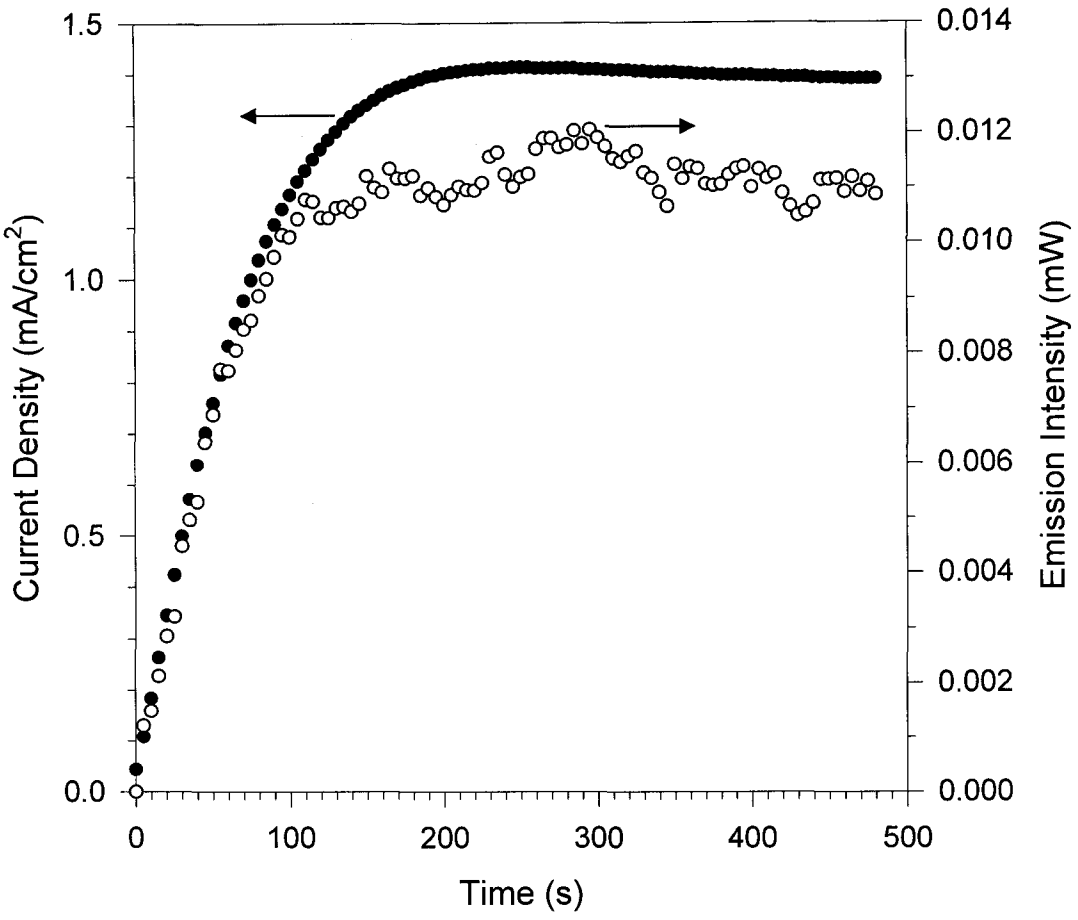

Figure 2.6: Current density (closed circles) and Intensity (open) vs time for a reused ECL device.

Finally, the mechanism by which charge is injected into **P2** is entirely electrochemical—it is as defined above, a "pure" ECL system. As such, the number of oxidized charge carriers ($[Ru(LL)_3]^{3+}$, "holes") and reduced charge carriers ($[Ru(LL)_3]^{1+}$, "electrons") injected per unit time must exactly match. Therefore, were it not for nonradiative processes, the material should exhibit a 100% ECL quantum efficiency (i.e., one photon/electron). In contrast, for polymeric and molecular electroluminescent materials such as poly-*p*-phenylenevinylene and tris(8-hydroxyquinoline)aluminum(III), charge injection is non-electrochemical.[15-18] For this reason in EL systems there is no a

priori requirement that the flux of holes and electrons match. Here the minority carriers are the "limiting reagent" in the light emitting reaction and their flux determines the maximum number of excited states generated per unit current.[19,20] Nonradiative processes notwithstanding, pure ECL systems should, in principle, be inherently more efficient than pure EL systems. In practice, prior to the present study, $Ru(LL)_3$-based pure ECL materials have not exhibited efficiencies that compare favorably with the better EL materials. Recently several reports have appeared on $Ru(LL)_3$-based materials which exhibit mixed modes of charge injection.[6,7] These materials have characteristics intermediate between those of either pure-mode materials (i.e., ECL and EL). In several instances *very* high external quantum efficiencies (1-3%) were reported.[6] These results are truly remarkable in that, in some instances at least, the internal electroluminescent quantum yields implied by the reported external quantum yields[14] significantly exceed the solution photoluminescence quantum yields for the same lumophore.[6]

Conclusion

By rational design of $[Ru(LL)_3]^{2+}$ complexes it is possible to enhance the properties of interest, including intensity of ECL emission. Furthermore, it has been demonstrated that the addition of active functions such as polymerizable groups spatially *distant* from the bipyridine moieties does not significantly alter the behavior of the parent metal complex. Finally, solid state devices retaining the intended properties found in the solution state can be fabricated from such specifically designed compounds, as has been done here employing **P2** films. These devices are capable of ECL efficiencies (greater than 4%) that are comparable with the best polymer-based light emitting devices known

to date[21,22] and considerably better than other ECL devices based on $Ru(LL)_3$ reported thus far. Quantitative stability testing of the devices in operation has been encouraging on the time scale of 10 minutes. At the same time, in observations with the naked eye the light emission of these devices has been greatly lowered (or even completely quenched) over the course of several hours. Long term stability in general is a common problem in ECL devices,[19] and one which must be addressed in order to produce real displays from this technology.

REFERENCES

(1) Juris, A.; Balzani, V.; Barigelletti, F.; Campagna, S.; Belser, P.; VonZelemsky, A. *Coord. Chem. Rev.* **1988**, *84*, 85.

(2) Wallace, W. L.; Bard, A. J. *J. Phys. Chem.* **1979**, *83*, 1350.

(3) Glass, R. S.; Faulkner, L. R. *J. Phys. Chem.* **1981**, *85*, 1160.

(4) Abruna, H. D.; Bard, A. J. *J. Am. Chem. Soc.* **1982**, *104*, 2641.

(5) Maness, K. M.; Terrill, R. H.; Meyer, T. J.; Murray, R. W.; Wightman, R. M. *J. Am. Chem. Soc.* **1996**, *118*, 10609.

(6) Lee, J. K.; Yoo, D.; Rubner, M. F. *Chem. Mat.* **1997**, *9*, 1710.

(7) Lee, J. K.; Yoo, D.; Handy, E.; Rubner, M. F. *Appl. Phys. Lett.* **1996**, *69*, 1686.

(8) Maness, K. M.; Masui, H.; Wightman, R. M.; Murray, R. W. *J. Am. Chem. Soc.* **1997**, *119*, 3987.

(9) Wacholtz, W. F.; Auerbach, R. A.; Schmehl, R. S. *Inorg. Chem.* **1986**, *25*, 227.

(10) Elliott, C. M.; Herschenhart, E. J. *J. Am. Chem. Soc.* **1982**, *104*, 7519.

(11) Oki, A. R.; Morgan, R. J. *Synth. Comm.* **1995**, *25*, 4093.

(12) Evans, J. P.; Spence, A.; Wilkenson, G. *J. Chem. Soc., Dalton Trans.: Inorg. Chem.* **1973**, *2*, 204.

(13) Elliott, C. M.; Freitag, R. A.; Blaney, D. B. *J. Am. Chem. Soc.* **1985**, *107*, 4647.

(14) Greenham, N. C.; Friend, R. H.; Bradley, D. *Adv. Mat.* **1994**, *6*, 491.

(15) Burroughs, J. H.; Bradley, D. D. C.; Brown, A. R.; Marks, R. N.; Mackay, K.; Friend, R. H.; Burns, P. L.; Holmes, A. B. *Nature* **1990**, *347*, 539.

(16) Gustafsson, G.; Cao, Y.; Treacy, G. M.; Klavetter, F.; Colaneri; Heeger, A. J. *Nature* **1992**, *357*, 472.

(17) Tang, C. W.; VanSlyke, S. A. *Appl. Phys. Lett.* **1987**, *51*, 913.

(18) Tang, C. W.; VanSlyke, S. A.; Chen, C. H. *J. Appl. Phys.* **1989**, *65*, 3610.

(19) Sheats, J. R.; Antoniadis, H.; Hueschen, M.; Leonard, W.; Miller, J.; Moon, R.; Roitman, D.; Stocking, A. *Science* **1996**, *273*, 884.

(20) Parker, I. D. *J. Appl. Phys.* **1994**, *75*, 1656.

(21) Yu, G. *Synth. Met.* **1996**, *80*, 143.

(22) Cao, Y.; G.Yu; Heeger, A. J.; Yong, C. Y. *Appl. Phys. Lett.* **1996**, *68*, 3218.

CHAPTER THREE

TERVALENT CONDUCTING POLYMERS WITH TUNABLE WORK FUNCTIONS: PREPARATION, CHARACTERIZATION, AND USE IN ELECTROLUMINESCENT DEVICES

A portion of the material presented in this chapter was published in

The Journal of the American Chemical Society, **2001**, *123*, 9436-9442.

I. Introduction:

Organic light emitting devices that operate via an EL mechanism are in some ways similar to ECL systems but have a different set of considerations shaping device design and construction.[1] These requirements provide a different set of constraints for organic emitting materials, as well as conductors employed as cathodes and anodes. While many different OLED designs have been examined, all are essentially variations on a theme. Again, these devices typically consist of one or more organic semiconductors, situated between a low work function metal cathode such as magnesium or calcium and a higher work function anode, often the transparent conducting oxide ITO.[1-3] When a sufficient potential bias is applied across the electrodes, electrons are injected from the cathode into the conduction band of the luminescent layer and holes are injected from the anode into the valence band. Depending on the chemical makeup of the material in question, it might be more appropriate to describe the injection of electrons and holes as being into LUMO's and HOMO's, respectively.[4] Also, charge carrier injection might or might not be directly from the respective electrode into the bands of the luminescent layer, again depending on the construction of the particular device under consideration. Layers of non-luminescent materials functioning for charge transport and other considerations are often employed to improve device performance.[2] Specific organic materials and device architectures will be discussed in detail below.

Following injection and driven by the potential field (rather than a concentration gradient as in an ECL device), electrons and holes migrate towards the center of the organic film, where they meet to form an exciton, or electron-hole pair. For polymer-

based systems, the exciton is generally delocalized to an extent dependent on the chemical structure of the polymer as well as the method of film deposition.[5-7] Several events are possible following the formation of the exciton. Because excitons in these materials are usually relatively long-lived, they may diffuse away from their origin.[8] When this occurs, if the exciton encounters defects or other quenchers including the electrodes, non-radiative recombination is likely to occur.[1,3,5,9] The goal in an OLED is of course light emission, and in a well-designed device there is a reasonably high probability of radiative recombination as the exciton decays back to the ground state. When this occurs, photons of an energy determined by the band gap (or HOMO/LUMO gap, as the case may be) are produced.

The number of charge carriers injected from the two electrodes is generally not equal. In this case, the current passed through the film is determined by the sum of majority and minority carriers, while the emission of light is limited by the minority carriers.[9] Optimum emission efficiency is thus obtained when the rates of hole and electron injection are matched. The exact mechanism whereby charge injection occurs is a matter of some controversy and, indeed, may vary for different materials and device construction motifs.[4,9] That point notwithstanding, there is at least an empirical relationship between the rates of charge carrier injection and the proximity of the Fermi level energies of the respective electrode to the energy of the band (or orbital) into which charge is injected. In other words, the Fermi energy of the anode should match the valence band energy while the Fermi energy of the cathode should match the conduction band energy.[1]

The simplest class of OLEDs are those composed of a single polymer layer between the two electrodes. Early work in this area focused on the conjugated polymer poly-*p*-phenylene vinylene (PPV, see **Figure 3.1**) as the EL material.[3] PPV is rather unwieldy for use in an OLED however, owing to very limited solubility in organic solvents. For this reason, PPV-based devices must be constructed using a precursor compound that can be deposited on a conductive substrate and subsequently treated to yield the desired EL polymer. On the other hand, the alkoxy-substituted analogue of PPV poly[(2-methoxy-5-(2'-ethylhexyloxy)-1,4-phenylenevinylene], also shown in **Figure 3.1** and generally referred to as MEH-PPV, is more easily employed as an EL material and has been widely utilized in EL devices.[3,9-13] More recently, structurally related polymers have been reported such as the alkoxyphenyl-substituted PPV known as BEHP-PPV.[5]

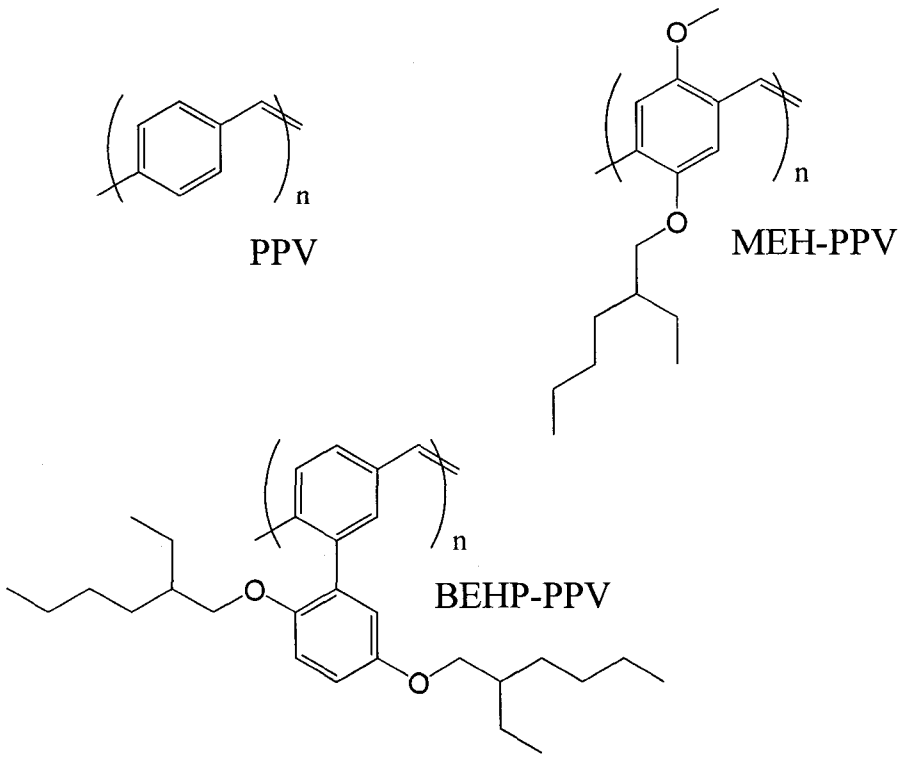

Figure 3.1: Structure of EL polymers PPV, MEH-PPV, and BEHP-PPV.

These substituted PPV polymers, which are soluble in organic solvents such as xylene, are typically spin coated onto an ITO substrate and a thin layer of a low work function metal is then deposited on top to act as the cathode. For MEH-PPV, the work functions of both the ITO anode and calcium cathode match up very well to the respective bands in the polymer. In the case of the cathode, the work function of calcium is 2.9 eV while the conduction band of MEH-PPV lies 2.8 eV below the vacuum level.[9] Theoretically then, this junction should be very close to ideal in terms of the relevant energy match; however, studies have indicated several complications. Localized destructive heating,[3] oxide layer buildup, and calcium doping into the polymer[11] are a few experimentally proven examples.

Following the pioneering work of Tang and VanSlyke,[2] an alternate approach in constructing OLED's employs small molecule organic compounds as EL materials in combination with one or more layers of charge transport materials.[1,2,4,8,13-15] A common system uses tris(8-hydroxyquinoline) aluminum(III) complex (Alq_3, as in **Figure 3.2**), applied via thermal vapor deposition, as both the EL and electron transport material. Because Alq_3 does not efficiently conduct holes,[2,8] an additional "hole transport material" layer is deposited between the anode and the EL layer. These materials are usually triarylamine based compounds such as N,N'-bis(3-methylphenyl)-N,N'-diphenylbenzidine (TPD, see **Figure 3.2**).[4] This multilayer architecture also has the advantage of producing excitons near the interface of the two organic films, thus relatively far away from the electrodes that could potentially quench emission. A typical literature device would thus consist of layers as follows: ITO anode/TPD/Alq_3/Metal cathode.[1] As with the polymer-

based devices, oxide buildup, degradation of the Alq_3, and other problems have been observed at the metal/organic interface.[15,16]

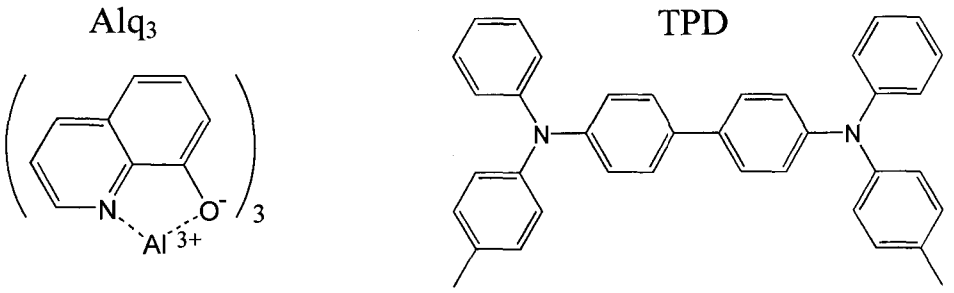

Figure 3.2: Structures of OLED materials Alq_3 and TPD.

Given these documented problems, replacing the metal cathodes in OLEDs with conducting polymers possessing equivalently low work functions might offer some significant advantages in device performance. First, a polymer-EL organic junction should be more compatible from a materials perspective. Second, impurities, oxides, or other degradation products would not necessarily be confined to the interface as they no doubt are with a metal contact. Finally, higher quantum efficiencies and/or longer lifetimes could result from increased stability imparted by such a more compatible junction.

In previous work, it has been demonstrated that $Ru(LL)_3$-based redox polymers similar to **P2** (which was employed as the emissive layer in the ECL device in **Chapter 2**) can be made much more conductive than polymers of the same chemical makeup but other redox compositions by careful electrochemical treatment.[17,18] In a procedure described in detail below, the polymer is electrochemically reduced such that the net charge of the film is zero, and all counterions have exited the polymer. Following the reduction, not only does the redox polymer become an effective conductor, but the E_F is

significantly raised to yield a low Φ conductor. The preparation of two additional redox polymers similar in structure to **P2** is described below. After electrochemical treatment, all three reduced polymers possess work functions that can be accurately predicted from the solution electrochemistry of the corresponding monomer and verified by ultraviolet photoelectron spectroscopy (UPS) on the polymers. Furthermore, by making appropriate synthetic modifications to the monomer, it is possible to "tune" polymer work functions in a predictable way. Specifically, the work functions of the specific polymers under consideration herein span from 3.7 to 3.0 eV. The lower end of this range matches the work function of many of the metals commonly used as cathodes in OLED's. This lowest work function polymer is successfully used to construct working devices based alternately on Alq_3 or BEHP-PPV as EL materials.

II. Experimental:

Chemicals.

Acetonitrile was Aldrich Optima grade, stored over 4Å molecular sieves and distilled over calcium hydride. Tetra-hydrofuran (THF) from Aldrich was freshly distilled under N_2 from sodium and benzophenone. Ammonium hexafluorophosphate ($NH_4^+PF_6^-$) was purchased from Elf Atochem. Other electrolytes, tetra-*n*-butylammonium hexafluorophosphate ($TBA^+PF_6^-$) and poly(diallyldimethylammonium hexafluorophosphate), $PDDA^+PF_6^-$, were prepared as described elsewhere.[19] 4,4′-Dimethyl-2,2′-bipyridine (DMB) was obtained from Reilly Industries and was recrystallized from ethyl acetate and dried under vacuum at room temperature for 12 hours prior to use. The EL material Alq_3 along with TPD were purchased from Aldrich

and purified by vacuum train sublimation with argon gas flow at 330°C and 250 °C, respectively. 3,4,9,10-perylenetetracarboxylic dianhydride (PTCDA, **Figure 3.3**) from Aldrich was used without further purification. BEHP-PPV was purchased from Aldrich and used as supplied.

PTCDA

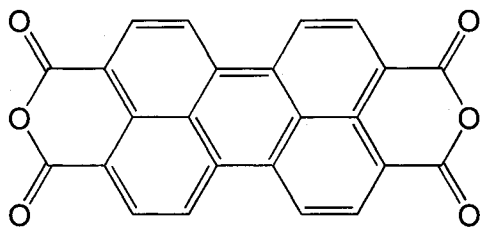

Figure 3.3: Structure of protective cap layer material PTCDA.

Synthesis of monomers M1 (Figure 3.4) and M2 (Figure 2.1):

The structure and synthesis of monomer **M2** is found in **Chapter 2**, and monomer **M1** was synthesized as previously reported in the literature.[19]

Synthesis of monomer M3 (Figure 3.4):

4,4′-Bis-(5-bromo-pentyl)-2,2′-bipyridine (**1**) All glassware was dried in a 150°C oven and cooled under N_2 flow. The reaction and all transfers were performed under N_2 and the reaction vessel cooled with dry ice/acetone at all times. 30 mL of dry THF was placed in a 1L 3 neck flask and cooled 30 min. Diisopropylamine (Aldrich) was filtered over neutral Al_2O_3 and purged with N_2 for 15 min. 7.80 mL (0.056 moles) of diisopropylamine was added by syringe into THF and cooled. 28.0 mL of *n*-butyllithium solution (2.0 M in cyclohexane, 0.056 moles) was slowly added via syringe and allowed to cool. 5.01 g of DMB (0.0273 moles) was dissolved in 350 mL of dry THF and placed in a 500 mL dropping funnel. The DMB solution was added dropwise with stirring over the course of 25 minutes, yielding a very dark red solution. After 2 hours, 13.0 mL of 1,4-

dibromobutane (Aldrich, N_2 purged for 15 min.) was added via syringe, following which the color slowly changed to turquoise. The reaction was cooled for 2 hours more and left under N_2 to warm slowly to room temperature. After 12 hours, 200 mL of deionized water was added to give a cloudy, slightly yellow mixture. Volatile organics were removed by rotoevaporation and the aqueous layer was extracted 4 times with ca. 200 mL CH_2Cl_2. Organic fractions were combined and dried over Na_2SO_4. The product **1** was purified by column chromatography with gradient CH_2Cl_2/acetone elution over flash silica gel.

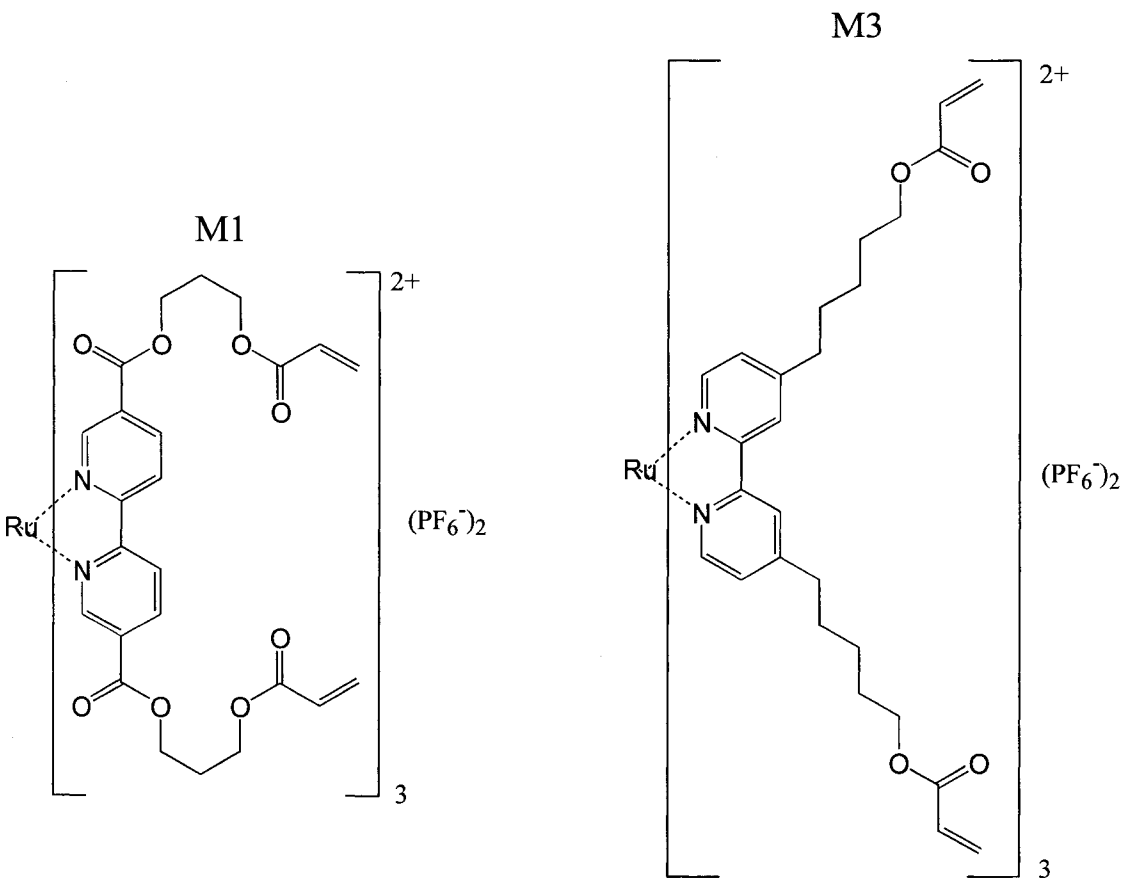

Figure 3.4: Structures of monomers **M1** and **M3** The structure of **M2** is depicted in **Figure 2.1**.

Acetic acid 5-[4′-(5-acetoxy-pentyl)-2,2′-bipyridinyl-4-yl]-pentyl ester (**2**). 500 mg of **1** was added to a solution of 200 mg sodium acetate (Aldrich) in 30 mL glacial acetic acid (Malinkrodt). The mixture was refluxed for 72 hours under N_2 and neutralized to pH 6, at which time **2** precipitated.

5-[4′-(5-Hydroxy-pentyl)-2,2′-bipyridinyl-4-yl]-pentan-1-ol (**3**): The crude product from the preparation of **2** was added to excess KOH in 250 mL of 95% ethanol. The solution was refluxed 12 hours under N_2. Following neutralization with dilute acetic acid, ethanol was removed by rotoevaporation, and **3** precipitated. The desired product was purified by column chromatography with gradient CH_2Cl_2/acetone elution.

Acrylic acid 5-[4′-(5-acryloyloxy-pentyl)-2,2′-bipyridinyl-4-yl]-pentyl ester (**4**). 300 mg of **3** was placed in 200 mL CH_3CN. 8 mL of acryloyl chloride (Aldrich) was added and solution refluxed for 6 hours under N_2. After rotoevaporation of the solvent, a brownish sludge remained, smelling strongly of acryloyl chloride. 150 mL of a 2% aqueous triethylamine solution was added, and extracted 4 times with 150 mL of CH_2Cl_2. Fractions were combined, dried, and purified in the same manner as product **1**. Overall yield of a colorless, greasy solid was approx. 10%. ^{1}H NMR in CD_3Cl (δ in ppm, multiplicity, integration); 1.4(p, 4H); 1.7(m, 8H); 2.7(t, 4H); 5.9(d of d, 2H); 6.2(m, 2H); 6.4(d of d, 2H); 7.2(d of d, 2H); 8.3(s, 2H); 8.6(d, 2H).

Tris-[acrylic acid 5-[4′-(5-acryloyloxy-pentyl)-2,2′-bipyridinyl-4-yl]-pentyl ester]ruthenium(II) hexaflourophosphate (**M3**). 4 mole equivalents of **4** (typically ≈150mg) was dissolved in absolute ethanol (50 mL). 1 mole equivalent (≈50 mg) of $Ru(DMSO)_4Cl_2$ was dissolved in 10 mL deionized water. The light yellow aqueous solution was added to the ligand solution, which quickly turned orange. The solution was

refluxed 2 hours under N_2. Solvent was rotoevaporated and H_2O added to 100 mL total volume. Excess (≈400mg) $NH_4^+PF_6^-$ was added, and an orange precipitate formed immediately. The solid was filtered, washed with water, and dissolved in CH_3CN. Solvent was evaporated to a small volume and the complex was precipitated again by addition of diethyl ether. The product was again filtered, washed with ether, twice with H_2O, redissolved in acetonitrile, and dried over Na_2SO_4. The product was purified by column chromatography over flash silica with gradient elution from 1:1 CH_3CN: H_2O to 50: 49:1 CH_3CN: H_2O: sat. aq. KNO_3. Yield of orange, oily solid approx. 70%. ^1H NMR in CD_3CN (δ in ppm, multiplicity, integration); 1.4(p, 4H); 1.7(m, 8H); 2.7(t, 4H); 5.9(d of d, 2H); 6.2(m, 2H); 6.4(d of d, 2H); 7.3(d, 2H); 7.7(m, 2H); 8.5(d, 2H).

Polymerization of monomers:

Thin films of **M1, M2** or **M3** can be cast in a variety of ways and polymerized either thermally or photochemically, producing the corresponding respective polymers **P1, P2,** and **P3.** In all of the work discussed herein, polymerization was effected thermally at 150°C. The exact polymerization conditions varied depending on the film thickness, the substrate material, whether polymerized in air or under inert atmosphere, etc. Detailed descriptions of the polymerization conditions for each experiment are provided below. Generally speaking, films reach the desired degree of polymerization more quickly in the absence of oxygen than in its presence, and more quickly on platinum than on ITO or glassy carbon. The addition of a radical initiator speeds the process but is not necessary and was not employed in the films discussed here. Films of the monomers and resulting polymers are flat, glassy and appear to be amorphous. Inspection visually,

by optical microscope, and by scanning electron microscopy does not reveal any secondary structure.

Electrochemistry:

Preparation of materials for electrochemical prediction of Fermi level energies. Monomer films approximately 400 nm thick (Sloan DekTak profilometer) were drop coated from acetonitrile on a polished and cleaned glassy carbon electrode, polymerized approximately 6 hours at 150°C, and washed with CH_3CN. Cyclic voltammetry was performed in a Luggin capillary cell with Ag/Ag^+ 0.1 M in DMSO reference (+0.41 V vs NHE), Pt wire counter, and 0.1 M $TBA^+PF_6^-$ in acetonitrile electrolyte. Scan rates were 50 mV/sec or 100 mV/sec. Electronics consisted of P.A.R. model 173 Potentiostat and model 175 Programmer with output to Yokogawa X/Y recorder.

Preparation of materials for UPS spectroscopy. Thinner films of the monomer (approx. 100 nm) were drop coated from CH_3CN on an ultrahigh vacuum (UHV) sample plate covered by Pt foil (previously flame cleaned and sonicated in absolute ethanol) and polymerized for 2 to 3 hours at 150°C. Samples were then introduced into a N_2 glove box and washed with CH_3CN. Alternately, the samples can be coated and polymerized entirely inside the box. Electrochemical reduction was done in a glass vial cell using the same conditions as above, but with a 0.05 M solution of the polymeric electrolyte $PDDA^+PF_6^-$ in acetonitrile. The polymer coated working electrode (WE) was scanned only in the reductive direction at 2 mV/sec to approximately 300 mV past the second reduction wave (for example, **P3** film scanned to -2.1 V). The potential was held for 30-60 seconds before disconnecting the WE. Upon reduction, all three films exhibit modest but quite obvious color changes. Samples were washed 3 times in clean CH_3CN and

placed behind the gate valve inside a UHV transfer rod. The gate valve was closed while still inside the glove box before removing the transfer assembly.

UPS Studies:

All UPS data were collected in an Omicron multiprobe UHV chamber (base pressure $5*10^{-11}$ torr) equipped with a VSW EA125 single channel analyzer. The transfer rod assembly was affixed to the entry chamber and pumped down to vacuum prior to introducing the samples into the analysis chamber. A helium lamp was used as the UV light source, providing a HeI line at 21.22 eV and a HeII line at 40.81 eV. A -5.00 V bias was applied to the samples to separate the sample and spectrometer high binding energy cutoffs. Kinetic energy analysis of electrons emitted normal to the sample was done using a 10 eV pass energy. The spectrometer was calibrated with an Ar^+ ion sputtered copper standard.

A straight line was fit on the secondary edge of the UPS HeI spectra. The intercept of this line with the abcissa determines the high binding energy cutoff (HBEC). A value of 0.1 eV was subtracted from the HBEC to correct for spectrum broadening due to thermal and analyzer effects.[16] The work function was determined by subtracting this value from the source energy of 21.22 eV.

OLED Construction:

An acetonitrile solution of **M3** was spin cast on a patterned ITO substrate. The homemade spin caster consisted of an Oster variable speed blender with a modified base peg such that flat substrates could be attached with double stick tape. The lowest blender speed is 4000 rpm; in order to achieve slower rates a variac was used. Films for devices were cast inside the glove box at about 2000 rpm using this method. While still in the

glove box, films were polymerized for 3 hours at 150 C, rinsed, and electrochemically reduced. Samples were then placed inside the vacuum deposition chamber (Denton DV502A turbo model) which is directly interfaced to the box. At pressures below $6 \cdot 10^{-6}$ torr, the organic materials and covering metal were sequentially thermally deposited. Thickness of Alq_3 and TPD layers were approximately 450 Å while the gold anode layer was about 800 Å, as measured by Leybold Inficon quartz crystal microbalance and XTM-2 Deposition Monitor. In OLEDs employing PTCDA, the protective cap layer was approximately 50 Å in thickness. For EL devices employing the light-emitting polymer BEHP-PPV, a film of **M3** was polymerized, electrochemically reduced, and cleaned in the same manner as above. A thin film of BEHP-PPV was then deposited by spin coating from a saturated (~1% by weight) solution in THF, followed by vapor deposition of a gold anode. In all cases, device testing was done using the electrochemical instrumentation described above, with an added simple external circuit (shown in **Figure 3.5**) to provide 3x multiplication of voltage output from the potentiostat. Light output was measured with a Hamamatsu photomultiplier tube (PMT) driven at 400 V to 800 V.

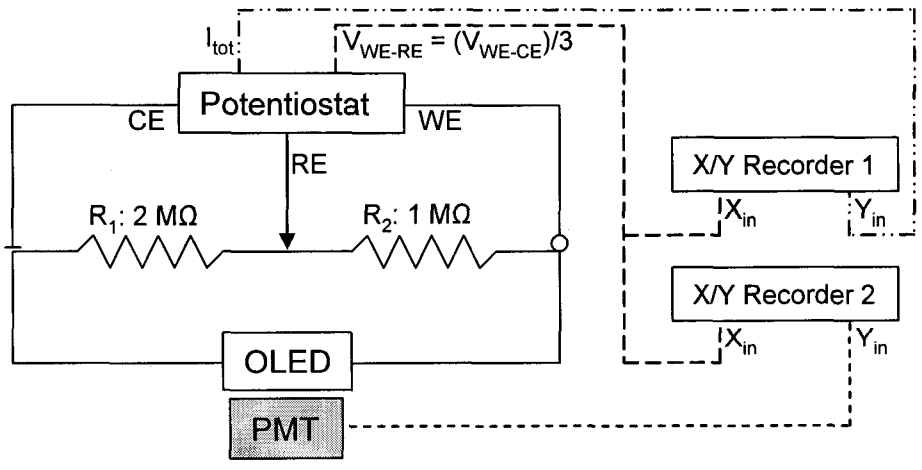

Figure 3.5: Diagram of the apparatus used to measure I/V and light/V data for OLEDs. The circuit is designed such that resistances $R_1 + R_2 >> R_{OLED}$, thus $I_{tot} \sim I_{OLED}$.

III. Background and Theory:

General considerations. Under the conditions used to form polymers **P1, P2** and **P3**, it can be estimated from earlier IR studies that, on average, approximately 1-1.5 of the six total acrylate groups per monomer are consumed in the polymerization process—the remainder are unchanged.[20] At this level of crosslinking, the polymers swell in contact with most electrochemical solvents. Standard electrolyte ions (e.g., TMA^+ or PF_6^-) can freely move between the polymer and solution during electrochemical changes in oxidation state. The concentration of $[Ru(LL)_3]^{2+}$ redox sites is estimated to be between 1.5 and 3.0 M. Spectral and electrochemical data show no indication of strong site-site interactions; consequently, it is assumed that the mechanism of electron transport through the polymer is by electron hopping from one localized site to another.

Up to this point, consideration of a $[Ru(LL)_3]^n$-based polymer has been limited to the formal Ru(III) and Ru(II) oxidation states. As previously discussed, in this case several generalizations can be made about the conductivity of these films. When a $[Ru(LL)_3]^n$ polymer is sandwiched between two metallic contacts, it will have measurable electronic conductivity only when mixed valent in the usual sense (i.e., when n is a non-integer). Furthermore, if the counterions present in the polymer are mobile, redox state gradients will form under an applied potential.[21] Even when the counterions have limited local mobility, as in a dry film at low temperature, mixed-valent materials of this sort are still semiconductors. In this case the oxidation state gradients are simply prevented from forming.[22] Finally, since the metal-based redox couple is well separated from other redox processes in the polymer (by ≥ 2.4 V), the only necessary criterion for

determining mixed valency is the value of *n* (i.e., whether it is 3, 2 or something in between).

When consideration is expanded to encompass other $[Ru(LL)_3]^n$ oxidation states, the situation with regard to conductivity becomes more complex. When the difference between the apparent standard potentials for two redox processes approaches RT/nF, integer values of *n* can no longer be used to establish single valency. *Irrespective of the value of n*, pure single oxidation states at the molecular level can no longer exist due to disproportionation. The value of *n* thus reflects only the average charge per redox site and not the actual molecular-level site-valency. For **P1-P3,** the ligand based redox potentials are such that these materials are significantly mixed-valent, and thus conductive, over the entire potential range spanning from the 2+/1+ to the 3-/4- formal redox couples.

In order to more quantitatively expand the preceding discussion it is useful to consider a simplified system consisting of a hypothetical polymer having only two redox processes. For the sake of illustration these two redox processes will be assumed to involve 1+/0 and 0/1- couples having a separation in formal potential, ΔE_o, of 0.140 volts.

$$\Delta E_o = E_o(1+/0) - E_o(0/1-) \qquad (1)$$

The Nernst equation (2), where [*red*] and [*ox*] are the concentrations of the reduced and oxidized forms of a couple, can be used to predict the redox composition of this polymer, which can in turn be mapped as a function of potential.

$$E = E^o - RT/nF \ln\left([red]/[ox]\right) \qquad (2)$$

Figure 3.6 is a plot of the concentration of each oxidation state (normalized for the concentration of total redox sites in the polymer) vs. potential. The potential axis lacks specific voltage values because it represents a generic example; however, the separation between the two E_o corresponds to 0.140 volts. Because the system has been restricted to three formal oxidation states, at potentials significantly more positive than $E_o(1+/0)$ or significantly more negative than $E_o(0/1-)$ the polymer would be essentially monovalent (either 1+ or 1-, respectively) and, therefore not electronically conductive. In contrast, when the applied potential is precisely midway between the two E_o's,

$$E_{(0,max)} = [E_o(1+/0) + E_o(0/1-)]/2 \qquad (3)$$

the net charge on the fixed redox sites is zero ($n = 0$); but, because of significant disproportionation, the material is mixed-valent and should be conductive.

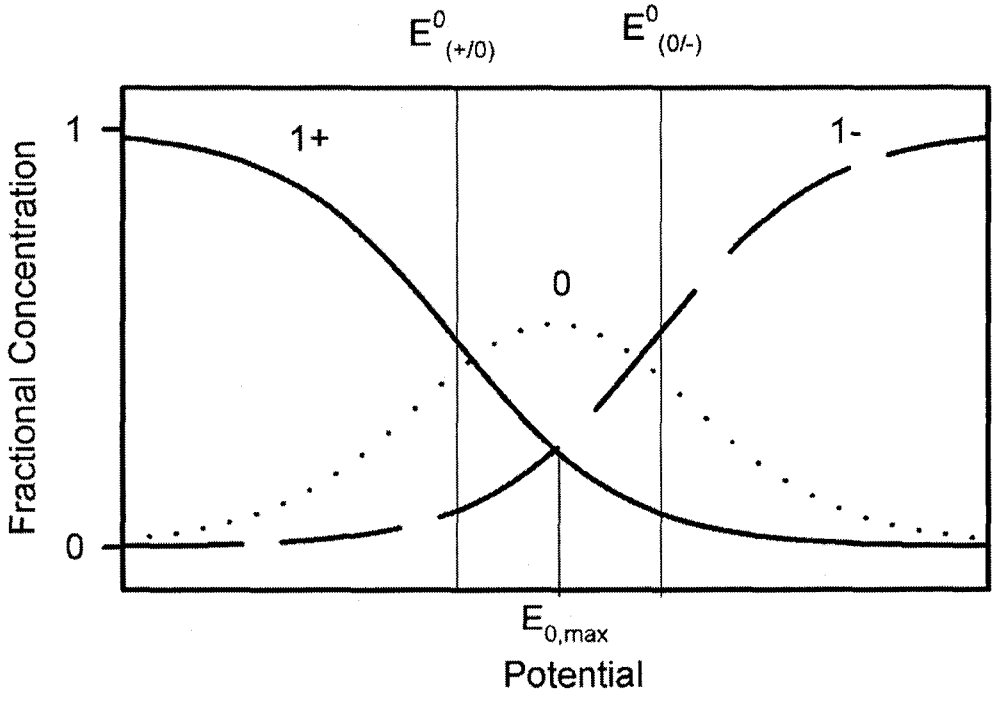

Figure 3.6: Normalized concentration vs potential at room temperature in a redox polymer system with two couples separated by 140 mV, as determined by the Nernst equation.

Up to this point nothing considered has been unique to the case of $n = 0$. An otherwise identical polymer having any three formal oxidation states (m, m-1, and m-2) would produce exactly the same type of composition vs potential distribution as illustrated in **Figure 3.6**. The unique consequence of having $n = 0$ is that the polymer requires *no* physically mobile counterions to maintain charge balance. Since redox sites with 1+ and 1- charges are mutually compensating, other counterions are not necessary. As a result, redox gradients are not possible because charge neutrality requires that [1+] = [1-] at every point within the polymer. Electron-hopping conduction can still occur by electron exchange between 0/1+ and 1-/0 sites, but the redox composition must remain uniform throughout the polymer.

Polymers formed from $[Ru(LL)_3]^{2+}X^-_2$ complexes have considerably more complex redox chemistry than the hypothetical example just discussed. Irrespective of that complexity, they all have in common with the example polymer stable and accessible 1+, 0 and 1- formal oxidation states. Moreover, the separation in potential, ΔE_o in equation 1, for each polymer is small enough that there is substantial tervalent character to the formal zero-valent form. Before considering how these zero-valent materials can be formed, a few more theoretical and practical points are worthy of consideration. First, there are certain ways in which these neutrally charged tervalent materials are conceptually analogous to intrinsic semiconductors. The HOMO of the redox sites is analogous to the valence band and the LUMO to the conduction band. The HOMO-LUMO energy separation, which again is ΔE_o as defined in equation 1, is the analogue of the bandgap. The 1+ and 1- sites are, respectively, analogous to thermally generated holes and electrons. A major difference is that the HOMO's and LUMO's of redox sites

in these $[Ru(LL)_3]^n$-based polymers are highly localized; in semiconductor parlance this would correspond to very narrow bandwidths with relatively immobile charge carriers. At the same time, the band gap analog ΔE_o is small; therefore, the relatively low charge carrier mobility is largely offset by the fact that the charge carrier concentrations are approaching 0.1 M at room temperature.

As in any electron-hopping polymer, electron transport in **P1-P3** is an activated process, as discussed above. In a mixed-valent polymer containing electroinactive counterions, a majority of that activation energy (E_a) can come from the need for local motions of these counterions. For the zero-valent form of these polymers, both 1+ and 1- sites are mobile by electron hopping. Experimentally, the absolute conductivities of these polymers are much larger when $n = 0$ than when it has any other value.[17]

The validity of a small bandgap intrinsic semiconductor model for these reduced polymers is further illustrated by examining the temperature dependence of the conductivity (σ). For charge carriers produced in a traditional intrinsic semiconductor by thermal excitation over the energy gap (E_g), the following simple relation holds (where k_B is the Boltzmann constant, T is the temperature in Kelvin, and σ_o is a constant).[23]

$$\sigma = \sigma_o e^{-E_g/2k_BT} \tag{4}$$

From this relation it follows that:

$$\ln\sigma = \ln\sigma_o - E_g/2k_BT \tag{5}$$

A plot of lnσ (or by extension lnR, where R is resistance) vs 1/T for a semiconductor should be linear, as was shown to be the case for a reduced film of **P1**.[18] Following the model, the value of E_g can be readily calculated from the slope of the lnσ vs 1/T plot. For the data previously obtained on **P1**,[18] such an analysis yields a calculated E_g of 0.60 eV. This is significantly larger than the ΔE_o value predicted from electrochemical data (see below), which is approximately 0.15 to 0.30 eV. This inconsistency most likely arises because the above model does not take into account activation energy for the movement of charged species from site to site.

The relationship presented in equation 4 can be expanded to include a term correcting for the activation energy of electron hopping between redox sites as follows:

$$\sigma = \sigma_o e^{-E_g/2k_BT} e^{-E_a/2k_BT} = \sigma_o e^{-(E_g+E_a)/2k_BT} \qquad (6)$$

In this case:

$$\ln\sigma = \ln\sigma_o - (E_g + E_a)/2k_BT \qquad (7)$$

From the slope of the same lnσ vs 1/T plot, the sum of E_g and E_a is now 0.60 eV. It is not possible from this model to quantitatively decouple the two variables; however, assuming an E_g between 0.15 and 0.30 eV (as predicted from cyclic voltammetry) yields E_a values of 0.30 to 0.45 eV, or 6 to 10 kcal/mole. In comparison, for the diffusion of charges in typical "mixed valent" redox systems such as polymerized films of vinylferrocene and ruthenium complexes of vinylbipyridine, (derived from chronoamperometric data at varying temperatures) E_a have been reported as 3 to 6 kcal/mole.[24,25] It is perhaps somewhat encouraging that the magnitude of E_a estimated

here is on the same order as those reported in the literature for similar systems. On the other hand, it might be expected that E_a for the specially treated "zero-valent" polymers described here would be *lower* than in other electron hopping materials, due to the absence of charged counterions. Indeed, a lower E_a for electron hopping in the reduced state vs other "mixed-valent" states *in a given polymer* seems the most likely explanation for the higher σ observed following reduction. It is possible that the apparent discrepancy arises in comparing E_a estimated for the polymers considered here to those previously reported in the literature (where the site-to-site distance is likely significantly smaller). On the other hand, this somewhat unexpected result may simply be an indication that the intrinsic semiconductor analogy presented here is a useful concept, but is not perfect.

Imperfections in the model notwithstanding, as in an intrinsic semiconductor,[23] the Fermi level energy of the zero-valent polymer should lie in the middle of the "bandgap." That energy is defined for the polymers as $E_{(0,max)}$ in equation 3. The redox processes which produce the formal 1+, 0 and 1- oxidation states (and thus define $E_{(0,max)}$) are largely ligand based states. The potentials of those processes are therefore superbly sensitive to substitutions on the bipyridine rings.[26] As a consequence, there is a huge capacity to tune those potentials, and thus the work function, by synthetic means. Ideally then, a monomer can be designed to produce a polymer with an a priori determined work function. Moreover, in general the potentials of the relevant redox processes are such that these types of conducting polymers should have relatively low work functions, in the 2.5 to 4.0 eV range.

Preparation of the zero-valent polymer. In principle it seems straightforward to electrochemically convert a poly-$[Ru(LL)_3]^{2+}$ film into its zero-valent form; in practice it is less so. Under typical electrochemical conditions, there is a single potential where n will be precisely zero. Accurately predicting this potential would require that both the 1+/0 and 0/1- redox processes be ideal. Furthermore, even if this potential could be identified, there is no certainty that the film would truly be free of redox-inactive ions. When $n = 0$ there is no *requirement* that counterions be incorporated to balance charge; however, there is also no requirement that the polymer be free of ions as long as the cation and anion concentrations are equal. Each of these problems can be avoided by employing an electrolyte solution in which the cation is polymeric.

In earlier work, it has been shown that poly(diallyldimethylammonium hexafluorophosphate), $PDDA^+PF_6^-$, can be used as a supporting electrolyte.[17] The very large $PDDA^+$ cation is completely sterically blocked from entering each of the polymers considered here; consequently, the films cannot be reduced beyond the $n = 0$ form because there are no cations in solution which can enter the film to maintain charge neutrality. Moreover, if cations cannot enter the film, it follows that the film cannot contain anions either (i.e., no salt). For this reason, cyclic voltammetry on the polymer films in a $PDDA^+PF_6^-$ electrolyte solution reveals only two possible reduction processes.[17,18] Cyclic voltammetry on **P2** films in electrolyte solutions of $PDDA^+PF_6^-$ and $TBA^+PF_6^-$, where TBA^+ is the relatively small tetrabutyl ammonium cation, along with the **M2** monomer in solution, are shown in **Figure 3.7**. It is readily apparent that in the case of the polymeric electrolyte the third and subsequent reductions are blocked.

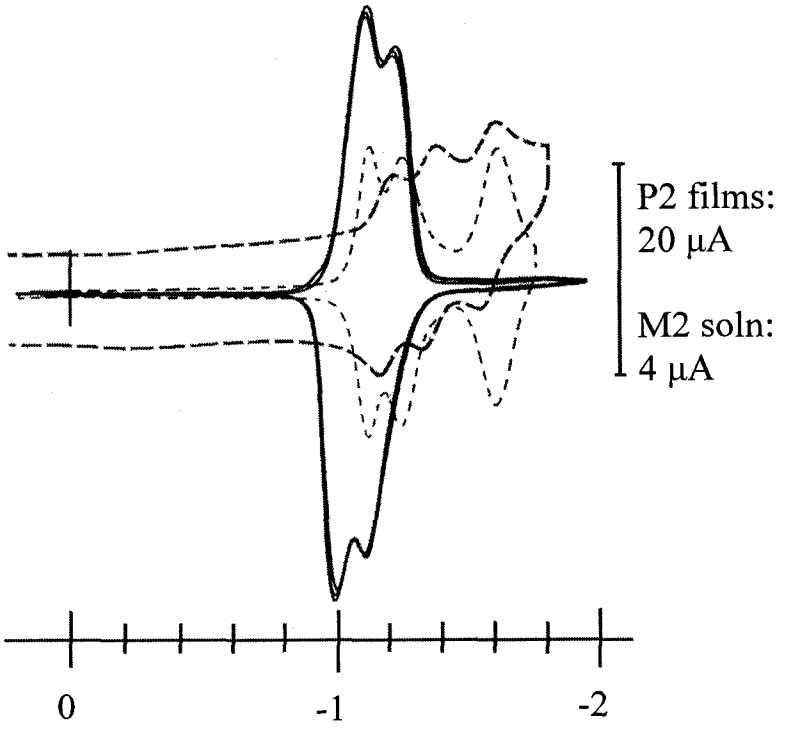

Figure 3.7: Cyclic voltammograms of **P2** films and **M2** monomer in CH_3CN.
Key: —— P2 film in $PDDA^+PF_6^-$ electrolyte; ····· P2 film in $TBA_+PF_6^-$; – – · M2 solution.
Conditions: WE: glassy C, RE: Ag/Ag^+ 0.1 M in DMSO, CE: Pt wire. Scan rate: 50 mV/sec.

Films of **P1-P3** electrochemically reduced in a solution of $PDDA^+PF_6^-$ well past $E_0(0/1-)$ will indeed have been stripped of all counter anions and will be in the $n = 0$ state, as described above. At that point, the applied potential can be removed and the film will remain in this state, provided that it does not encounter oxidizing agents. Resistivities (ρ) of such films at room temperature are on the order of 10^3 Ω·cm (or 10 Ω·m).[18] The consequences of this for an OLED application are made clear by considering the simple relationship between R and ρ for a film with a given thickness (ℓ) and cross-sectional area (A).

$$R = \rho \ell / A \qquad (8)$$

For a typical EL device, $\ell \sim 100$ nm and A ~ 0.1 cm. Thus, for a conductive polymer layer of these dimensions, R = 0.1 Ω. For the layers of luminescent materials employed in OLEDs, generally R is on the order of 1-100 kΩ, thus the resistance of the conducting $[Ru(LL)_3]^0$ film should be negligible in this application.

IV. Results and Discussion:

Fermi energies. Thin polymer films were prepared on electrode surfaces from monomers **M1, M2** and **M3** as described in the Experimental Section. Electrochemical data obtained from these films are presented in **Table 3.1**, along with solution data from each of the three monomers in the same electrolyte (a $TBA^+PF_6^-$ in acetonitrile solution). Fermi levels (E_F) were calculated from each set of data as the average of the $E_{½}$ of the second and third reductions. The use of either electrochemical data set for calculating E_F requires some caution. The solution data cannot account for any environmental or chemical effects on $E_{½}$ introduced by the polymerization process. The polymer data, on the other hand, is complicated by the effects of both sterics and Donnan potentials on the $E_{½}$'s.[27] Since the problems associated with the polymer data are dependent on both the composition and concentration of the electrolyte and because it is not clear how one might quantitatively deconvolute these effects from the data, the solution results probably more accurately reflect redox values relevant to the calculation of E_F (it is for this reason that ΔE_o for the data in **Figure 3.6** was calculated from the *solution* voltammogram of **M1** as ~ 140 mV). Despite these caveats, the values of E_F calculated from both sets of data and displayed in **Table 3.1**, are in very close agreement with each other for all three

polymers. That agreement suggests that the various perturbations on the redox processes considered above are, in the final analysis, fairly minor.

Table 3.1: Redox potentials, predicted Fermi energies, and work functions for polymers and monomers.

	$E_{½}$ vs Ag/Ag^+ ref.		$E_{½}$ vs NHE ref.		E_F calc.	Φ, calc.	Φ, UPS
	$E_{½}$ 1+/0	$E_{½}$ 0/1-	$E_{½}$ 1+/0	$E_{½}$ 0/1-			
P1 Film	-1.02 V	-1.32 V	-0.61 V	-0.91 V	-0.76 V	**3.84 eV**	**3.6 eV**
P2 Film	-1.26 V	-1.61 V	-0.85 V	-1.20 V	-1.03 V	**3.57 eV**	**3.5 eV**
P3 Film	-1.85 V	-2.00 V	-1.44 V	-1.59 V	-1.52 V	**3.08 eV**	**3.0 eV**
M1 Monomer Solution	-1.11 V	-1.27 V	-0.70 V	-0.86 V	-0.78 V	**3.82 eV**	
M2 Monomer Solution	-1.35 V	-1.58 V	-0.94 V	-1.17 V	-1.06 V	**3.54 eV**	
M3 Monomer Solution	-1.92 V	-2.15 V	-1.51 V	-1.74 V	-1.63 V	**2.97 eV**	

From these calculated E_F values, approximate work functions (Φ) are available. The energy required to remove an electron from the Fermi level to the vacuum energy level, which is ca. -4.60 eV vs normal hydrogen electrode (NHE) in the electrochemical potential scale,[28] is defined as Φ. Work functions can thus be taken as the difference between –4.60 eV and the calculated E_F.

The work function of a conducting material, along with other information about the valence level electronic structure, can be determined directly using ultraviolet photoelectron spectroscopy. In photoelectron spectroscopy, a sample is placed in an ultrahigh vacuum environment ($P < 10^{-10}$ torr) and bombarded by photons of a known energy, *hv*. After absorption of light energy, photoelectrons are released which escape

the material with a kinetic energy (E_{KE}) which is measured in an electron analyzer. Under most conditions the binding energy (E_{BE}) for an electron can be calculated by the following simple relationship:[29]

$$E_{BE} = h\nu - E_{KE} \tag{9}$$

In UPS, the incident photons are in the ultraviolet region of the electromagnetic spectrum, and thus are of an appropriate energy to dislodge electrons from the valence orbitals. Meanwhile, the x-rays used in the analogous method of XPS are of a sufficient energy to release photons from core orbitals.[29] Photoelectron spectra in general consist of two regions, which are defined by the E_{BE} as determined by equation 9. Electrons escaping with the full E_{KE} with which they were released are indicative of the energy of a specific orbital. In UPS spectra the region from approximately 0 – 14 eV binding energy (where an E_{BE} of 0 eV corresponds to the Fermi level) contains in large part these electrons from determinate valence orbital levels, and is thus referred to as the valence region. On the other hand, electrons with a lower measured E_{KE} (and thus a higher binding energy) are referred to as secondary electrons, and in UPS are found in the portion of the spectrum with $E_{BE} > 14$ eV. These photoelectrons were initially released with a higher E_{KE}, but lost some amount of this energy through collision processes with the material prior to escaping. At the secondary photoelectron edge, electrons are escaping with the least possible E_{KE}, and the work function is determined by the difference in energy between this cutoff and the known photon energy $h\nu$.[29]

Full UPS spectra for all three polymers were acquired, after each film was electrochemically reduced in an inert atmosphere glove box, thoroughly rinsed with pure

solvent, and transported into the UHV system without contacting ambient air (as described in the Experimental Section). Spectra of reduced polymers analyzing for photoelectrons dislodged by photons from both HeI and HeII source lines, with energies of 21.22 eV and 40.81 eV respectively, are presented in **Figures 3.8-3.10**. For the sake of comparison, UPS spectra from an untreated P2 film are also displayed in **Figure 3.11**. The structure of the valence region is in general much sharper in the HeII spectra, as is typical for photoelectrons liberated by the higher energy photons. These bands are not rigorously assigned here, but in analogy to conducting polymer systems reported in the literature, peaks are most likely due to the ligand conjugated π systems, underlying σ bonding orbitals, and (in the case of the native **P2** film) PF_6^- counterions.[30,31] Comparing the two **P2** films, detailed analysis of the low E_{BE} region also reveals a new HOMO peak shifted toward the Fermi level in the reduced film, ostensibly due to population of ligand-based π^* orbitals.

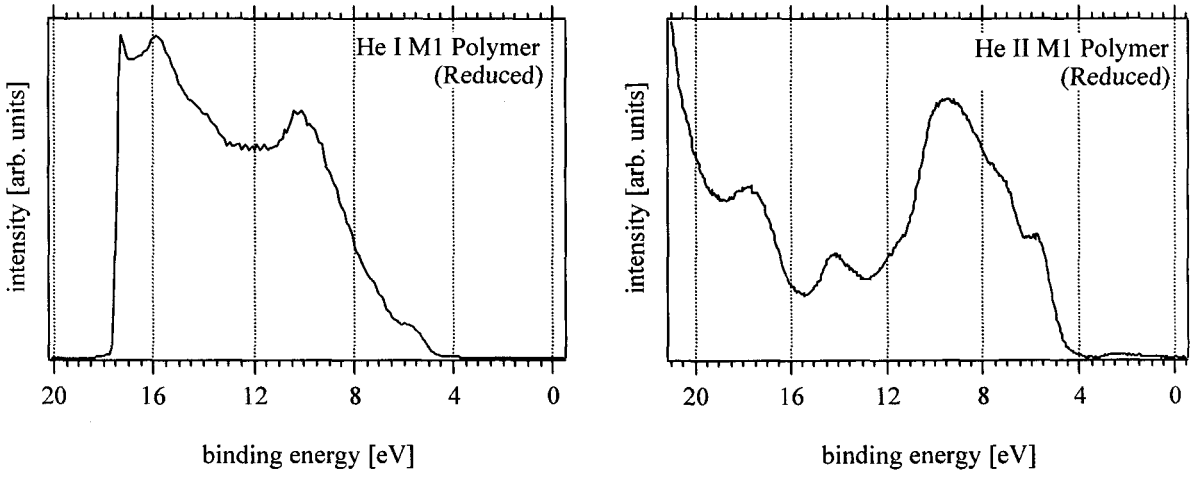

Figure 3.8: HeI and HeII UPS spectra for an electrochemically reduced P1 film.

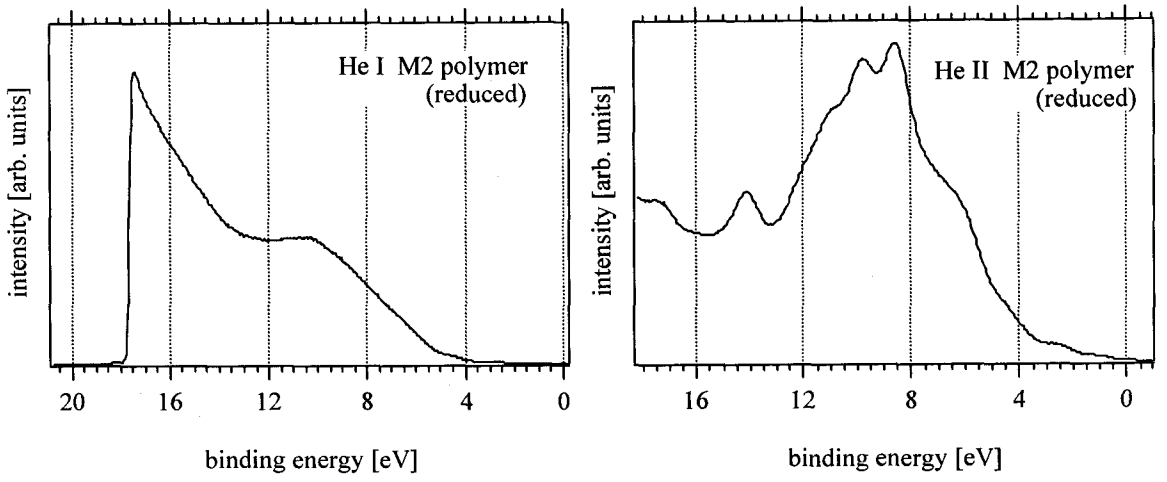

Figure 3.9: UPS spectra for a reduced P2 polymer film.

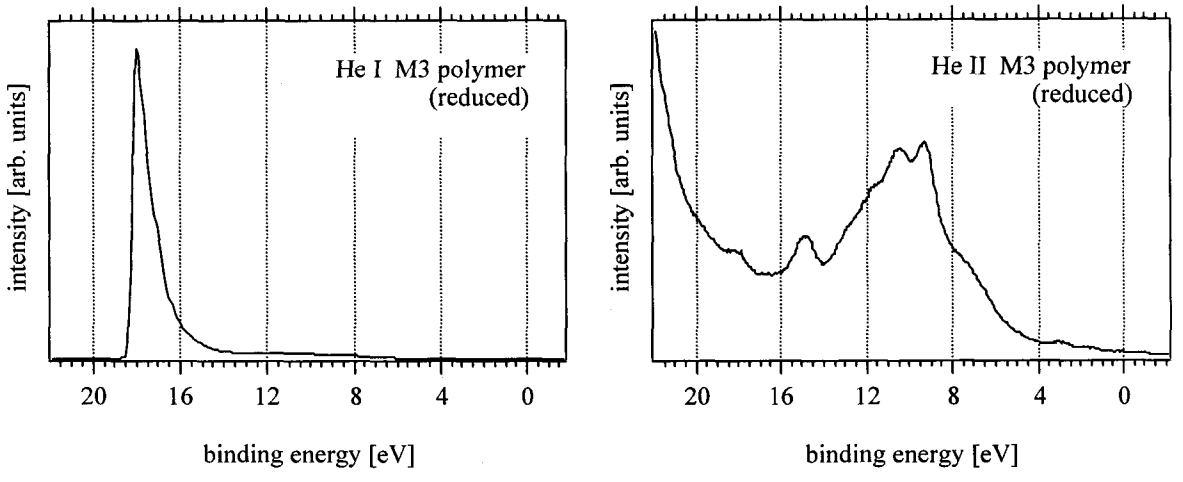

Figure 3.10: UPS spectra for an electrochemically treated P3 film.

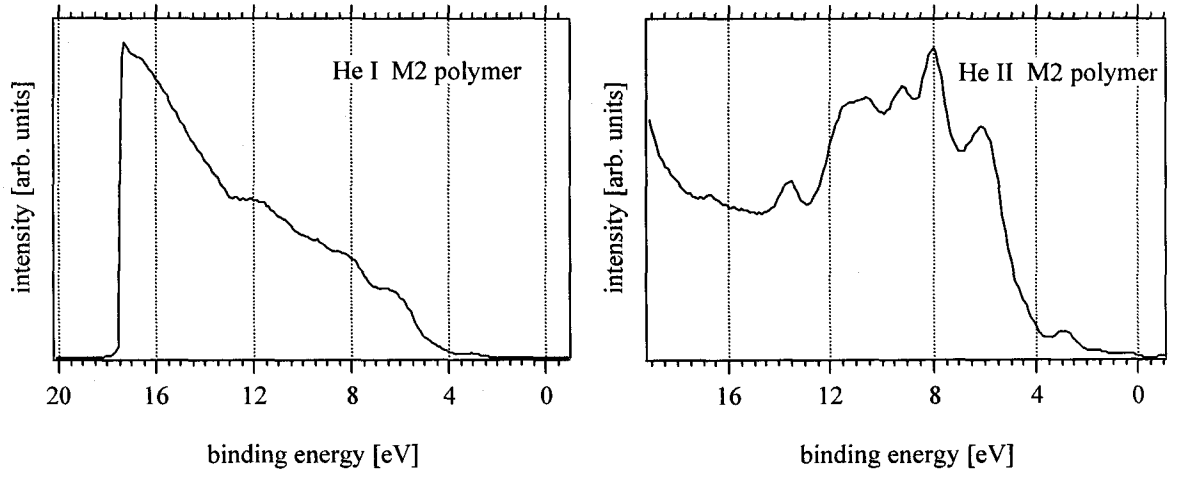

Figure 3.11: UPS spectra for an untreated P2 film.

The principle utility of the HeI spectra in this study is for analysis of the secondary electron region in order to determine Φ. To further demonstrate the elucidation of work functions via UPS, **Figure 3.12** is a blowup of the high E_{BE} portion of the HeI spectrum for the same reduced **P3** film reported in **Figure 3.10**. A line fit to the secondary electron edge is shown, with the 0.1 eV adjustment in HBEC due to thermal and analyzer broadening included.[16] Again, Φ for a given film is determined by comparing this final HBEC value to the incident photon energy of 21.22 eV. To check for any effects due to interaction of the films with the platinum substrate, photoelectron spectroscopy was also performed on reduced **P2** films coated on highly ordered pyrolytic graphite (HOPG). Both work functions and valence structures from the films on HOPG substrates agree well with those on platinum.

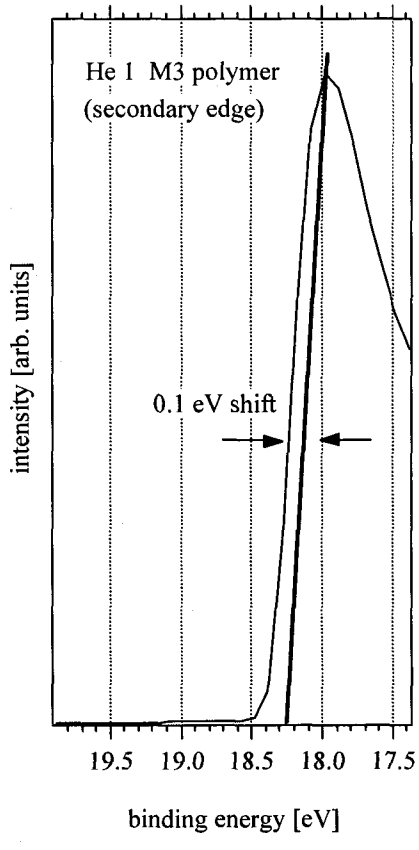

Figure 3.12: Blowup of the HBEC region of the HeI spectrum for a reduced **P3** film.

Work functions obtained from UPS experiments are tabulated in **Table 3.1**. The spectrally determined values of Φ are all quite close to the values predicted from the electrochemical data, a result which validates the premise that electrochemistry can reliably be used to predict work functions of these zero-valent polymers. Furthermore, given the ability to synthetically tune the redox properties of the monomer, it follows that it should be possible to predetermine the work function of a corresponding reduced polymer film.

Performance of Alq_3-based devices with a reduced **P3** cathode: The work function of the reduced **P3** polymer is approximately 3.0 eV. Consequently, like calcium with $\Phi = 2.9$ eV, it should be capable of injecting electrons into the conduction band of several common EL materials. In an effort to verify this assumption, first generation OLED devices using Alq_3 as the EL material were constructed, replacing the traditional metal cathode with the electrochemically treated **P3** polymer. The **M3** monomer was spin coated on a patterned ITO substrate, thermally polymerized, and electrochemically reduced all in a N_2 glove box. Successive layers of Alq_3, TPD, and gold were thermally deposited in a vacuum chamber coupled to the glove box. The layers were thus as follows: ITO substrate/reduced **P3** polymer cathode/Alq_3/TPD/Au anode (see Experimental Section for details). In order to electrochemically reduce the polymer prior to the addition of other layers, the **P3** cathode material must be deposited on a conductive surface. For this purpose, ITO serves quite adequately and is optically transparent. The reduced polymer itself has several intense absorption bands across the visible region of the spectrum. However, at the thickness employed the polymer is almost completely

transparent, and imparts only a slight purplish tinge to the ITO. Since this cathode is essentially transparent, it is possible to construct these OLEDs with the anode on top and the light escaping through the cathode, which is an inverted arrangement relative to most devices in the literature. A few OLEDs with an inverted construction have been reported previously. In those cases a metal cathode was first deposited on a silicon substrate, followed by the organic layers and finally a transparent ITO anode.[32] In addition, an ITO/copper phthalocyanine layer has previously been reported as a transparent cathode material.[33]

The performance of OLEDs constructed with a **P3** cathode is somewhat variable from one device to another, with a relatively high incidence of electrical shorting. This problem was not unexpected and is almost certainly due, at least in part, to defects caused by particulate matter present in the lab and glove box. Every effort has been taken to minimize the problem and a fair percentage of the devices have performed as expected. At the same time, other defects such as pinholes are also possible sources of shorting. Current density vs voltage and light output vs voltage curves for a typical non-shorted device are shown in **Figure 3.13**. At approximately 9 Volts there is a sharp increase in current and light output. For these experiments calibrated light output data is not available, thus the units for light power are arbitrary. Qualitatively, however, the devices produce green colored light that is easily visible to the naked eye at potentials at or above 10 Volts. It should be noted that the presence of the reduced **P3** film is essential to generating light in these devices. Identical devices constructed omitting the polymer layer have never been observed to produce light even with biases as large as 30 V.

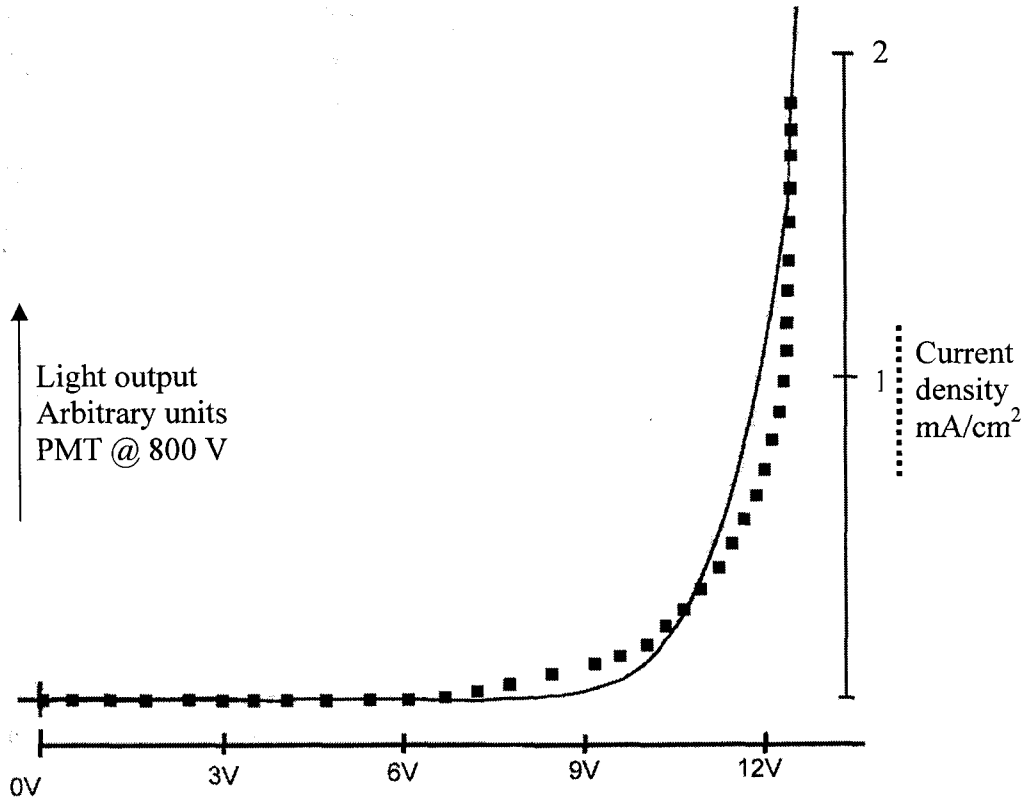

Figure 3.13: Performance for an OLED constructed with a **P3** cathode and Alq_3 EL layer.

While these results demonstrate that these new low work function polymers can serve as electron injecting contacts, the performance of these first generation EL devices is less than ideal. The shorting problems, as stated above, are largely of known origin and should be greatly improved with better "clean-room" conditions. At the same time, the turn-on voltages, emission intensity and lifetime of these devices are sub-optimum. One suspected culprit in those regards is the hole transport layer, TPD. Upon microscopic analysis, numerous devices have shown noticeable crystallization of the TPD layer. This is no doubt caused by heating or other damage upon thermal deposition

of the adjacent gold layer. Indeed, anode deposition directly on TPD has been shown to adversely affect device performance through this very mechanism.[32] In order to mitigate against this problem, the use of a very thin (~50 Å) layer of a more thermally stable "protective cap" such as the perylene-based material PTCDA (structure in **Figure 3.3**) prior to anode deposition has been successful.[32]

Second generation OLEDs constructed exactly as above, but with the addition of PTCDA as a protective cap layer displayed noticeably different performance compared with devices lacking this layer. Figure **3.14** depicts the current and light vs voltage for such a device. The turn-on voltage and light emission for OLEDs using the PTCDA layer are much improved. While the y-axis for light emission in for these devices is still in arbitrary units, it is important to note the high voltage bias for the photomultiplier tube, which is now 400 V as opposed to 800 V for the first generation OLEDs. The PMT response is quickly saturated when using the higher voltage setting in light measurement for the devices containing PTCDA, indicating a significantly greater total emission power in these second generation devices. At the same time, the current passed by the two types of devices is roughly equivalent, thus the emission efficiency is greater in devices including the cap layer. This is most likely a consequence of significantly better balanced charge carrier injection (that is, the number of holes and electrons injected at a given voltage are more closely matched). Microscopic analysis of devices containing the PTCDA protective cap layer does not reveal any crystallization or damage to the organic materials upon thermal deposition of gold. Presumably for this reason, the proportion of devices that operate successfully is much higher when the PTCDA layer is added. On the other hand, the shape of the I/V and light/V curves in this case is curious and not ideal.

Because the increase of current and light with voltage is not nearly as steep as in most OLEDs, ultimate current densities and light emission are not as great as might be hoped. While the reason for this behavior is uncertain, it can likely be attributed to a higher electrical resistance owing to the insulating PTCDA layer.

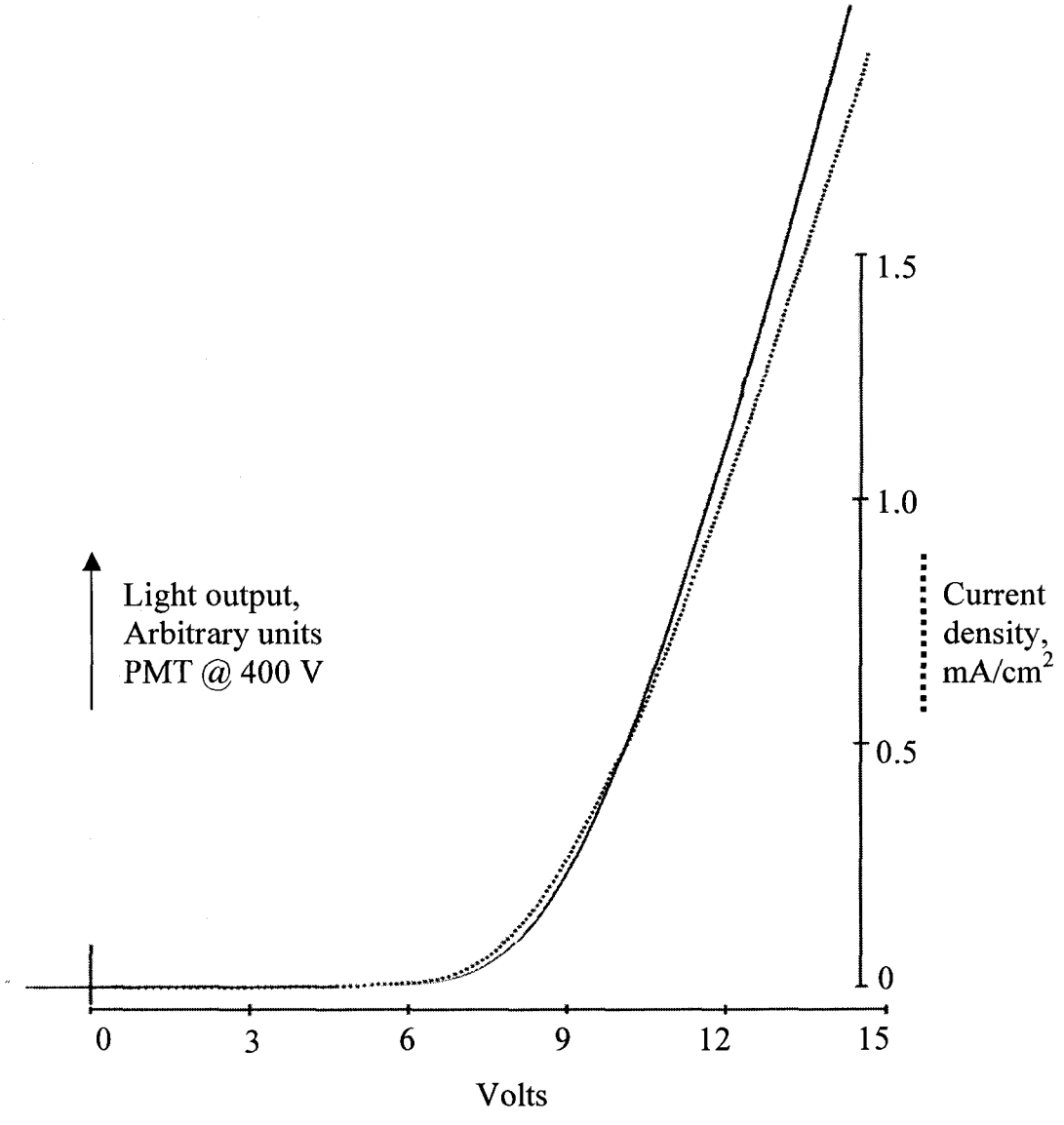

Figure 3.14: Performance for an OLED constructed with a **P3** cathode, Alq_3 EL layer, and PTCDA as a protective cap layer prior to deposition of the gold anode.

Devices containing the EL polymer BEHP-PPV: OLEDs employing reduced **P3** as the cathode and the EL polymer BEHP-PPV, directly covered by a gold anode, have also been constructed and tested. The performance for one of these polymer-based OLEDs is shown in **Figure 3.15**. In this case, the emission is relatively intense (the PMT is again at 400 V), but is not evident until a rather high voltage of approximately 11 V. On the other hand, increased current is evident in the neighborhood of 7 V. This large difference in turn-on voltages for light emission as compared to current likely indicates that the barrier for charge injection at one of the electrode/organic interfaces is significantly larger than predicted. Whether this is occurring at the cathode or the anode is not clear from the experiment.

V. Conclusions.

Through this study several things have been demonstrated. First, it is possible to generate low work function conducting polymers which can serve as electron injecting cathodes in OLED's. Second, it is possible to tune the Fermi energies (and thus work functions) of these materials in predictable ways by synthetic modifications of the monomer. Finally, solution electrochemical data from the monomer can be used to predict the work function of the respective polymer with excellent accuracy, a result which was verified through the use of photoelectron spectroscopy.

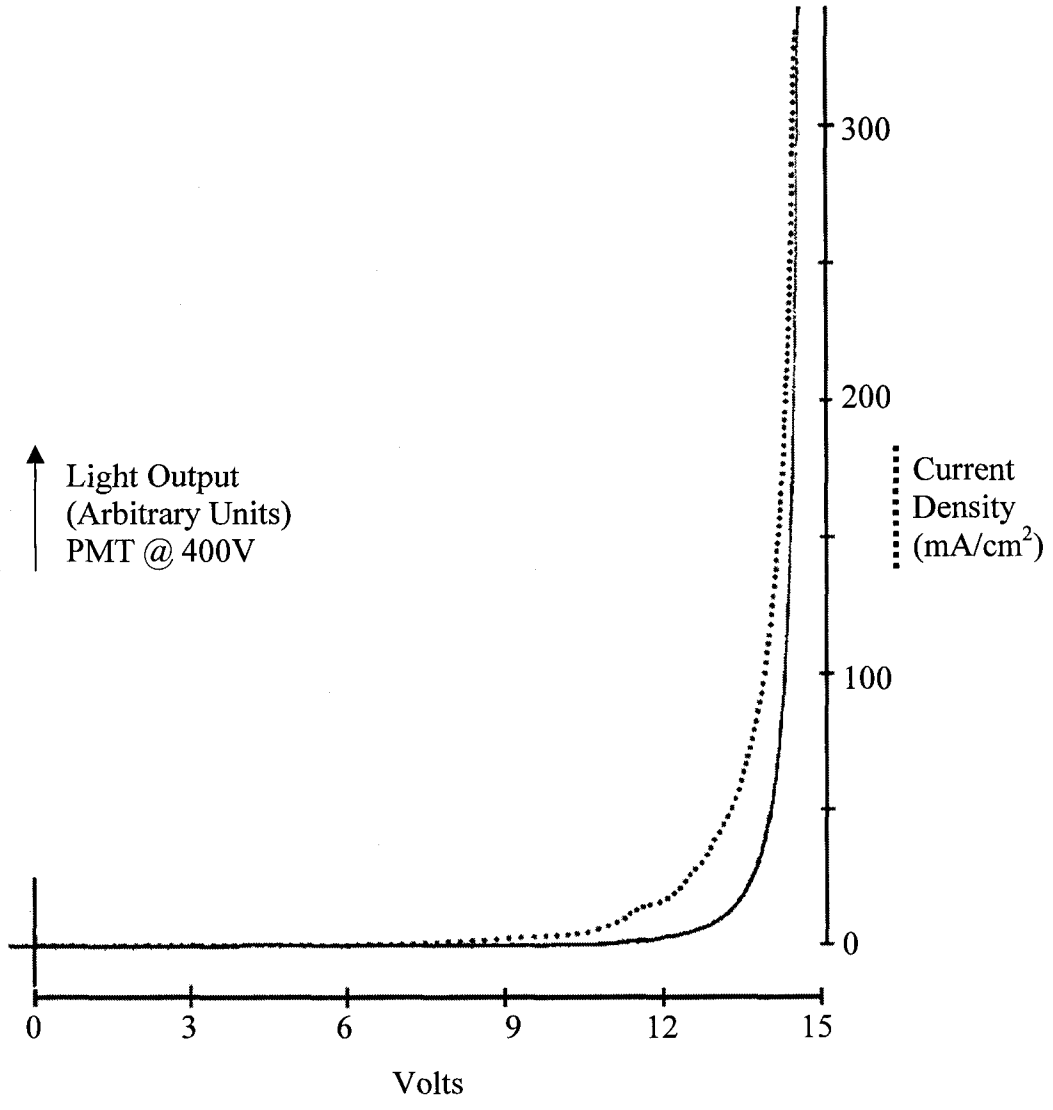

Figure 3.15: Performance of an OLED with a reduced **P3** cathode and EL polymer BEHP-PPV.

As a consequence of the level of control one can exert over the electronic properties, in principle polymeric cathodes can be tailored to match the band structure of each EL material. The availability of a series of different polymer cathode materials may provide an opportunity to study the EL material interface with polymers having very similar chemical compositions but varying work functions. Such fundamental studies

should be relevant to important practical considerations in OLED operation such as stability, efficiency and turn-on voltage.

On the other hand, EL devices constructed to date employing a reduced **P3** polymer as the cathode material have suffered from mediocre performance, at least in part as a consequence of practical constraints their use places on OLED design. Specifically, the necessity of placing the polymer on the bottom of the device (along with the need for subsequent electrochemical treatment of the film) has proven problematic for ultimate OLED performance. While these issues may eventually be surmountable, thus far the device characteristics and ability to evaluate the nature of the cathode/organic interface have been hampered. These problems may ultimately limit the importance of these materials both in terms of device performance and fundamental studies.

REFERENCES

(1) Sheats, J. R.; Antoniadis, H.; Hueschen, M.; Leonard, W.; Miller, J.; Moon, R.; Roitman, D.; Stocking, A. *Science* **1996**, *273*, 884.

(2) Tang, C. W.; VanSlyke, S. A. *Appl. Phys. Lett.* **1987**, *51*, 913.

(3) Burroughs, J. H.; Bradley, D. D. C.; Brown, A. R.; Marks, R. N.; Mackay, K.; Friend, R. H.; Burns, P. L.; Holmes, A. B. *Nature* **1990**, *347*, 539.

(4) Burrows, P. E.; Forrest, S. R. *Appl. Phys. Lett.* **1994**, *64*, 2285.

(5) Johansson, D. M.; Srdanov, G.; Yu, G.; Theander, M.; Inganas, O.; Andersson, M. R. *Macromol.* **2000**, *33*, 2525.

(6) Nguyen, T. Q.; Martini, I. B.; Lu, J.; Schartz, B. J. *J. Phys. Chem. B* **2000**, *104*, 237.

(7) Nguyen, T. Q.; Kwong, R. C.; Thompson, M. E.; Schwartz, B. J. *Appl. Phys. Lett.* **2000**, *76*, 24524.

(8) Tang, C. W.; VanSlyke, S. A.; Chen, C. H. *J. Appl. Phys.* **1989**, *65*, 3610.

(9) Parker, I. D. *J. Appl. Phys.* **1994**, *75*, 1656.

(10) Gustafsson, G.; Cao, Y.; Treacy, G. M.; Klavetter, F.; Colaneri; Heeger, A. J. *Nature* **1992**, *357*, 472.

(11) Birgeson, J.; Fahlman, M.; Brohms, P.; Salaneck, W. R. *Synth. Met.* **1996**, *80*, 125.

(12) Lazzaroni, R.; Bredas, J. L. *Plast. Engin.* **1998**, *43*, 185.

(13) Miyata, S.; Nalwa, H. S. *Organic Electroluminescent Materials and Devices*; Gordon and Breach: Netherlands, **1997**.

(14) Hamda, Y.; Sano, T.; Fujita, M.; Fujii, T.; Nishio, Y.; Shibata, K. *Jpn. J. Appl. Phys.* **1993**, *32*, L514.

(15) Choung, V. E.; Mason, M. G.; Tang, C. W.; Gao, Y. *Appl. Phys. Lett.* **1998**, *72*, 2689.

(16) Schlaf, R.; Schroder, P. G.; Nelson, M. W.; Parkinson, B. A.; Merritt, C. D.; Crisafulli, L. A.; Murata, H.; Kafafi, Z. H. *Surface Science* **2000**, *450*, 142.

(17) Elliott, C. M.; Redepenning, J. G.; Balk, E. M. *J. Electroanal. Chem.* **1986**, *213*, 203.

(18) Elliott, C. M.; Redepenning, J. G.; Balk, E. M.; Schmittle, S. J. *Electronically Conducting Films of Poly(trisbipyridine)-Metal Complexes;* ACS Symposium Series 360 (Inorganic and Organometallic Polymers), American Chemical Society: Washington, DC, **1988**, p. 420.

(19) Elliott, C. M.; Redepenning, J. G. *J. Electroanal. Chem.* **1986**, *197*, 219.

(20) Sprinkle, R. B. *Ph.D. Thesis*; Chemistry Department: Colorado State University, Fort Collins, CO, **1990**.

(21) Jernigan, J. C.; Murray, R. W. *J. Phys. Chem.* **1987**, *91*, 2030.

(22) Chidsey, C. E. D.; Murray, R. W. *J. Phys. Chem.* **1986**, *90*, 1479.

(23) VanVlack, L. H. *Elements of Materials Science and Engineering*; Sixth ed.; Addison-Wesley: Reading, MA, **1989**.

(24) Daum, P.; Lenhard, J. R.; Rolison, D.; Murray, R. W. *J. Am. Chem. Soc.* **1980**, *102*, 4649.

(25) Oyama, N.; Anson, F. C. *J. Electrochem. Soc.* **1980**, *127*, 640.

(26) Elliott, C. M.; Herschenhart, E. J. *J. Am. Chem. Soc.* **1982**, *104*, 7519.

(27) Naegeli, R.; Redepenning, J.; Anson, F. C. **1986**, *90*, 6227.

(28) Trasatti, S. *Pure Appl. Chem.* **1986**, *58*, 955.

(29) Ertl, G.; Kuppers, J. *Low Energy Electrons and Surface Chemistry*; VCH Verlagsgesellschaft mbH: Weinheim, Germany, **1985**.

(30) Fahlman, M.; Bredas, J. L.; Salaneck, W. R. *Synth. Met.* **1996**, *78*, 237.

(31) Nelson, A. J.; Glenis, S.; Frank, A. J. *J. Chem. Phys.* **1987**, *87*, 5002.

(32) Bulovic, V.; Tian, P.; Burrows, P. E.; Gokhale, M. R.; Forrest, S. R.; Thompson, M. E. *Appl. Phys. Lett.* **1997**, *70*, 2954.

(33) Parthasarathy, G.; Burrows, P. E.; Khalfin, V.; Kozlov, V. G.; Forrest, S. R. *Appl. Phys. Lett.* **1998**, *72*, 2138.

CHAPTER FOUR

LOW WORK FUNCTION REDUCED METAL COMPLEXES AS CATHODES IN ORGANIC ELECTROLUMINESCENT DEVICES

A portion of the material presented in this chapter will be published in *The Journal of Physical Chemistry B* in the spring of 2003.

I. Introduction

The exact mechanism for electron injection from the cathode of OLEDs into the adjacent organic layer is still a subject of debate, and likely differs depending on the exact nature of the device in question.[1] In some cases, a Fowler-Nordheim tunneling mechanism applies, where electrons tunnel *through* an energy barrier determined by the characteristics of the materials in the interface and the applied potential.[2] Others have asserted that the injection of electrons is limited by thermionic emission *over* an energy barrier,[3] or alternately by a space-charge limited mechanism.[4] While the conflicting models can in some instances be explained by differences in device makeup, at other times there is disagreement on the mechanism for identical or very similar OLEDs.[3,4] Whatever the exact mechanism, to a first approximation a low barrier for injection should be provided when the Fermi energy of the cathode is closely matched to the LUMO energy of the emitting (or electron transport) layer. Again, for this reason low work function (Φ) metals such as magnesium, calcium and aluminum, or their alloys with silver are the most commonly used materials for cathodes and are most commonly interfaced directly with the EL organic layer.[3-7]

Advances have more recently been made utilizing very thin layers of insulators and wide bandgap semiconductors between the conducting cathode and the active organic material. Specifically, inorganic insulators such as LiF, Li_2O, MgF_2, and MgO under aluminum metal have been widely used[8-11], and copper phthalocyanine (CuPc) has been paired with the high work function conducting metal oxide indium tin oxide (ITO)[12] to produce a reasonably efficient transparent OLED. Doping of lithium metal into Alq_3 by

codeposition has also been reported.[13] The presence of these extra layers clearly changes the nature of the cathode/organic interface, and several arguments have been made to explain the success of these more complex systems. The formation of Li metal by reaction with Al has been proposed to explain the use of LiF[10], while others assert the mechanism is electron tunneling through the insulating salt[9,11] or band bending in the organic layer.[8] In the case of a metal oxide on CuPc, the formation of midgap states due to damage by the deposition of the ITO onto the organic was thought to decrease the barrier to injection.[12] This latter result is particularly interesting, as there is no low work function material involved at all.

In the previous chapter a series of low Φ conducting polymers composed of redox active substituted transition-metal diimine complexes was described as another alternative to low Φ metals in EL devices. The **P3** polymer, with a work function of 3.0 eV, was used in conjunction with ITO as a cathode in several "inverted type" OLEDs of the following general composition: ITO/reduced **P3**/active-organics/Gold The "active organics" portion of the devices was alternately composed of multiple layers of small molecule or polymer EL materials. While this type of device produced light under a moderate voltage bias, the performance was not optimal. Most likely this was due to inherent limitations of the inverted geometry, the requirement of electrochemical reduction of the polymer, and the instability of the TPD/gold interface.[14] These problems made it difficult to draw definitive conclusions about the nature of the **P3** polymer/organic interface.

This chapter describes the use of a similar class of low Φ organic materials (LWOMs) composed of redox active metal complexes and shown in **Figure 4.1**, but ones that can be

deposited by thermal evaporation. Accordingly, these compounds are simpler to use, and allow more flexible design of OLEDs. Devices of the type Metal/LWOM/Alq_3/TPD/ITO were constructed using silver and gold (both of which have relatively high Φ) in conjunction with the LWOM as a cathode, and their performance was evaluated.

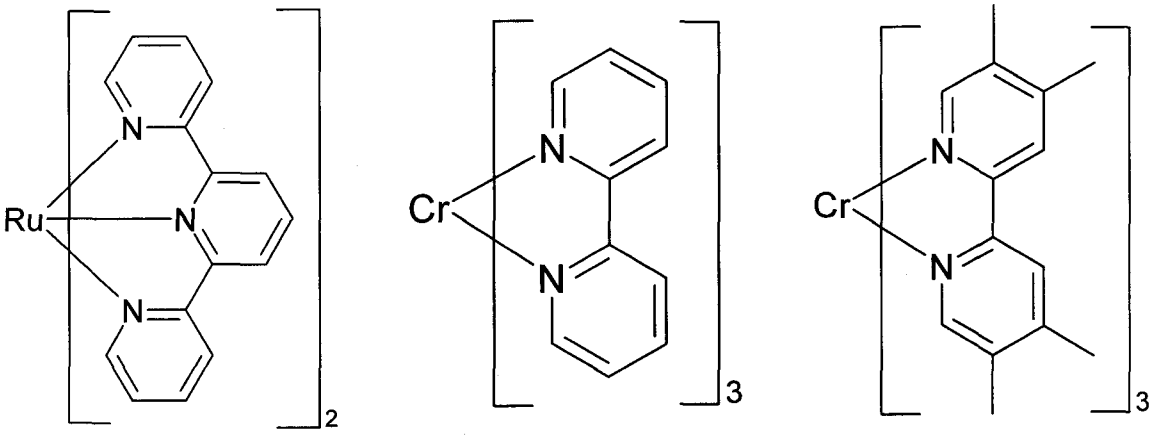

Figure 4.1: Structures of three electrochemically active coordination complexes employed as cathode materials in EL devices. Detailed synthesis is reported below.

II. Experimental Section

Chemicals. Acetonitrile was Aldrich Optima grade, stored over 4 Å molecular sieves and distilled from CaH_2. Ammonium hexafluorophosphate (NH_4^+ PF_6^-) was supplied by Elf Atochem and tetra-*n*-butylammonium hexafluorophosphate ($TBA^+PF_6^-$) electrolyte was prepared as described elsewhere.[15] The ligand 4,4′,5,5′-tetramethyl-2,2′-bipyridine (TMB) was produced by a coupling reaction of 3,4-lutidine (Aldrich) over Pd on C, followed by recrystallization from ethyl acetate. 2,2′-bipyridine (bpy) was purchased from Baker, and 2,2′:6′,2″-terpyridine (terpy) from Aldrich, and both were used without further purification. Alq_3 and TPD, from Aldrich, were purified by vacuum train sublimation with Argon gas flow at 330°C and 270°C, respectively. Chromic

chloride was supplied by Fisher. Gold of purity 99.99% was purchased from Alfa Aesar, and 99.9999% pure silver from Sargent-Welch. The conducting polymer dispersion, poly(styrenesulfonate)-poly(2,3-dihydrothieno-[3,4-*b*]-1,4-dioxin) 1.3 % by weight in H_2O (PEDOT-PSS), was supplied by Aldrich. ITO, 4-8 Ω/sq. on glass, was purchased from Delta Technologies, Ltd.

Synthesis of $[Ru(terpy)_2]^{2+}(PF_6^-)_2$, Figure 4.1. Terpyridine (100 mg, 0.429 mmol) in 10 mL ethylene glycol was added to $Ru(DMSO)_4Cl_2$ (95 mg, 0.196 mmol) in 4 mL 1:1 methanol:water. The mixture was heated under N_2 via an oil bath held at 100°C for 2.5 hours, producing a dark reddish solution which was then cooled to room temperature. Water was added to reach a total volume of 75 mL and NH_4^+ PF_6^- was added whereupon a red/orange precipitate formed. The solid was washed well with H_2O and recrystallized from methanol to yield brick red crystals.

Synthesis of $[Cr(bpy)_3]^{3+}(ClO_4^-)_3$, Figure 4.1. A modified literature procedure was used.[16,17] $CrCl_3 \cdot 6H_2O$ (1.33 g, .0050 mol) was heated at reflux under N_2 in 0.05 M $HClO_4$ (Mallinkrodt) over Al metal (Baker) to produce a blue/green solution likely containing both Cr^{2+} and Cr^{3+} ions. This solution was added to a N_2 purged suspension of bpy (7.81 g, 0.050 mol) in aqueous $HClO_4$ of pH 2. A black suspension was quickly formed, which slowly turned yellow (indicating formation of the $[Cr(bpy)_3]^{3+}$ complex) upon bubbling with O_2 for 2 hours. The yellow solid was collected by filtration, washed well with water, ethanol, and CH_2Cl_2 (to remove excess ligand), and finally recrystallized from water.

Synthesis of $[Cr(TMB)_3]^{3+}(ClO_4^-)_3$, Figure 4.1. The above procedure was changed only slightly, using much less TMB ligand (0.50 g), as the large excess was in this case unnecessary and difficult to remove, and 0.285 g chromic chloride. The resulting yellow solid was only sparingly soluble in hot water, and was purified by washing with hot water and ethanol rather than recrystallization.

Electrochemistry. Cyclic voltammetry was performed in a Luggin capillary cell with a Ag/Ag^+ 0.1 M in DMSO (0.41 V vs NHE) reference electrode, Pt wire counter, and glassy carbon working electrode, in 0.1 M $TBA^+PF_6^-$ in CH_3CN electrolyte. Scan rates were 50 mV/sec. Electronics consisted of a P.A.R. model 173 Potentiostat and model 175 Programmer with output to a Yokogawa X/Y recorder.

Electrocrystallization. The three complexes were reductively electrocrystallized following a modification of a method described in the literature.[18,19] A three compartment bulk electrolysis cell was used in an inert atmosphere glove box with the same electrolyte, reference and counter electrodes as above, and a Pt mesh working electrode (WE). To produce $[Ru(terpy)_2]^0$, 50 mg of $[Ru(terpy)_2]^{2+}(PF_6^-)_2$ was added to the WE compartment, and vigorously stirred. The WE was held at a constant potential of –2.00 V (several hundred mV past the second reduction as determined from cyclic voltammetry) until the current decayed from approx. 500 mA to under 100 μA over the course of several hours. The WE, which was covered with purple/black crystals of the reduced complex, was disconnected from the potentiostat and removed from the electrolysis solution. These crystals were dislodged from the WE in fresh CH_3CN,

collected on a fritted filter, and washed with more acetonitrile. The solid was dried by passage of glove box atmosphere over the solid with a vacuum pump, and scraped into a boat for thermal deposition. Crystals of $[Cr(bpy)_3]^0$ and $[Cr(TMB)_3]^0$ were prepared in the same manner, but at controlled potentials of –1.90 V and –2.15 V vs Ag/Ag^+ 0.1 M in DMSO, respectively.

Photoelectron Spectroscopy. All photoelectron spectroscopy work was performed in an Omicron multiprobe UHV chamber (base pressure $5 \cdot 10^{-11}$ torr) equipped with a VSW EA125 single-channel analyzer. A transfer rod assembly was used which could be moved into the glove box for sample preparation, and the sample isolated from the atmosphere behind a gate valve. This assembly was affixed to the entry chamber of the UHV system and pumped down to vacuum prior to introducing the sample into the analysis chamber. The X-ray source was the Mg Kα line at 1253.6 eV. The UV light source was a helium arc lamp, providing a He(I) line at 21.22 eV and a He(II) line at 40.81 eV. A –5.00 V bias was applied to the sample to separate the spectrometer and sample high binding energy cutoffs. Kinetic energy analysis of electrons emitted normal to the sample was done using a 10 eV pass energy. The spectrometer was calibrated with an Ar^+ ion sputtered copper standard.

A straight line was fit on the secondary edge of the UPS He(I) spectrum (and the XPS spectrum). The intercept of this line with the abscissa determines the high binding energy cutoff (HBEC). A value of 0.1 eV was subtracted from the HBEC to correct for spectrum broadening due to thermal and analyzer effects.[20] The work function was determined by subtracting this value from the source energy of 21.22 eV.

OLED Construction. After rinsing in ethyl acetate and isopropyl alcohol, patterned ITO substrates were cleaned in a laminar flow hood by successive sonication in a 5% aqueous solution of VWR aquasonic cleaner followed by Millipore water. For devices including PEDOT-PSS, the polymer suspension was filtered through a 0.2 μm cellulose acetate syringe filter (Nalgene) and spin coated onto an ITO substrate at approximately 1000 rpm using a modified commercial blender. The substrates were introduced first into the glove box and then the vacuum deposition chamber (Denton DV 502A Turbo model) that is directly interfaced with the glove box. Organic materials and metals were sequentially deposited at pressures below $3 \cdot 10^{-6}$ torr, yielding devices with an active area of ca. 0.1 cm^2. The thickness of the various layers was measured by a Leybold Inficon quartz crystal microbalance and XTM-2 Deposition Monitor. Device testing was performed using a Kiethley 2400 Sourcemeter and Newport 1830-C Optical Power Meter with 818-SL Photodiode detector driven by LabVIEW 6.0 Software.

III. Background and Theory

To review, the previous chapter described thin polymer films composed of substituted tris(bipyridine) ruthenium(II) complexes, which by nature have many closely spaced (in potential) redox couples at negative potentials. Electrochemical reduction of the active sites in the polymer to the formally zero-charged state afforded electronically conductive (resistivity $\rho \sim 1 \cdot 10^3$ $\Omega \cdot cm$) low Φ films.[21] The conductivity and low work functions are both explained by considering the consequences of the proximal redox processes, as predicted by the Nernst equation. Due to thermal energy, at least three

oxidation states (1+,0, and 1-, where the charged species are present in equal numbers) are present in moderate concentration at room temperature in the reduced films. Furthermore, because the LUMO energy of the free ligands can be controlled by synthetic alterations, the Φ of the resulting reduced films can be tuned. Photoelectron spectroscopy was used to verify that the Φ could be predicted by cyclic voltammetry of the monomers in solution from the average of the $E_{1/2}$ of the 1+/0 and 0/1- couples.

In principle, the same factors which apply to the conductivity and Φ of the previously described polymers should also apply to solids composed of neutral small-molecule organics with similar redox properties. Moreover, because in certain cases these materials can be thermally vapor deposited, they should provide some important advantages over the polymers in OLED applications. By eliminating the necessity of post-polymerization electrochemical processing, small molecule LWOMs would allow a much greater variety of device architectures, and no doubt would be inherently more pure. Redox active polypyridine complexes of transition metals are a natural choice, in that they posses numerous oxidation states with small voltage separations. Neutral complexes can be produced by electrochemical or chemical reduction of the complex, by adding a number of electrons equal to the initial positive charge. Also, by virtue of a lack of formal charge, isolation of the zero-valent form is often simple due to their different solubility than the charged species.

The solid state compounds $[Ru(bpy)_3]^0$ and $[Ru(terpy)_2]^0$, prepared by reductive electrocrystallization from the 2+ species, have been recently studied as interesting electronic systems.[18,19,22] The conductivity of single-crystalline $[Ru(bpy)_3]^0$ was reported as $\sigma \sim 1.5 \cdot 10^{-1}\ \Omega^{-1}cm^{-1}$ at 297 K, with a semiconductor-like temperature coefficient.[23]

Based on the conductivity, x-ray crystal structures, electron paramagnetic resonance, and magnetic properties of these systems, several possible models for the electronic structure (and thus mode of conduction) were proposed. In the simplest case, the two "extra" electrons provided by the reduction are seen as localized on individual ligands, but can undergo very facile intra- *and* intermolecular exchange due to efficient orbital overlap.[23] Alternately, an "expanded atom" model was considered, that treats the electrons as a completely delocalized pseudospherical ligand around the cationic core.[24] Finally, the more extreme possibility of an electride[25] was discussed, in which the electrons are essentially altogether freed from the complexes and exist as a "lattice gas", residing in cavities within the crystal lattice.[19,22] A definitive argument for any one of these models was not made, and it may be most appropriate to view these cases as three points along a continuum of electronic structure. Regardless of the actual mechanism, clearly electrons in these systems are fairly mobile; and while conductivity has been reported only for the bpy complex as a single crystal, it is reasonable to expect that thin polycrystalline or amorphous films of either species would be respectable conductors.

Extrapolating from the results with these neutral ruthenium complexes, one might expect $[Cr(bpy)_3]^0$ to also be conductive given its similar reduction electrochemistry. While the solid state conductivity of this system has not been reported, analysis of the electron transfer reaction between $[Cr(bpy)_3]^{1+}$ and $[Cr(bpy)_3]^0$ in *N,N*-dimethylformamide solution revealed a very fast second-order rate constant of $2.0 \cdot 10^9$ $M^{-1}sec^{-1}$.[26] This rate was rationalized in part by minimal inner-sphere reorganization upon electron exchange, which would be expected for all of these complexes, and would also be consistent with facile electron transfer in the solid state.

Attempts to vapor deposit $[Ru(bpy)_3]^0$ were unsuccessful; however, both $[Ru(terpy)_2]^0$ and $[Cr(bpy)_3]^0$ could be deposited at moderate temperatures and pressures below $6 \cdot 10^{-6}$ torr. Using the ligand-localized electron model, this difference in behavior can be attributed to the symmetry of these neutral complexes. When each added electron is assumed to be instantaneously localized on a single ligand, the symmetry of $[Ru(bpy)_3]^0$, $[Ru(terpy)_2]^0$ and $[Cr(bpy)_3]^0$ are respectively C_2, D_{2d}, and D_3. While all three complexes are uncharged, the point groups of the latter two species do not permit a dipole, whereas $[Ru(bpy)_3]^0$ in C_2 can, and presumably does, have a dipole. Moreover, if the electron were totally localized, the instantaneous dipole is predicted to be quite large (on the order of 20 Debye). Presumably a strong dipolar interaction in the solid significantly reduces the volatility of $[Ru(bpy)_3]^0$ relative to the other reduced complexes that both lack dipoles. This pattern indicates a further constraint for complexes to use as evaporable LWOMs: when the reductions are essentially ligand based, the number of ligands must be equal to the initial positive charge on the complex and therefore the number of electrons by which it is reduced. Interestingly, with regards to the models of electronic structure considered above, this result is particularly at odds with the expanded atom view, and most consistent with the localized electron description. If the expanded atom model were valid, it stands to reason that $[Ru(bpy)_3]^0$ could be evaporated in the same manner as $[Ru(terpy)_2]^0$.

In order to predict (via cyclic voltammetry) the Φ of "zero valent" polymeric materials reported in **Chapter 3**, a model was presented assuming discrete redox sites having 1+, 0, and 1- oxidation states and an overall neutral charge. This is conceptually analogous to a narrow bandgap intrinsic semiconductor, with a large (*and equal*) number

of electrons and holes produced by thermal excitation. In this picture, the Fermi level (E_F) should lie in the middle of the bandgap. Accordingly, the E_F can be estimated as the average potential for the redox processes creating the two singly charged species, and by extension the Φ can be calculated. In light of the more complex electronic models discussed above for the small molecule LWOMs considered here, the assumption of isolated charged sites is likely not entirely valid in a more ordered crystalline environment. Nonetheless, the energy levels of the reductions (i.e. $E_{1/2}$ $[Ru(terpy)_2]^{1+/0}$ and $E_{1/2}$ $[Ru(terpy)_2]^{0/1-}$), provided by cyclic voltammetry, should yield at least a rough estimate of the energy of electrons in the solid LWOMs.

IV. Results and Discussion:

Cyclic voltammograms of $[Cr(bpy)_3]^{3+}$ and $[Cr(TMB)_3]^{3+}$ are displayed in **Figure 4.2**, while electrochemical data for $[Ru(terpy)_2]^{2+}$ has been reported extensively in the literature[27] and is not duplicated here. The $E_{1/2}$ for the 1+/0 and 0/1- reductions, along with calculated E_F and Φ, of $[Ru(terpy)_2]^0$, $[Cr(bpy)_3]^0$, and $[Cr(TMB)_3]^0$ are presented in **Table 4.1**. Note that, as predicted, the TMB complex undergoes reductive processes at potentials significantly more negative than does the bpy analogue due to the electron donating nature of the methyl substituents on the ligands. Indeed, for this system, the fourth reduction (0/1-) is very near or outside the electrochemical window available in acetonitrile solvent and must be estimated by comparison to the other Cr complex. This seems to be a fair assessment, since the three corresponding measured reductions are each shifted by the approximately the same amount. The data were obtained using either a Ag/Ag^+ 0.1 M in DMSO or SSCE reference electrode. Potentials are also reported

relative to the standard electrode for electrochemical data, the normal hydrogen electrode (NHE), by subtracting the difference in potential of the RE used in the experiment from that of the NHE, 0.410 and 0.236 V respectively. The E_F vs NHE is calculated as the average of the half wave potentials for the 1+/0 and 0/1- reductions, and finally the Φ is estimated by comparison of the energy of the NHE to the energy of a free electron in vacuum, -4.60 eV.[28]

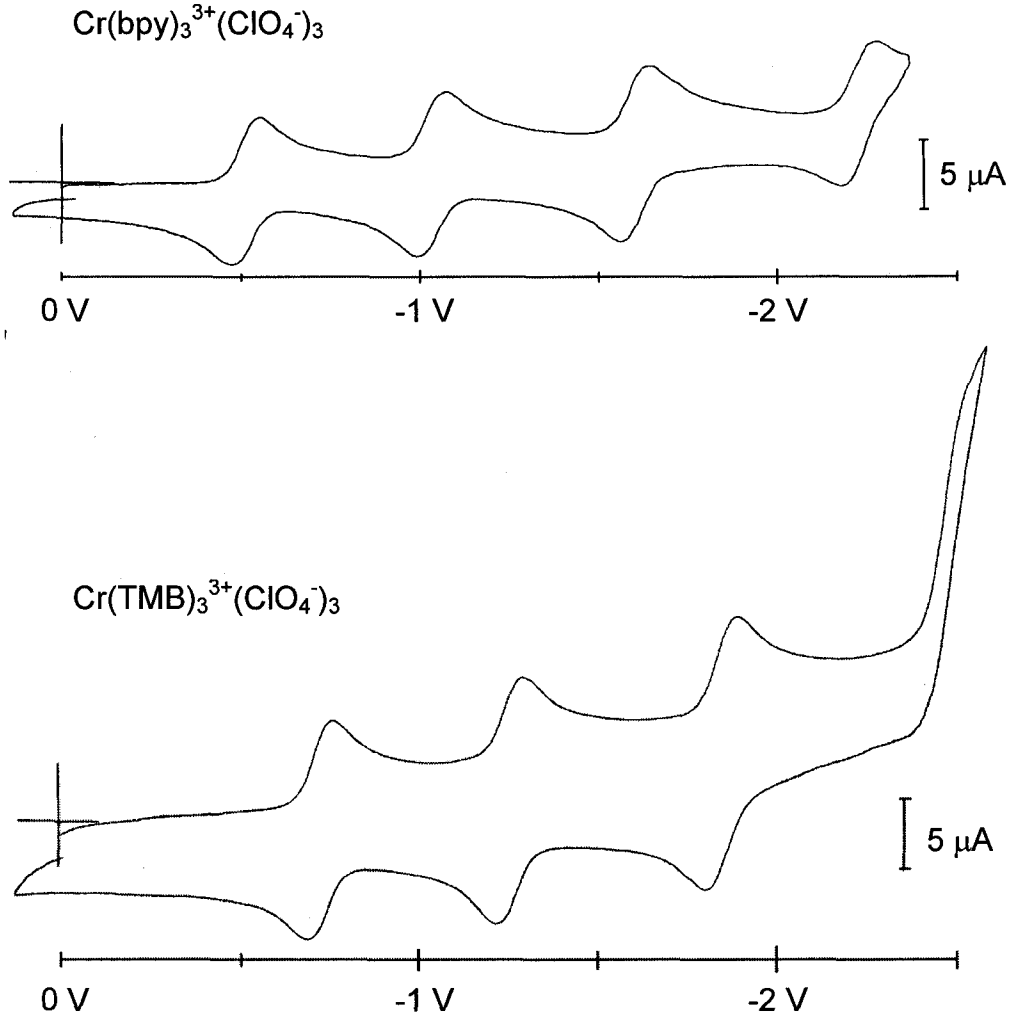

Figure 4.2: Cyclic voltammetry for Cr complexes. WE: glassy C, RE: Ag/Ag^+ 0.1 M in DMSO, CE: Pt wire, electrolyte: $TBA^+PF_6^-$ in CH_3CN, rate: 50 mV/sec.

Table 4.1: Electrochemical data for Cr and Ru complexes, along with predicted work functions of reduced complexes. *Taken from the literature.[27] †Estimated by comparison to the 0/1- couple for $Cr(bpy)_3$.

	$E_{1/2}$ vs Ag/Ag^+ 0.1 M in DMSO, V				$E_{1/2}$ vs NHE, V		E_F calc.	Φ, calc.
	3+/2+	2+/1+	1+/0	0/1-	1+/0	0/1-		
$Ru(terpy)_2$	---	-1.44*	-1.69*	-2.13*	-1.28	-1.72	-1.50 eV	3.10 eV
$Cr(bpy)_3$	-0.48	-0.98	-1.56	-2.18	-1.15	-1.77	-1.46 eV	3.14 eV
$Cr(TMB)_3$	-0.72	-1.25	-1.85	-2.46†	-1.44	-2.05†	-1.75 eV	2.85 eV

Photoelectron Spectroscopy: X-ray and ultraviolet photoelectron spectroscopy (XPS and UPS) were performed on a 200 Å thick film of $[Ru(terpy)_2]^0$ thermally deposited on Pt foil. XPS reveals the presence of carbon, nitrogen, and ruthenium (as expected), as well as oxygen, as shown in the survey spectrum in **Figure 4.3**. High-resolution XPS spectra of the carbon, ruthenium, and nitrogen regions are depicted in **Figure 4.4**.

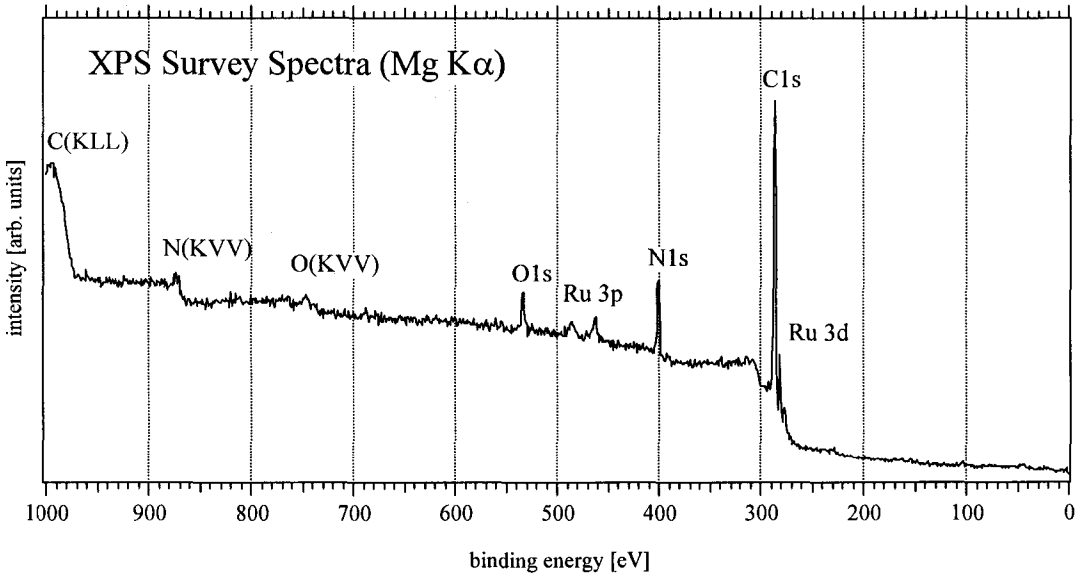

Figure 4.3: XPS survey spectrum for a vapor-deposited film of $[Ru(terpy)_2]^0$.

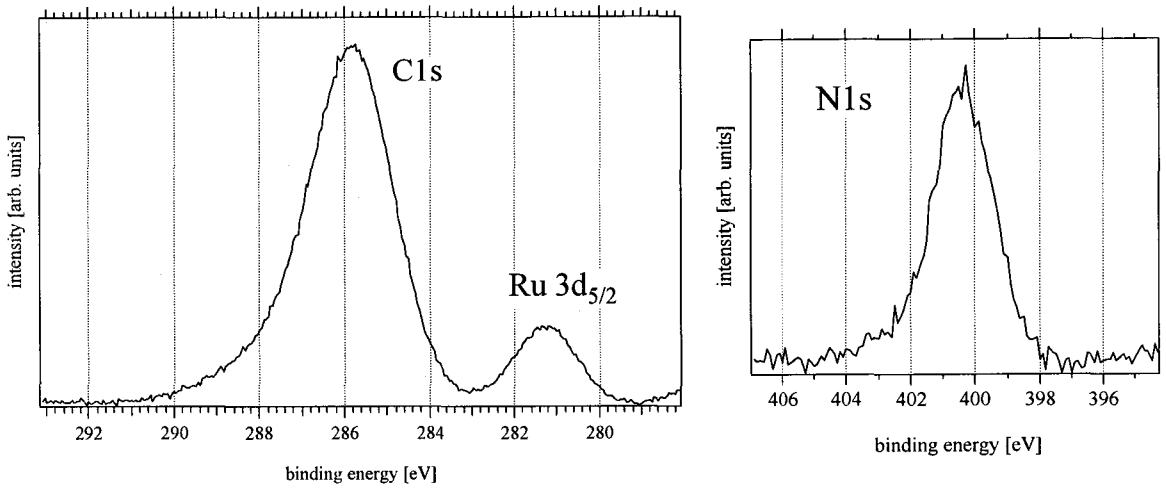

Figure 4.4: High-resolution XPS spectra of vapor deposited $[Ru(terpy)_2]^0$.

The presence of ruthenium, carbon, and nitrogen supports the assertion that the complex is vapor deposited intact, rather than decomposing to yield other carbonaceous material. However, there is no oxygen in the chemical structure for the complex, and the origin of the oxygen may be from materials non-specifically adsorbed to the Pt substrate. Alternately, the oxygen could indicate partial oxidation by air in the transfer of the sample from the glove box to the UHV chamber. UPS spectra for the vapor deposited film were also obtained, and the HeII spectrum is displayed in **Figure 4.5**.

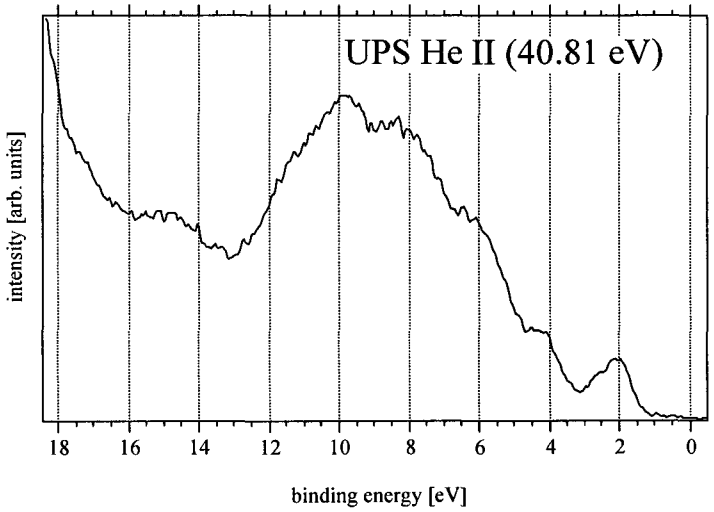

Figure 4.5: UPS HeII spectrum for a vapor deposited film of $[Ru(terpy)_2]^0$.

The signal-to-noise ratio for the above HeII spectrum is not optimum, but the shape of the underlying peaks is still evident. As might be expected, the data closely resembles the spectra reported in **Chapter 3** for the reduced $Ru(LL)_3$-based polymers. For the spectroscopic determination of the work function, the secondary edge region for both the XPS (with the x axis shifted in energy for direct comparison) and UPS HeI spectra are examined in **Figure 4.6**, and yield Φ values of 3.32 eV and 3.38 eV respectively.

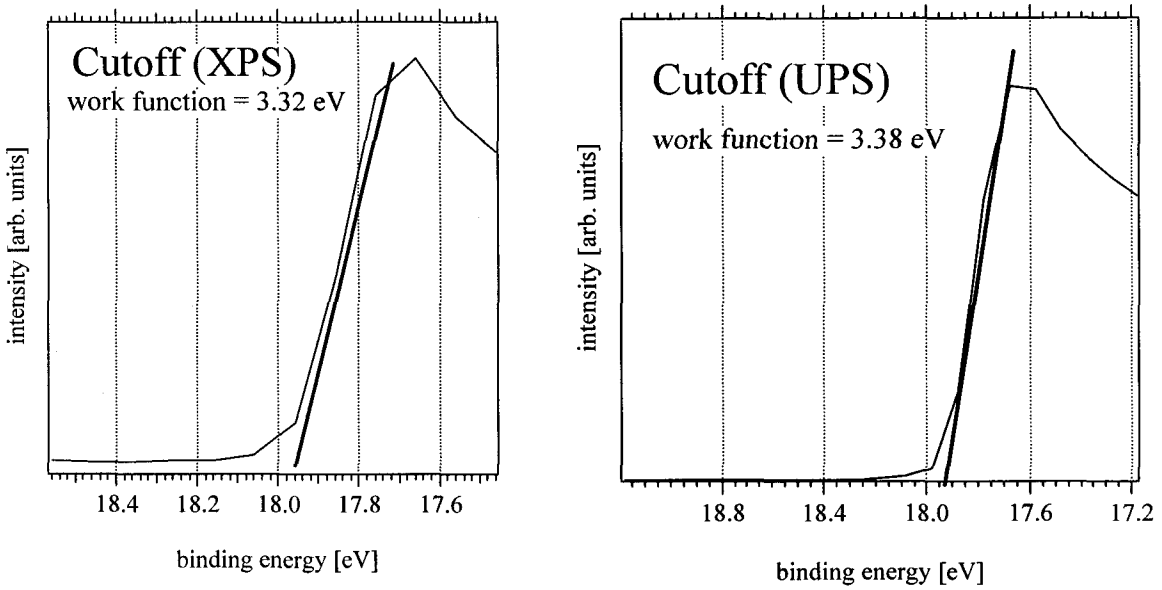

Figure 4.6: Secondary edge region of XPS and UPS spectra of $[Ru(terpy)_2]^0$.

These measured Φ, while in good agreement with each other, are slightly higher than the value of 3.10 eV predicted from the electrochemical data and are not as close to the predicted Φ as are the values obtained for similar conducting polymers. The difference from the predicted value could be rationalized in several ways; by a partial oxidation of the films while moving the sample into the UHV chamber, by solid-state effects in the crystal lattice, or by delocalization of electron density. Extensively delocalized electrons in the solid, in the model of an electride, would likely reside at a

lower energy than electrons in a corresponding isolated complex. Presumably this would result in a somewhat lower E_F, and thereby a greater work function. Aside from any such delocalization effects, the ordering of complexes in a crystalline environment could change the HOMO and LUMO energies (relative to the energies of an isolated complex in solution) in a systematic fashion. In contrast, the energies in an amorphous polymer environment, like those reported in the previous chapter, should be more randomly distributed about the value for an isolated unit. In any case, the Φ for $[Ru(terpy)_2]^0$ provided by photoelectron spectroscopy is within the range of commonly used metals for OLED cathodes (by comparison, Ca metal has a Φ of 2.9 eV), and is at least fairly close to the predicted value of 3.10 eV.

Device Performance: EL devices were initially constructed using $[Ru(terpy)_2]^0$ with the architecture Ag/LWOM/Alq_3(400 Å)/TPD(400 Å)/ITO. Performance for a typical device with approx. 140 Å of $[Ru(terpy)_2]^0$ as the LWOM is shown in **Figure 4.7**. As described above, current/voltage measurements for these devices were performed with a digital sourcemeter instrument, while light emission was detected with a calibrated photodiode and collected in digital form. As a consequence, data for device performance is now depicted in logarithmic plots to allow for more detailed analysis. In comparison to the devices employing reduced $Ru(LL)_3$ polymers presented in **Chapter 3**, turn-on voltage (as defined by the lowest voltage with measurable light output) is significantly lower. Because the light power in the previous generation of devices was measured in arbitrary units, it is not possible to quantifiably compare the total light output; however, by observation with the naked eye the emission intensity in the present devices is much

greater. Furthermore, in attempts to measure light power for these devices using the PMT employed in the previous chapter, the PMT response was saturated at a bias of approx. 7 V (with the PMT setting at 400 V). Total current passed is also in general much higher in these OLEDs employing LWOM materials as cathodes. Emission spectra for these devices peak in the 520 nm region typical of Alq_3 based OLEDs,[29] and the spectrum for a device with a $[Ru(terpy)_2]^0$/Ag cathode is plotted in **Figure 4.8**.

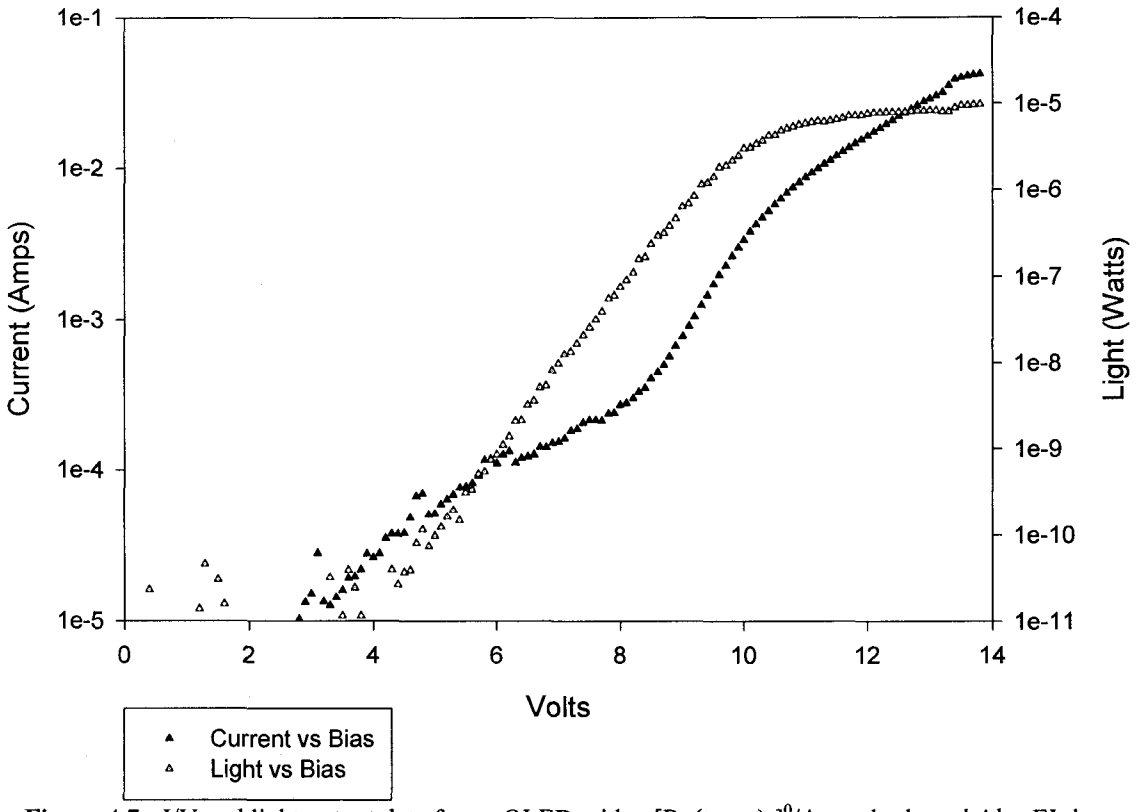

Figure 4.7: I/V and light output data for an OLED with a $[Ru(terpy)_2]^0$/Ag cathode and Alq_3 EL layer. Device areas throughout are approximately 0.07 cm^2.

Following this initial work, devices were prepared with the addition of a poly(thiophene)-based conducting polymer interlayer (PEDOT-PSS) between the ITO anode and the TPD hole transport material. This approach has been shown to improve device performance by reducing the barrier to hole injection at the anode,[30,31] resulting in increased device lifetime and efficiency in literature OLEDs. In this study, devices

containing a PEDOT-PSS layer for hole injection had a lower turn-on voltage, passed more current and produced more light at a given potential than did identical devices lacking the additional layer. The performance for a device composed of the layers Ag/$[Ru(terpy)_2]^0$/Alq_3/TPD/PEDOT-PSS/ITO is shown in **Figure 4.9**.

To investigate the role of the metal layer covering the LWOM, analogous OLED's were also made with gold, which has a very high Φ of 5.2 eV,[2] in place of silver as the metal contact. As is apparent in **Figure 4.9**, there is very little difference in device performance following this substitution. In contrast, devices constructed with only the metals as cathodes (i.e., no LWOM layer) work only poorly when made with silver and not at all with gold, due to a very large barrier for electron injection. This observation supports the assertion that the nature of the metal contact is of secondary importance to the underlying LWOM.

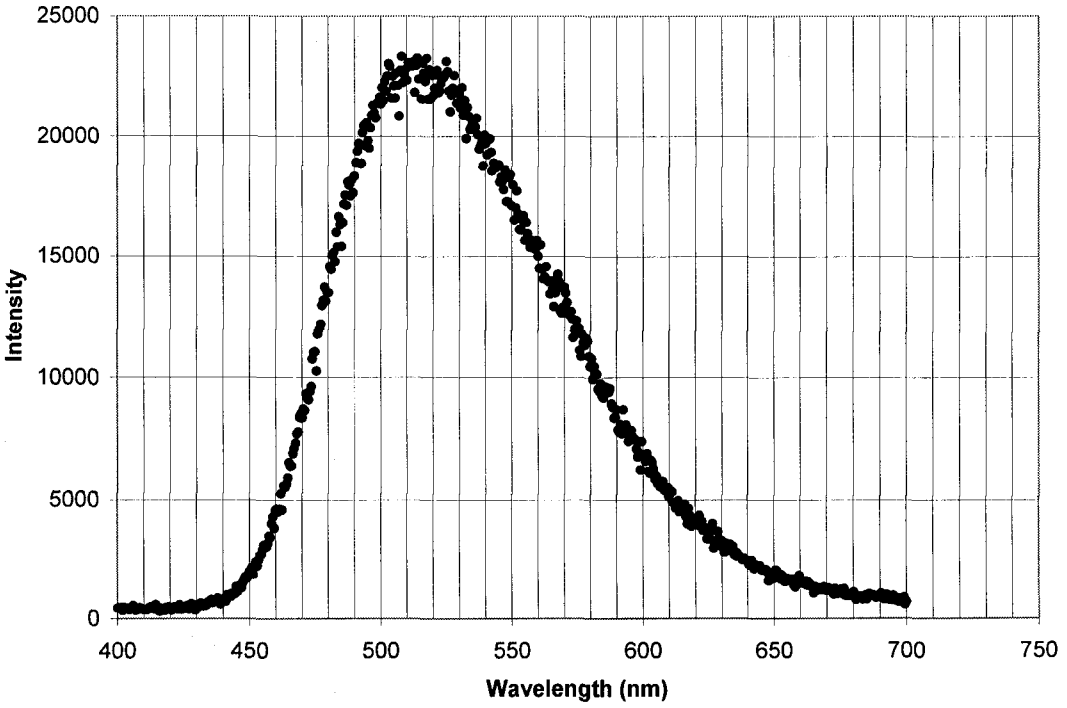

Figure 4.8: Emission spectrum for an EL device with a $[Ru(terpy)_2]^0$/Ag cathode. There is no evidence of emission from the LWOM layer, or perturbation of the Alq_3 emission.

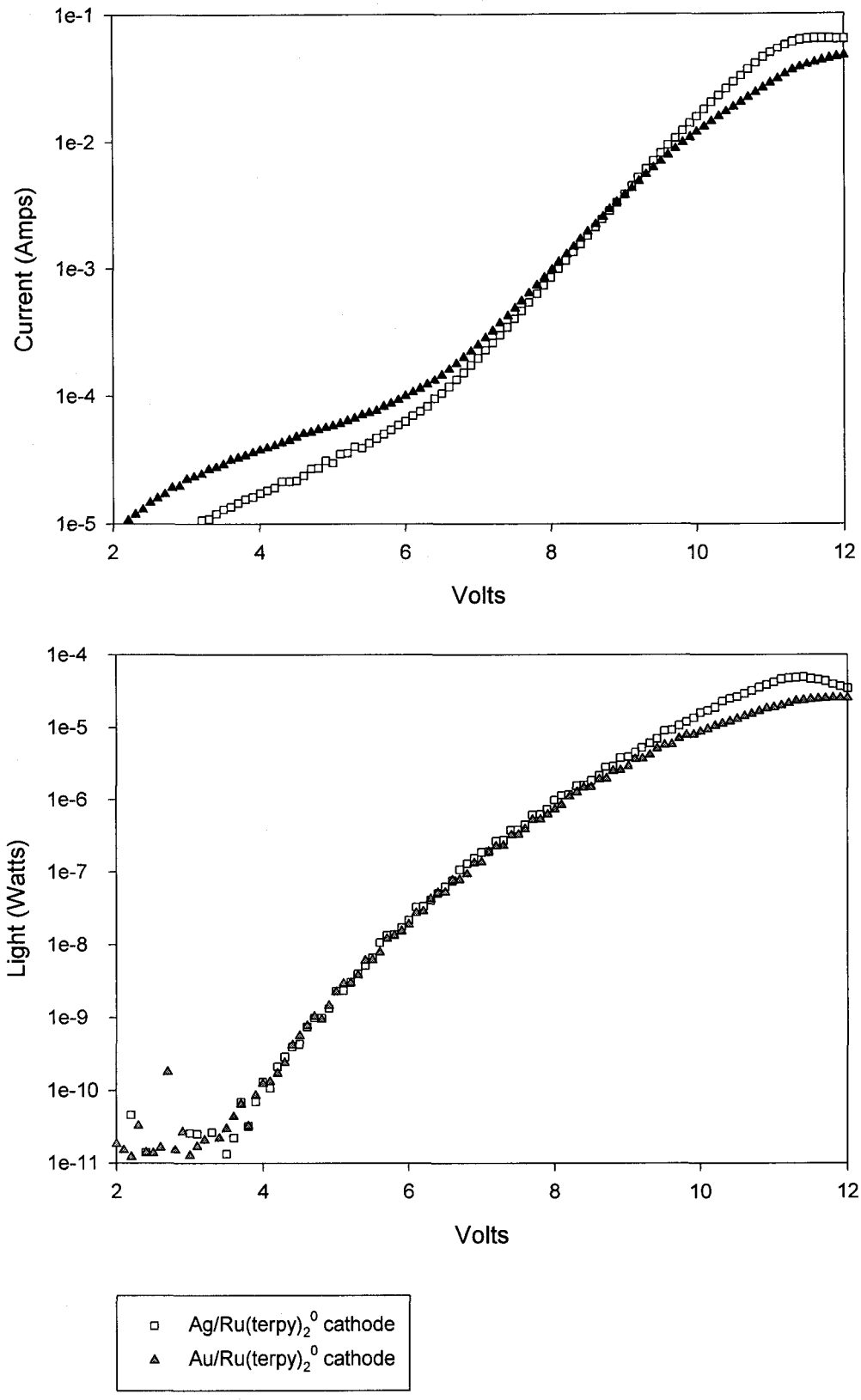

Figure 4.9: I/V (upper) and light output (lower) data for two OLEDs constructed with a PEDOT-PSS layer, a $[Ru(terpy)_2]^0$ cathode and Ag or Au metal covering the LWOM.

Analogous EL devices employing $[Cr(TMB)_3]^0$ and $[Cr(bpy)_3]^0$ as the cathode materials were also constructed. The performance of two typical OLEDs of this makeup is depicted in **Figure 4.10**. Comparing this data to the devices analyzed above, OLEDs containing the TMB complex emit more light (while also passing more current) than do comparable devices with $[Ru(terpy)_2]^0$. This may be attributed to the lower calculated Φ of the reduced complex, which would be expected to yield a lower barrier for electron injection. On the other hand, devices employing $[Cr(bpy)_3]^0$ produce noticeably less light emission, but with greater current at lower drive voltages, than do OLEDs with either of the other LWOMs, which cannot be easily explained based on the predicted work function alone. External quantum efficiencies ($\varphi_{ext.}$) of OLEDs containing $[Ru(terpy)_2]^0$ with silver and gold, as well as $[Cr(TMB)_3]^0$, are at a maximum of 0.04 – 0.05 % at 8 V bias. Devices with $[Cr(bpy)_3]^0$-based cathodes have a significantly lower maximum $\varphi_{ext.}$ at a bias of 10 V, of only 0.02 %. Again, the explanation for the differing performance of the devices employing $[Cr(bpy)_3]^0$ is not clear.

Notably, the performance of OLEDs having a relatively thick layer of LWOM is superior to those with thin layers (i.e. < 100 Å). This is in contrast to what was observed in the literature for more insulating materials such as inorganic salts[8,10,11] and CuPc,[12] where only very thin layers of less than 50 Å are effective. Light emission from several devices (of makeup Ag/$[Cr(bpy)_3]^0$/Alq_3/TPD/PEDOT-PSS/ITO) differing only in the thickness of LWOM is displayed in **Figure 4.11**. The OLEDs having thicker layers (89 or 185 Å) of $[Cr(bpy)_3]^0$ produce several orders of magnitude more light than do those with only 37 Å. These results are further consistent with the model of electron injection directly from conducting LWOMs into the Alq_3 EL layer.

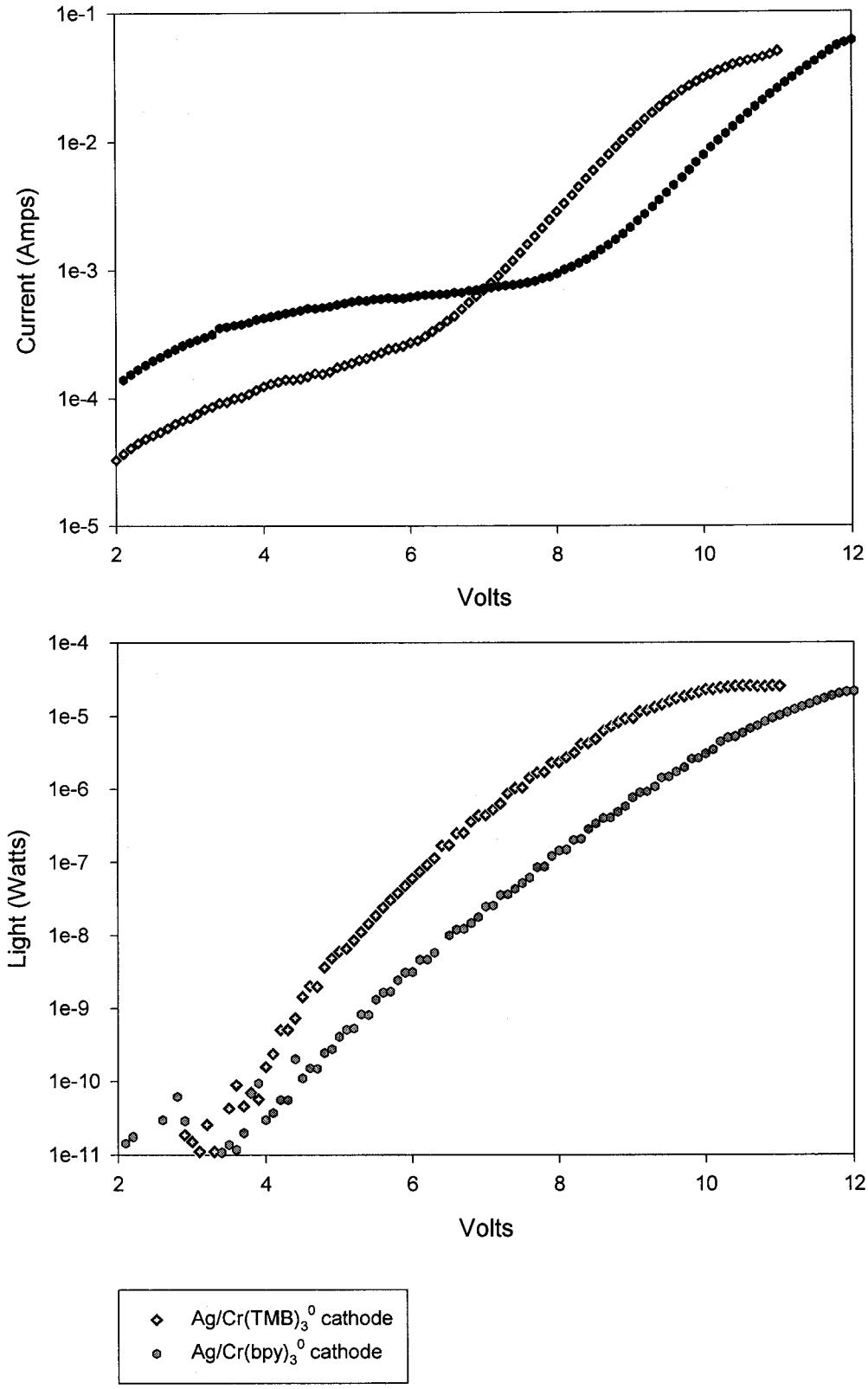

Figure 4.10: Performance of two OLEDs with cathodes composed of reduced Cr complexes.

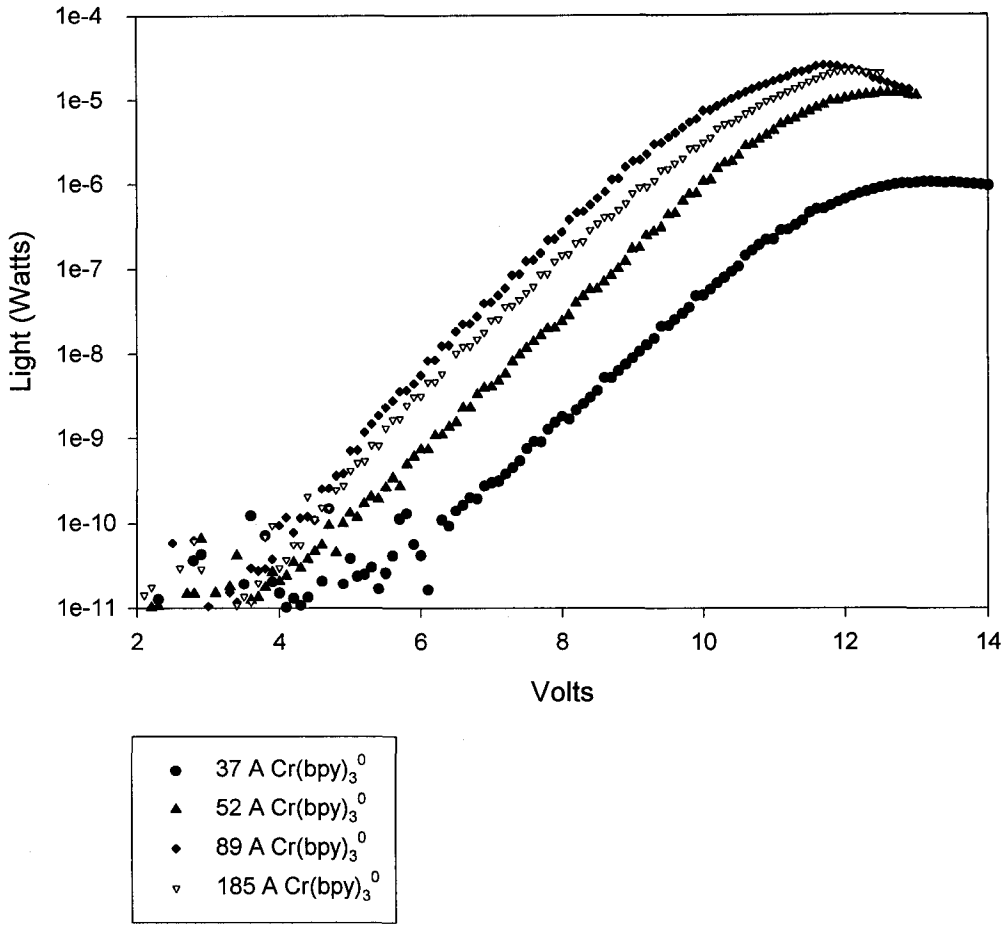

Figure 4.11: Emission data for Ag/$[Cr(bpy)_3]^0$/Alq_3/TPD/PEDOT-PSS/ITO devices. All four OLEDs are identical in all respects other than LWOM thickness.

Interpretation of the data in **Figure 4.11** displaying the dependence of device performance on LWOM thickness becomes more complex when consideration of the morphology of the films is taken into consideration. The actual property of the film being directly measured during vapor deposition (by quartz crystal microbalance, as described above) is mass. From this quantity the thickness of the film is calculated using known or estimated properties, most importantly density. However, the assumption is also made that the film is uniform in morphology. It is instead possible that initially the material deposits in an "islanding" mode, where there may be incomplete coverage of the

underlying Alq_3 material. If this were the case here, the data above could be indicative of the portion of the device actually covered by the LWOM, rather than the thickness of the layer. Analysis of the devices by electron microscopy indicates that the LWOM layers are most likely polycrystalline, but it was not possible to determine whether or not there is complete coverage with the deposition of small amounts of material.

Stability of Devices in Operation: The performance of any light emitting device with time is of critical importance. In **Figure 4.12**, current and light intensity vs time are depicted for a typical OLED (with layers Ag/$[Ru(terpy)_2]^0$/Alq_3/TPD/PEDOT-PSS/ITO) held at 7 Volts for ca. 4 hours. Over this time period, the current passed and light emission were both attenuated, by approximately 20% and 40%, respectively. The shape of these curves is not unusual, and suggests that device performance may be reaching a plateau where the current and light will change only very slowly with time. However, the ultimate lifetime of one of these devices cannot be assessed with certainty from this data. The physical cause of the decay of emission and current in these OLEDs with time is also not known. Nevertheless, emission from these devices, which have been constructed with a minimum of optimization, is stable for time scales on the order of hours as is necessary for any real-world application. A systematic study of the mechanism for device degradation in these systems would likely provide both a better fundamental understanding of any stability problems, as well as potential solutions.

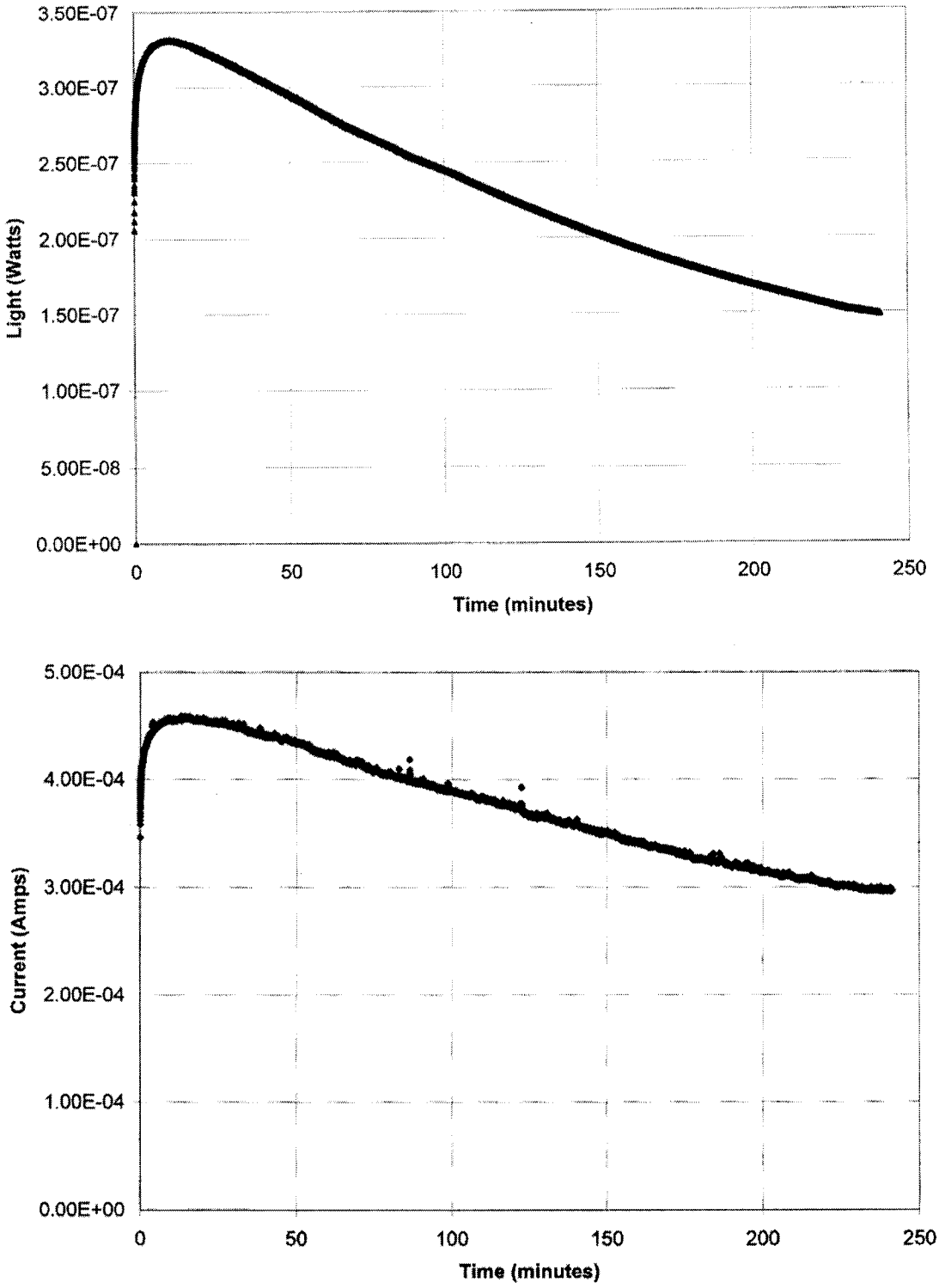

Figure 4.12: Performance of an EL device with a Ag/$[Ru(terpy)_2]^0$ cathode over time.

Analysis of the Injection Mechanism: By closer analysis of the I/V curves, it may be possible to gain a deeper understanding of the nature of the electron injection process in these devices. As discussed in the introduction, several models have been developed to account for charge injection and transport in OLEDs. It is commonly asserted that the shape of the current-voltage curve for an OLED is indicative of the mechanism for charge carrier introduction from the electrodes.[1,2,4] For devices governed by trap-limited electron conduction in the Alq_3 layer, the power law equation (1) describes the I/V relationship.[4] In this case, the current is limited by transport characteristics of the Alq_3, rather than a barrier to injection at the interface with one or both electrodes. In equation 1, I_o is a constant current (which is often omitted) and a is a constant containing several terms including device area, electron mobility in Alq_3, and layer thickness.[4]

$$I = I_o + aV^m \quad (m = 7-9) \tag{1}$$

If $I_o = 0$, it follows that:

$$\log(I) \propto m\log(V) \tag{2}$$

For the OLEDs constructed here, fits to the power law relation have been unsatisfactory. The I/V performance in the useful operating range of 4-10 V of the previously discussed $[Ru(terpy)_2]^0$ containing device (with PEDOT-PSS and Ag metal), along with a best fit to the equation $I = I_o + aV^9$, is shown in **Figure 4.13**. Clearly, the agreement with this model is quite poor (as were fits with other m). A plot of log(I) vs log(V) is also displayed in **Figure 4.13**, and is obviously not linear. Thus there is no m for which the power law would describe the data. It follows that the above mentioned trap-limited conduction in the Alq_3 layer is not the governing mechanism for this device.

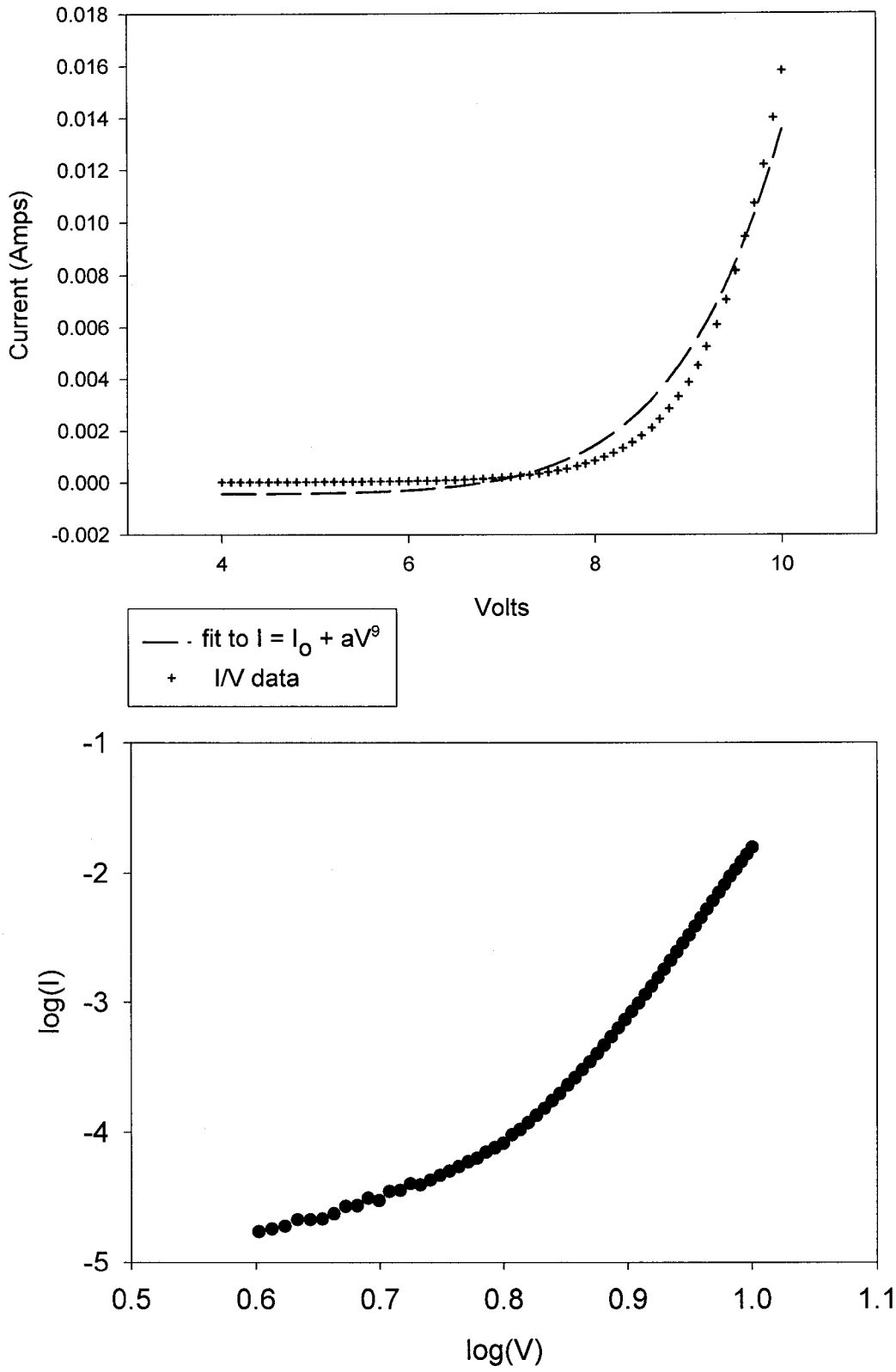

Figure 4.13: Current vs voltage data for the same OLED previously reported with layers of Ag/$[Ru(terpy)_2]^0$/Alq_3/TPD/PEDOT-PSS/ITO. **Upper:** data along with a best fit to the power law equation (1), performed by Sigmaplot 6.0 software. **Lower:** log/log plot, as in equation (2), for the same data.

The Fowler-Nordheim tunneling model, where an electron is assumed to tunnel through a triangular energy barrier (dependent on the potential field and the difference between electrode Φ and CB energy in the organic), has been successfully applied mainly to MEH-PPV based EL devices.[1,2] The current vs voltage response for EL devices governed by this mechanism follows the relationship below in (3), where A and B are constants and F is the strength of the electric field in V/m. It has been asserted that this model is effective only in cases where the energy barrier for electron injection is relatively large.[1,32] Fits to this model were also unsatisfactory in describing the current/voltage characteristics of OLEDs in this work, which is perhaps not surprising considering that other evidence at hand suggests a small barrier for injection at the cathode/organic interface.

$$I = AF^2 e^{\left(-B/F\right)} \qquad (3)$$

While neither Fowler-Nordheim tunneling nor trap limited conduction in Alq_3 were adequate models, the simple exponential equation (4) fits the data very well, as shown in **Figure 4.14**. This suggests that the performance of these devices is limited by some manner of injection *over* an energy barrier. It is interesting to note that this expression is of the same form as the "diode equation" (5) for a forward-biased inorganic *p-n* junction diode[4,33] In this formula, q is the elementary charge, and k is Boltzmann's constant.

$$I = ae^{bV} \qquad (4)$$

$$I = I_o e^{qV/kT} \qquad (5)$$

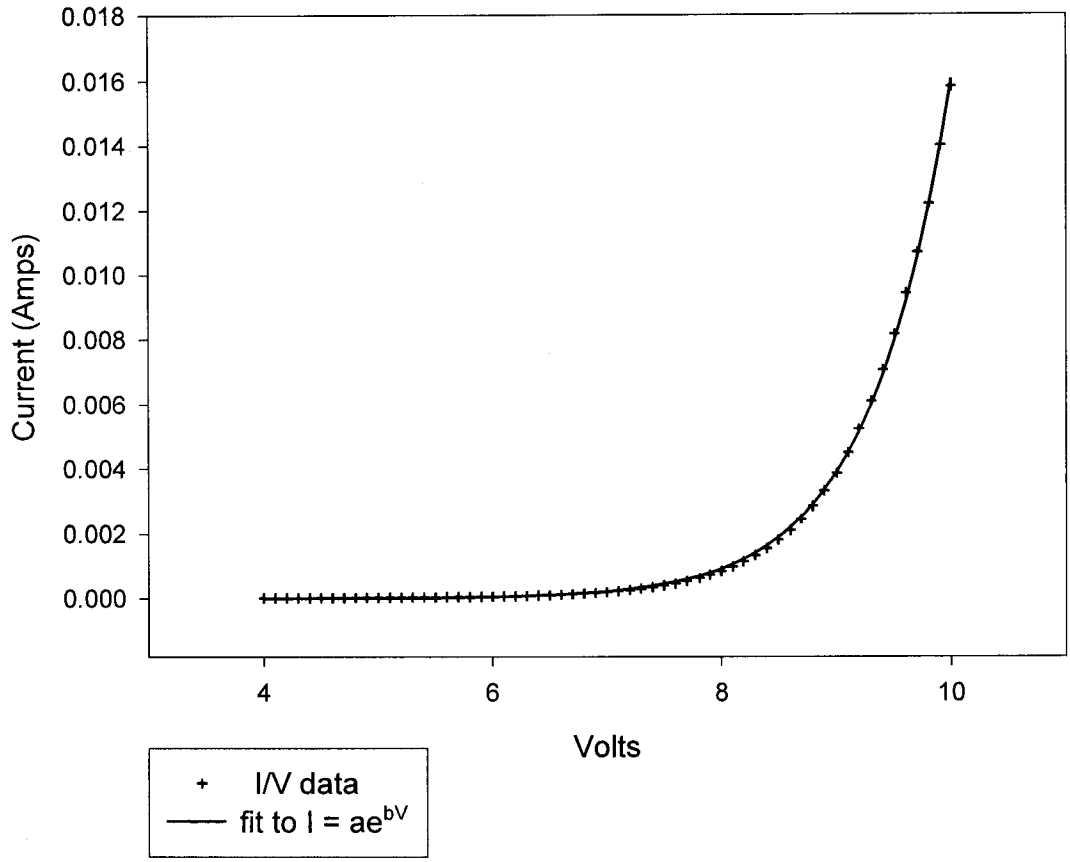

Figure 4.14: A fit of the current vs voltage data with the simple exponential equation (4) where $a = 1.07 \cdot 10^{-8}$ Amps, and $b = 1.42\ V^{-1}$.

The most commonly identified model for injection over an energy barrier in organic EL devices is the thermionic emission mechanism, in which the current/voltage characteristics are described by the somewhat more complex relationship in equation 6, where J is current density (in Amps/m^2), while A and C are constants.[3] If the thermionic emission model holds, a plot of ln(J) vs $V^{1/2}$ *at a given T* should result in a linear expression. Such a plot is shown in **Figure 4.15,** again using data from the same device (operated at room temperature) as the previous examples.

$$J \propto AT^2 e^{C\sqrt{V}/kT} \qquad (6)$$

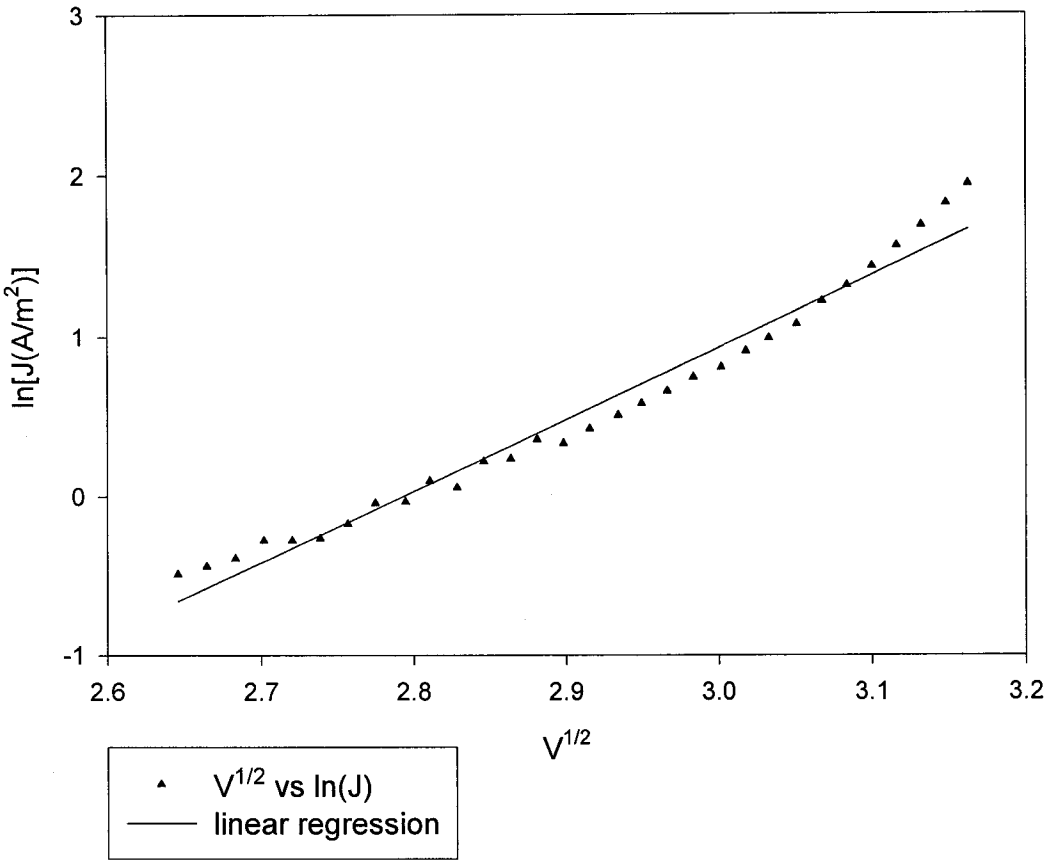

Figure 4.15: A plot following the behavior predicted by the thermionic emission model for the same device analyzed above.

The agreement with the thermionic model, as evidenced by the plot in **Figure 4.15**, is not altogether satisfactory. There appears to be a systematic deviation from the linear relationship predicted by the thermionic emission mechanism. Analysis of the temperature dependence of device performance would also be instructive, as there is clearly a strong temperature effect in the above theoretical expression describing the thermionic model. Such studies have not been undertaken here for these devices. What is clear is that OLEDs constructed with the cathode materials under discussion here do *not* adhere to the commonly cited trap-limited conduction mechanism for other Alq_3-based devices, and likely also do not follow the thermionic emission mechanism. At the same time, strictly applying the model used for inorganic LEDs of charges moving over

the energy barrier at the *p-n* junction as a consequence of applied voltage seems inappropriate here. If this model were strictly correct, the parameter *b* in equation 4 would be equal to *q/kT* (38.6 C/J), as in equation 5. However; from the fit in **Figure 4.14**, *b* = 1.42 C/J. Apparently the simple diode equation is also inadequate to describe the current/voltage behavior of these devices. Injection of electrons from this new class of low Φ materials may require yet another new model that takes into account their unusual electronic structures. Regardless of the exact mechanism, it has been demonstrated that these materials provide for effective electron injection into organic layers for EL devices.

Inverted EL Devices with LWOM cathodes: All of the OLEDs discussed in this chapter have been constructed using the common architecture of an ITO anode on the bottom, organic materials in the middle, and a cathode deposited to form the top contact. The LWOMs presented here should also afford the possibility of building "inverted" EL devices, as was done in **Chapter 3** using cathodes composed of electrochemically reduced polymers (coated on ITO) as the bottom contact and a thermally deposited gold anode on top. As previously outlined, there are some inherent disadvantages in this setup, not the least of which is the TPD/gold interface. This problem was dealt with in part by the addition of a "protective cap layer" of PTCDA prior to gold deposition. While the performance of devices of this sort using a **P3** polymer cathode have been less than ideal, it seems nonetheless informative to compare the results of analogous OLEDs in which a vapor deposited LWOM is used in place of the treated polymer. With this in mind, **Figure 4.16** contains performance data for a device with layers as follows; ITO/$[Ru(terpy)_2]^0$ (50 Å)/Alq_3 (400 Å)/TPD (400 Å)/PTCDA (50 Å)/Gold.

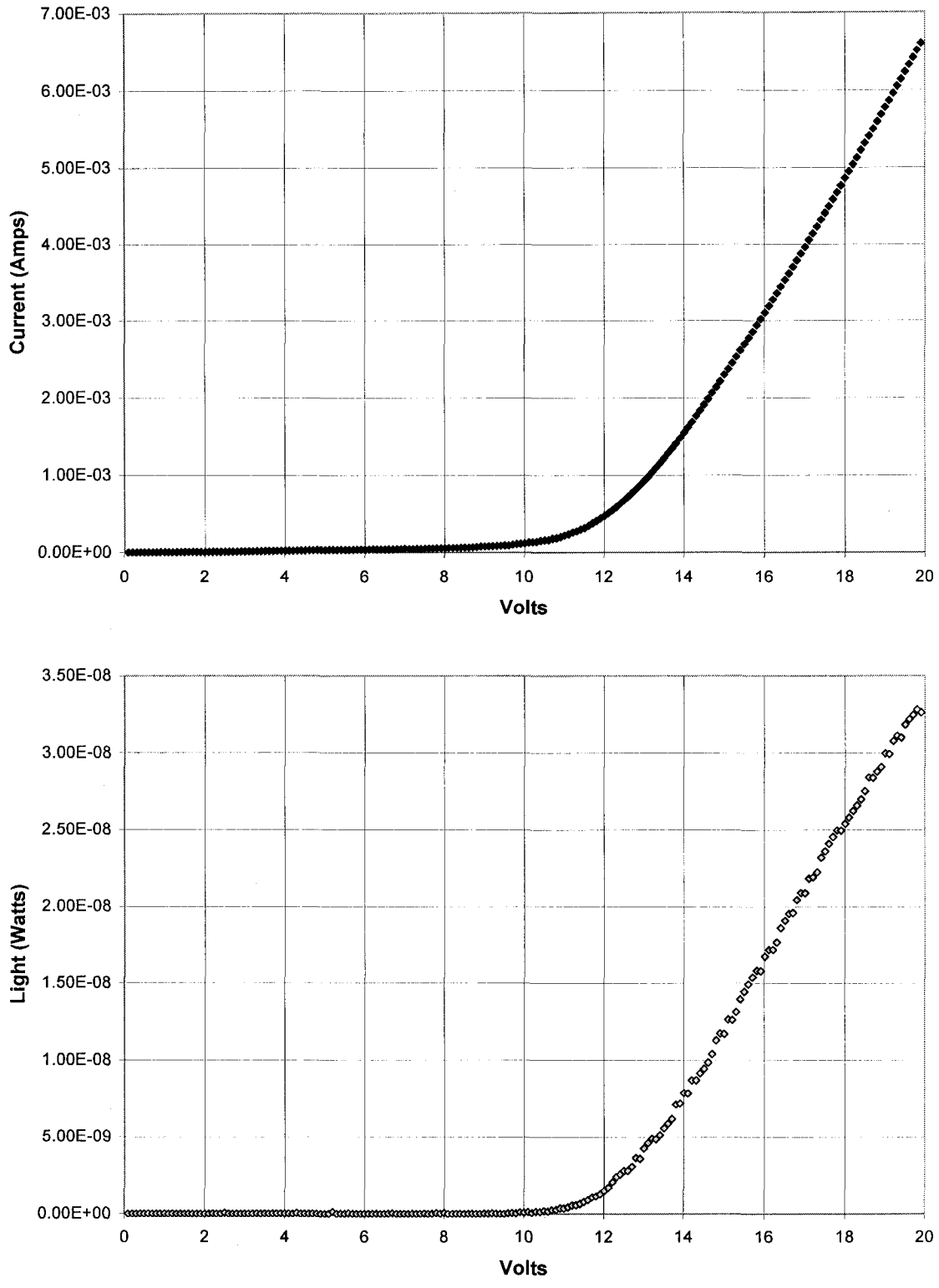

Figure 4.16: Current vs voltage and light output vs voltage for an inverted OLED with a $[Ru(terpy)_2]^0$ cathode. Both **y axes are linear** for direct comparison with the data in **Figure 3.14**. Since device area is approx. 0.1 cm^2, multiplication of the y axes by 10 yields current density in A/cm^2 (and light in $Watts/cm^2$).

Several conclusions can readily be drawn from inspection of the data in **Figure 4.16**. First, the performance of this inverted device is significantly inferior to the OLEDs previously described in this chapter in terms of both turn-on voltage and total light output. Comparing the output of this device to the data in **Figure 3.14** (the analogous device with a **P3** cathode), the general shape of both the I/V and light output curves are quite similar. The turn-on voltage for light emission appears to be higher in the device with the $[Ru(terpy)_2]^0$ cathode; however, this may be due to the lower sensitivity of the photodiode used for light measurement (as opposed to the PMT employed in **Chapter 3**). For this same reason, the absolute magnitude of light emission cannot be directly compared for the two cases. The current response for the two devices is fairly comparable in terms of total current passed, but the potential at which the current deviates from an ohmic response is somewhat higher for the device with the LWOM cathode (at ~ 9 V compared to ~ 6 V with the **P3** polymer). This result suggests that the actual turn-on voltage for light emission is likely indeed higher for this device as well. Taken as a whole, the characteristics of the two devices appear to be roughly similar, with the present device being somewhat less impressive. This leads to the conclusion that the generally poor performance of the OLEDs containing a reduced **P3** cathode (as compared to the devices presented earlier in this chapter) is largely due to problems associated with the inverted architecture, rather than issues relating to the polymer itself or the electrochemical reduction.

V. Conclusions:

A new class of electrochemically active transition metal complexes that can be reduced and isolated in a zero charged form has been introduced. As with the related polymeric systems reported in the previous chapter, these reduced materials are electronically conducting and posses low work functions. Unlike polymers, the discrete molecule systems presented here can be thermally vapor deposited in the conducting form. As such, these materials are advantageous for use as electron injecting contacts in OLEDs using common emitting materials such as Alq_3. It has further been demonstrated that the identity of the metal contacting these relatively thick conducting organic layers has only a very minor effect on device performance, allowing the use of air stable metals such as silver or gold. This suggests the possibility of replacing the metal with a transparent conducting oxide such as ITO, yielding a completely transparent device. In addition, these new materials could be employed in situations where metal deposition is problematic due to thermal damage in underlying organic layers, opacity, or other issues. Many other novel OLED designs could be envisioned due to the flexibility these materials provide both in their work functions and practical use in devices.

While the performance of EL devices constructed with these new LWOMs as cathode materials is promising, the precise nature of the mechanism for charge injection is still not fully understood. It has been clearly shown, however, that some of the models commonly employed to explain the characteristics of similar devices with more traditional cathode materials are not satisfactory for these new devices. Thus at this time, the effort towards a better general understanding of the nature of the cathode/organic interface in OLEDs is still unfinished.

REFERENCES

(1) Sheats, J. R.; Antoniadis, H.; Hueschen, M.; Leonard, W.; Miller, J.; Moon, R.; Roitman, D.; Stocking, A. *Science* **1996**, *273*, 884.

(2) Parker, I. D. *J. Appl. Phys.* **1994**, *75*, 1656.

(3) Matsumura, M.; Akai, T.; Saito, M.; Kimura, T. *J. Appl. Phys.* **1996**, *79*, 264.

(4) Burrows, P. E.; Forrest, S. R. *Appl. Phys. Lett.* **1994**, *64*, 2285.

(5) Tang, C. W.; VanSlyke, S. A. *Appl. Phys. Lett.* **1987**, *51*, 913.

(6) Burroughs, J. H.; Bradley, D. D. C.; Brown, A. R.; Marks, R. N.; Mackay, K.; Friend, R. H.; Burns, P. L.; Holmes, A. B. *Nature* **1990**, *347*, 539.

(7) Gustafsson, G.; Cao, Y.; Treacy, G. M.; Klavetter, F.; Colaneri; Heeger, A. J. **1992**, *357*, 472.

(8) Hung, L. S.; Tang, C. W.; Mason, M. G. *Appl. Phys. Lett.* **1997**, *70*, 152.

(9) Jabbour, G. E.; Kawabe, Y.; Shaheen, S. E.; Wang, J. F.; Morrell, M. M.; Kippelen, B.; Peyghambarian, N. *Appl. Phys. Lett.* **1997**, *71*, 1762.

(10) Matsumura, M.; Jinde, Y. *Appl. Phys. Lett.* **1998**, *73*, 2872.

(11) Lee, C. H. *Synth. Met.* **1997**, *91*, 125.

(12) Parthasarathy, G.; Burrows, P. E.; Khalfin, V.; Kozlov, V. G.; Forrest, S. R. *Appl. Phys. Lett.* **1998**, *72*, 2138.

(13) Kido, J.; Matsumoto, T. *Appl. Phys. Lett.* **1998**, *73*, 2866.

(14) Bulovic, V.; Tian, P.; Burrows, P. E.; Gokhale, M. R.; Forrest, S. R.; Thompson, M. E. *Appl. Phys. Lett.* **1997**, *70*, 2954.

(15) Elliott, C. M.; Redepenning, J. G. *J. Electroanal. Chem.* **1986**, *197*, 219.

(16) Pecsok, R. L.; Lingane, J. L. *J. Am. Chem. Soc.* **1950**, *72*, 189.

(17) Baker, B. R.; Mehta, B. D. *Inorg. Chem.* **1965**, *4*, 848.

(18) Perez-Cordero, E.; Buigas, R.; Brady, N.; Echegoyen, L. *Helv. Chim. Acta* **1994**, *77*, 1222.

(19) Pyo, S.; Perez-Cordero, E.; Bott, S. G.; Echegoyen, L. *Inorg. Chem.* **1999**, *38*, 3337.

(20) Schlaf, R.; Schroder, P. G.; Nelson, M. W.; Parkinson, B. A.; Merritt, C. D.; Crisafulli, L. A.; Murata, H.; Kafafi, Z. H. *Surface Science* **2000**, *450*, 142.

(21) Elliott, C. M.; Redepenning, J. G.; Balk, E. M.; Schmittle, S. J. *Electronically Conducting Films of Poly(trisbipyridine)-Metal Complexes;* ACS Symposium Series 360 (Inorganic and Organometallic Polymers); American Chemical Society: Washington, DC, **1988** p. 420.

(22) Perez-Cordero, E.; Campana, C.; Echegoyen, L. *Angew. Chem. Int. Ed. Engl.* **1997**, *36*, 137.

(23) Wagner, M. J.; Dye, J. L.; Perez-Cordero, E.; Buigas, R.; Echegoyen, L. *J. Am. Chem. Soc.* **1995**, *117*, 1318.

(24) Echegoyen, L.; Xie, Q.; Perez-Cordero, E. *Pure Appl. Chem.* **1993**, *65*, 441.

(25) Dye, J. L. *Inorg. Chem.* **1997**, *36*, 3816.

(26) Saji, T.; Aoyagui, S. *Bull. Chem. Soc. Japan* **1973**, *46*, 2101.

(27) Morris, D. E.; Hanck, K. W.; DeArmond, M. K. *J. Electroanal. Chem.* **1983**, *149*, 115.

(28) Trasatti, S. *Pure Appl. Chem.* **1986**, *58*, 955.

(29) Tang, C. W.; VanSlyke, S. A.; Chen, C. H. *J. Appl. Phys.* **1989**, *65*, 3610.

(30) Troadec, D.; Veriot, G.; Antony, R.; Moliton, A. *Synth. Met.* **2001**, *124*, 49.

(31) Elschner, A.; Bruder, F.; Heuer, H. W.; Jonas, F.; Karbach, A.; Kirchmeyer, S.; Thurm, S.; Wehrmann, R. *Synth. Met.* **2000**, *111-112*, 139.

(32) Vestweber, H. *Synth. Met.* **1995**, *68*, 263.

(33) Mayer, J. W.; Lau, S. S. *Electronic Materials Science: For Integrated Circuits in Si and GaAs*; Macmillan: New York, **1990**.